Control of reactive oxygen species (ROS) machinery to maintain the cellular homeostasis

活性酸素種による細胞動態恒常性調節機構の解析

February, 2024

Kenly WUPUTRA
吳　念吉

Control of reactive oxygen species (ROS) machinery to maintain the cellular homeostasis

活性酸素種による細胞動態恒常性調節機構の解析

February, 2024

Waseda University
Graduate School of Advanced Science and Engineering

Kenly WUPUTRA
呉　念吉

Index

List of illustrations

Abstract:

Regulation of oxidative stress and redox control processes is one of the most important mechanisms for development, maintenance of characteristics, self-renewal, and reprogramming of stem cells. Regulation of the equilibrium of oxidative stress and antioxidation involves the acryl hydrocarbon receptor–Jun dimerization protein 2–nuclear factor (erythroid-derived 2)-like 2 (AhR–Jdp2–Nrf2) axis through mitochondrial integrity. By elucidating the balance mechanism of reactive oxygen species (ROS) generation through the redox pathway that involves Jdp2, I will provide insights into the role of the AhR–Jdp2–Nrf2 gene battery in determining the plasticity of differentiation and cell fate.

In this study, I first discuss AhR–Jdp2 axis activation through stimulation by dimethyl sulfide (DMSO), a commonly used polar organic solvent. The promoter of the *AhR* gene was significantly upregulated via a Dioxin response element (DRE), which increased ROS production and resulted in apoptosis of mouse embryonic fibroblasts. The mechanism of AhR promoter upregulation is Jdp2 dependent. Moreover, the interaction of AhR with Jdp2 and the phase II-dependent transcription factor, small Maf basic zipper Transcription Factor K (MafK), has been detected by co-immunoprecipitation and chromosome immunoprecipitation on the DRE of the AhR promoter region. Take these results together, Jdp2 forms a complex with the phase I enzyme factor, AhR, and the phase II enzyme factor, Nrf2. Furthermore, this complex plays an important role in the AhR promoter activation in response to DMSO.

To further confirm the crosstalk between the AhR–Jdp2–Nrf2 axis, we identified Nrf2 as one of the factors critical activation of AhR-promoter by the phase I enzyme ligand 2,3,7,8-tetrachlorodibenzo-p-dioxin, in a spatiotemporal *cis*-element-dependent manner. These findings identified the role of the AhR–Jdp2–Nrf2 gene battery in modulating ROS production, controlling cytoskeletal remodeling, cell spreading, migration, and tumor progression.

In pancreatic carcinoma, we demonstrated that tumor growth is significantly affected by the Jdp2–AhR–Nrf2 gene battery modulating ROS production. Regorafenib, one of the most commonly used multi-kinase inhibitors functioning as an anticancer drug for the treatment of hepatocellular carcinoma (HCC), is known to generate ROS for anticancer activities and inhibit angiogenesis. Here, we generated HepG2_Rego_R, a regorafenib-resistant HepG2 HCC cell line, inducing forkhead box protein M1

upregulation. This upregulation was crucial for the survival of cancer cells treated with regorafenib; in this case, ROS control was critical for drug resistance. Taken together, these studies of the AhR–Jdp2–Nrf2 gene battery provide basic and compelling evidence for the application of ROS balance in the search for new therapeutics targeted to the AhR–Jdp2–Nrf2 gene battery in cancers or other diseases in the future.

Abbreviations

Abbreviation	Full name
AhR	Acryl hydrocarbon receptor
ANOVA	Analysis of variance
AP-1	Activator protein 1
ARE	Antioxidant response elements
ARNT	AhR nuclear translocator
BaP	6-formylindolo [3,2-*b*] carbazoleand benzo[*a*]pyrene
bHLH	Basic helix–loop–helix
CAF	Cancer associated fibroblasts
ChIP	Chromosome immunoprecipitation
Co-IP	Co-immunoprecipitation
CSC	Cancer stem cells
DME	Drug metabolizing enzymes
DMSO	Dimethyl sulfide
DRE	Dioxin response elements
EMT	Epithelial- mesenchymal transition
FL	Full-length
FOXM1	Forkhead box protein M1
GSH	Glutathione
HCC	Hepatocellular carcinoma
Jdp2	Jun dimerization protein 2
Keap1	Kelch-like ECH-associated protein 1
KO	Knockout
LCC	Lewis lung carcinoma
MafK	Maf bZIP Transcription Factor K
MDA	Malondialdehyde
MEF	Mouse embryonic fibroblast
NQO1	NAD(P)H quinone oxidoreductase 1
Nrf2	Nuclear factor (erythroid-derived 2)-like 2
pMLC2	Phosphorylated MLC2 at position serine 19
ROS	Reactive oxygen species
shRNA	Short hairpin RNA
siRNA	Small interfering RNA
TCDD	2,3,7,8- dtetrachlorodibenzo-p-dioxin
WT	Wild type

Chapter I Introductions

1.1 Environmental toxin 2,3,7,8-tetrachlorodibenzo-p-dioxin (TCDD) and the ROS increase through AhR activation

Environmental toxins can be harmful to organisms existing in the living environment. 2,3,7,8-tetrachlorodibenzo-p-dioxin (TCDD), one of the most notorious toxins, has been reported to cause systemic effects on organisms including tumorigenesis, immunological dysfunction, and metabolic disorders [1]. The acryl hydrocarbon receptor (AhR) is known to display various enzymatic and nonenzymatic responses to xenobiotic chemicals such as allergies, inflammation, immunity, cell differentiation, and cancer progression [2]. Reports have shown that TCDD directly interacts with the AhR complex through the AhR heat-shock protein 90 ligand binding pocket [3]. In these studies, AhR functioned as a ligand-activated transcriptional factor. It directly bound to two classes of chemicals: synthetic halogenated aromatic hydrocarbons, including polycyclic aromatic hydrocarbons [4], and natural components such as indirubin and indigo [5]. In the absence of ligands, AhR was localized in the cytoplasm and constituted a complex with heat shock protein 90 and several other proteins including HBV X-associated protein 2 and aryl hydrocarbon receptor-interacting protein, immunophilin homolog (ARA9) [6]. On interaction with ligands, AhR disassociated from its chaperone protein complex and translocated into the nucleus where it dimerized with the AhR nuclear translocator (Arnt). The AhR–Arnt complex can bind to dioxin response elements (DRE) containing a core sequence of 5′-TNGCGTG-3′ resulting in changes in gene expression [3,7]. Further evidence has shown that AhR can be activated by directly associating with TCDD and translocating to the nucleus, further activating downstream transcription [8] (Fig. 1A). The protective response of AhR activation results in a significant increase in reactive oxygen species (ROS) [9] and can lead to a sharp increase in the immune response and cell apoptosis [10].

1.2 The balance mechanism of ROS through response with phase II enzymes

Activation of the AhR signaling pathway leads to a significant increase in ROS by binding to drug-metabolizing enzymes (DMEs) of cytochrome P4501a1 (Cyp1a1), Cyp1a2, and Cyp1b1 promoters [9,11-14]. This phenomenon is also known as a phase I enzyme response to sequential activation of DMEs.

To summarize, DME can be classified into three phases: step-wise activation of phase I enzymes that oxidize xenobiotics or drugs, phase II enzymes that conjugate phase I products, and phase III enzymes that extrude or transport the metabolites out of the cells [15]. Upregulation of ROS can activate phase II enzymes that act as a master regulator responsible for the cellular antioxidant response, nuclear factor (erythroid-derived 2)-like 2 (Nrf2) [16]. When oxidative stress increases intra- or extracellularly, Nrf2 dissociates from Kelch-like ECH-associated protein 1 (Keap1) and shuttles into the nucleus to bind to small Maf protein family members (MafK, MafG, and MafF). By interacting with small Maf proteins, Nrf2 forms a transcriptionally active complex that binds to antioxidant response elements (AREs; 5′-G/ATGACNNNGC-3′) [17,18]. This, in turn, will activate the antioxidant response of phase II enzymes and maintain the homeostasis of ROS induced by the AhR–Arnt complex [19] (Fig. 1B).

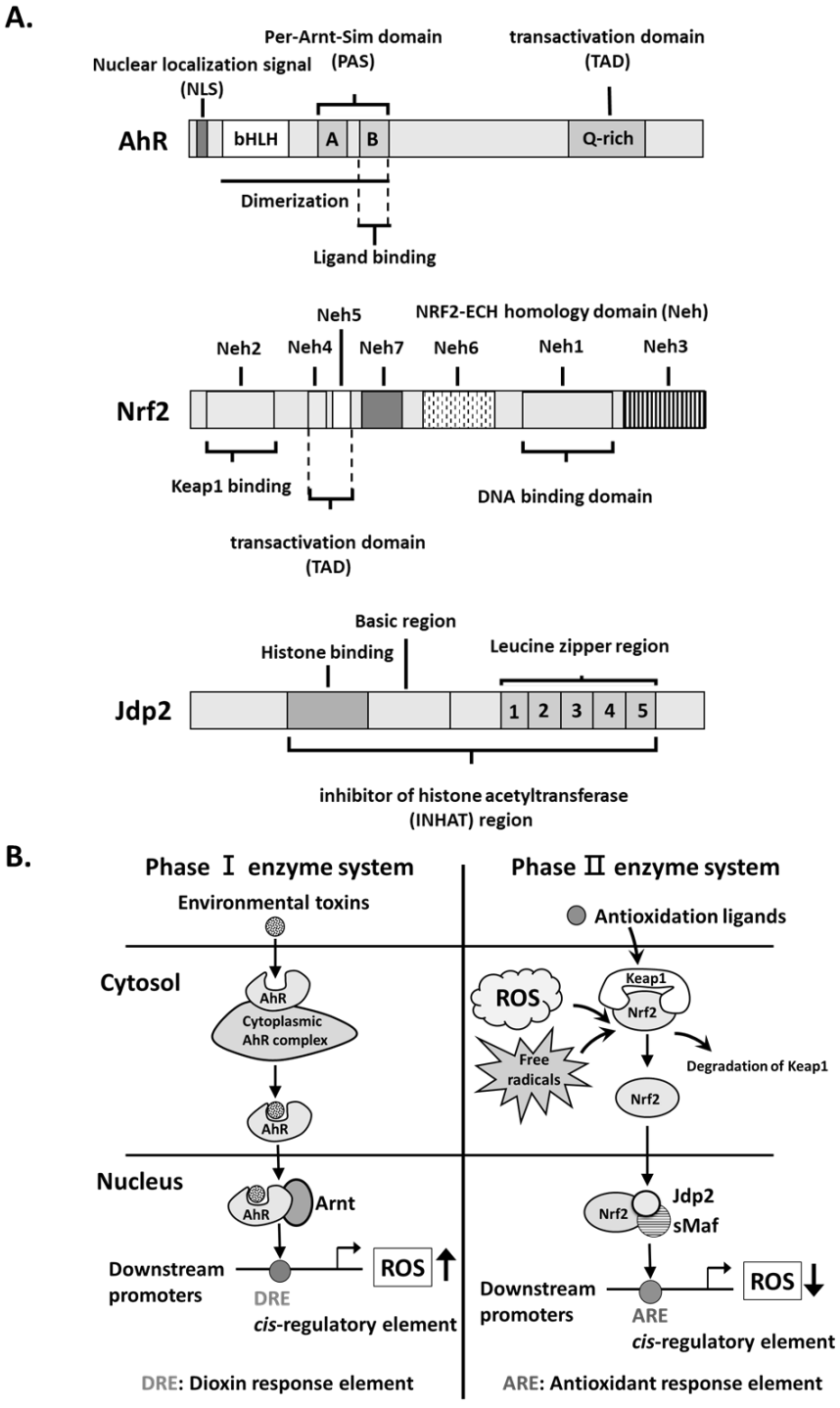

Fig. 1 Protein domains of AhR, Nrf2, Jdp2, and DME system. (**A)** The functional protein domains of AhR, Nrf2, and Jdp2. (**B**) Simplify cartoon description of DME system.

1.3 AhR–Nrf2 gene battery and the interaction of Jdp2

The concept of "AhR–Nrf2 gene battery" was first proposed by Yeager et al. [20]. The term is used to describe AhR and Nrf2 signaling crosstalk to control phase I- and phase II-related gene promoters. The AhR gene controls the phase I enzyme genes of the p450 families some examples are P4501a1 (Cyp1a1), Cyp1a2, Cyp1b1, and Cyp1b2. Nrf2 proteins regulate the expression of phase II enzymes, some examples are nicotinamide adenine dinucleotide phosphate (NAD(P)H) quinone oxidoreductase 1, heme oxygenase 1, and UGT1A10 [21,22]. These two signals exhibit their functions coordinately. Although AhR and Nrf2 signals are critical for maintaining ROS balance and cell homeostasis, the detail of each target regulation in phase I and phase II genes remains unclear. The balance between AhR detoxification and ROS maintenance is critically influenced by Nrf2 antioxidant pathway activation. One of the cofactors of the Nrf2 complex, Jun dimerization protein 2 (Jdp2), regulates ARE interaction and ROS homeostasis [23,24]. It has been well documented that Jdp2, one of the family member of activator protein 1 (AP-1) transcription factor, is responsible for transcription repression through various mechanisms involving DNA interactions, inactivation of AP-1 family member heterodimer, histone deacetylase recruitment to inhibit histone acetylation, and chromatin assembly regulation [25,26]. Besides its contribution to the Nrf2 antioxidant pathway, Jdp2 was also reported to be critical for AhR activation and modulation of ROS accumulation in mouse embryonic fibroblasts (MEFs) [27]. These researches suggest that Jdp2 may be a crucial modulator of phase I and phase II responses. Jdp2 signaling affecting cancer progression was described by Barvbarov et al. [28]. The deficiency of Jdp2 expression in JDP2$^{-/-}$ Lewis lung carcinoma (LLC) displayed a reduced rate of metastasis through the regulation of LLC chemokines. These researchers revealed the correlation of ROS response with tumor progression.

1.4 Cancer stem cells and acquisition of drug resistance

Cancer stem cells (CSCs) are characterized by their ability for self-renewal and extensive proliferation. Cancer progression of tumors relies on tissue organization, with CSCs at the top of the hierarchy [29]. CSCs were defined in hepatocellular carcinoma (HCC) by liver stem cell markers which were commonly used: CD44, CD90/THY-1, CD133/PROM-1, Sal-like protein 4, CD13, aldehyde dehydrogenase, CD117/c-kit, intercellular adhesion molecule 1, CD24, epithelial cell adhesion molecule (EpCAM),

and delta-like 1, and cytokeratin 19 [30,31]. In the tumor environment, elevated ROS was detected as an outcome of high metabolic activity and gene mutations [32]. The elevate level of ROS may contribute to the progression of cancer, while cancer-associated fibroblasts (CAFs) may actively facilitate tumor microenvironment homeostasis. The increased ROS level may promote the transformation of CAFs to become active through TGFβ signaling [33]. Regorafenib, one of the commonly used multi-kinase inhibitors serving as anticancer drugs for treating HCC, is also known to inhibit TGFβ signaling and induce ROS production [34]. Reports show that regorafenib can induce ROS-dependent apoptosis [35]. However, the clinical efficacy of regorafenib is rather limited even though this drug exerts its toxic effect on cancer cells and displays a potential clinical advantage in increasing survival rate [36]. A recent study has suggested that elevated forkhead box protein M1 (FOXM1) expression is correlated with a poor prognosis [37]. Inhibition of FOXM1, leads to inhibition of proliferation and migration and induction of cell death through apoptosis [35,38]. These observations suggest that studies of the underlying mechanism characterizing regorafenib are crucial for the future treatment of HCC.

1.5 The specific aim of this study

The regulation of redox balance is important for an organism to survive various challenges including environmental stress. The aim of this study was to characterize the AhR–Jdp2–Nrf2 gene battery and determine whether the retardation of ROS modulation through the AhR–Jdp2–Nrf2 gene battery is crucial for HCC survival benefit. In this study, the mechanism of AhR activation was investigated. Interactions between phase I and phase II detoxification reactions show that the role of Jdp2 is important for the modulation of the AhR and Nrf2 pathways. Furthermore, Jdp2 interacting with AhR and Nrf2 on *cis*-elements was detected during TCDD treatment, suggesting a complex formation that includes AhR and Nrf2. The formation of this complex indicates that AhR is involved in cross talk between phase II enzymes. Upregulation of FOXM1 in CSC demonstrated a gain of regorafenib resistance that was associated the increased acquisition of CSC features and the induction of epithelial–mesenchymal transition (EMT). This finding supports the notion that FOXM1 may be a therapeutic target that reverses drug resistance in HCC.

Chapter II AhR–Jdp2 axis controls ROS level in mouse embryonic fibroblasts through DMSO stimulation

This chapter is a modified version of the original work reported in Cell Biology of Toxicology (2021). The publisher Springer licensed the respective authors in accordance with the Creative Commons Attribution (CC-BY) 4.0 license, which has allowed me to use this paper as a part of my doctoral dissertation.

AhR, functioning as a protein possess of ligand-binding ability, it can respond to aromatic hydrocarbons in the environment and activates downstream transcription of detoxification phase I proteins through the binding of *cis*-element DREs when activated [4,7]. Dimethyl sulfide (DMSO), a commonly used organic solvent in oxidative stress research and also in the study of toxicology [39], penetrates the cell membrane by interacting with phospholipids and facilitates molecules to permeate the intracellular space [40]. DMSO displays a variety of characteristics including anti-inflammatory, vasodilatory, and bacteriostatic activities [41]. Despite its cytotoxicity and interference with cellular activities, DMSO is still an optimal solvent for biochemical experiments [42-45]. In this chapter, our results revealed that the activation of AhR expression was enhanced by dosing with low concentrations of DMSO. Activation required the regulation of the Ap-1 transcriptional regulator, Jdp2. In fact, Jdp2 positively regulates the promoters of ARE-dependent phase II genes [23,24], this protein is likely to serve as a bifunctional protein in AhR–Nrf2 responses, maintaining homeostasis of ROS and supporting apoptosis response in DMSO treatment.

2.1 Characterization of DMSO effect on mouse embryonic fibroblasts.

Normal mouse embryonic fibroblasts (MEFs) were prepared from mouse embryo between 14.5 and 15.5 gestation days; they formed the structure with a spindle shape as a typical structure of fibroblast when *in vitro* culture was performed. MEFs were used commonly as co-culture feeder layer in order to maintain pluripotent property for supporting the growth of target embryonic stem cells [46]. MEFs were known to be regulated by the activation of AhR in cellular structure, adhesion ability, and migration ability [47-51], and shown to be useful for determining gene function in studies; MEFs can also gathered from Jdp2 knockout (KO) mice, despite with Jdp2 gene knockout, the

mice showed no variable offspring [52]. In this chapter, MEFs were used to evaluate gene activity. As a commonly used organic solvent, DMSO at the concentration of 0.1% was examined for the effect on cell spreading, cytotoxicity, and ROS elevation levels.

2.1.1 Effect of DMSO treatment on spreading of cell and F-actin dynamic

The control dose for 0.1% DMSO was tested initially for cell spreading. From the result, more than 6.0-fold increase in fluorescence intensity of F-actin in wild type (WT) MEFs was detected when compared with the non-treatment control (Fig.2A, B). This result of F-actin spreading was not observed in the AhR-depleted MEFs (Fig.2B); the finding was consistent with the previous report [53]. Phosphorylated MLC2 at the site of serine 19 (pMLC2) was identified to be critical for the remodeling process of actin stress fiber [54]. Notably, pMLC2 fluorescence signal intensity increased more than 3-fold when compared with that of non-DMSO treatment as control in WT MEFs. This result was also not observed in the AhR-depleted MEFs (Fig.2C). In order to observe the effect of cytokinesis actin remodeling in the treatment of 0.1% DMSO, western blot was performed and protein expressions of pMLC and MLC were normalized by dividing β-actin after WT MEFs were exposed to 0.1% DMSO for 2 h. The analysis demonstrated the expression of pMLC2/MLC/β-actin in the treatment of DMSO was 1.4-fold higher than without DMSO treatment (Fig.2D, E).

These results shown 0.1% DMSO can induce MEFs cell spreading and flatten out the structure. To further assess the impact of DMSO, we inspect the changes of cytotoxicity and proliferation to different concentrations by using WT MEFs.

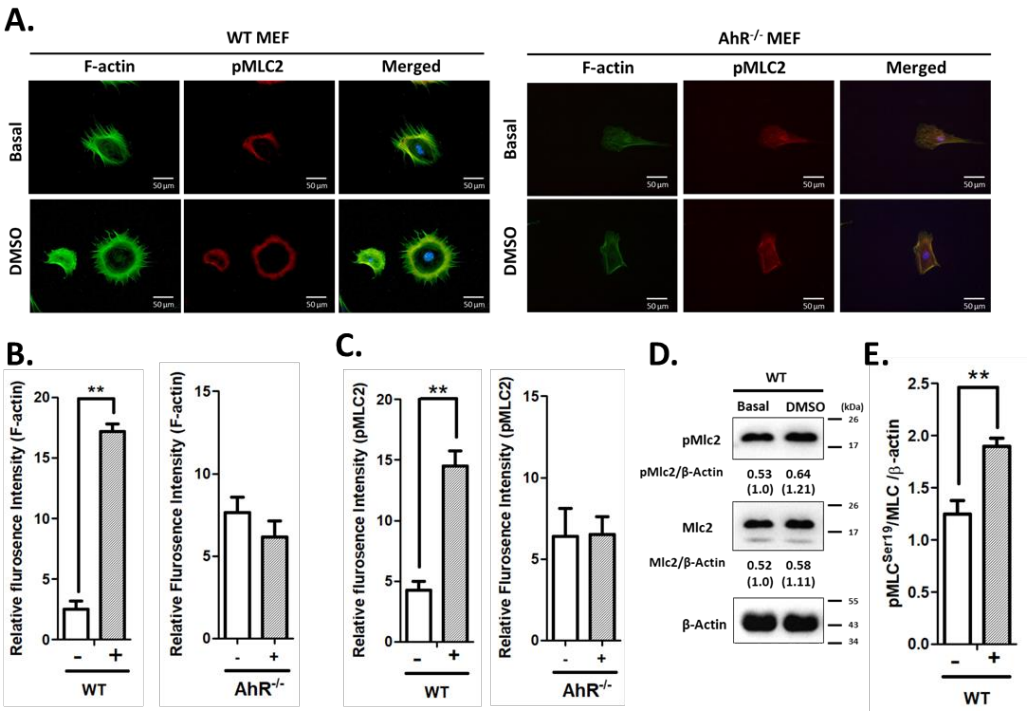

Fig. 2 DMSO exposure effects actin stress fibers extension and cell structure spreading in MEFs. (**A**) 0.1% DMSO were treated for 2 h, MEFs were labeled with phosphorylated myosin light chain and F-actin. Nuclei were labeled with DAPI, as indicated with colors of three fluorescence merged. (**B**) F-actin fibers signal quantifications. *AhR*$^{-/-}$ and WT MEFs with or without the treatment of 0.1% DMSO for 2 h. Results were shown as mean ± SEM (n = 5), $^{**}P < 0.01$. (**C**) pMLC2 signals quantification. *AhR*$^{-/-}$ and WT MEFs with or without the treatment of 0.1% DMSO for 2 h. Results were shown as mean ± SEM (n = 5), ** $P < 0.01$. (**D**) Mlc2 and pMlc2 representative expressions. (**E**) MEFs collected after 2 h with the treatment of 0.1% DMSO were quantified. Results were shown as mean ± SEM (n = 5). Above statistical analyses were conducted by using student's t-test (** $P < 0.01$). Dimethyl sulfoxide stimulates the AhR-Jdp2 axis to control ROS accumulation in mouse embryonic fibroblasts © 2023 by Wuputra K is licensed under CC BY 4.0.

2.1.2 Proliferation and cytotoxicity effect of DMSO

By exposing MEFs to different concentrations of DMSO ranging from 0.01% to 10%, cytotoxicity, apoptosis and necrosis were being investigated (Fig. 3A, B, C). As 0.1% of DMSO were commonly used as concentration for control solvent, we observed metabolic process were maintained more than 85% (Fig. 3A). Significant increase of necrosis and apoptosis was also detected at the concentration of 0.1% DMSO (Fig. 3B, C). The induction of apoptosis may be a result of Fas-Fas ligand-caspase 8 dependent pathway [55]. The protein level of FAS, FAS-L, caspase 3, caspase 8, and Bax were detected (Fig.3D). These data indicated DMSO at the concentration of 0.1% can reduce metabolic activity and cell proliferation, in addition to inducing cytotoxicity. Thus, further investigation of DMSO exposure is examined.

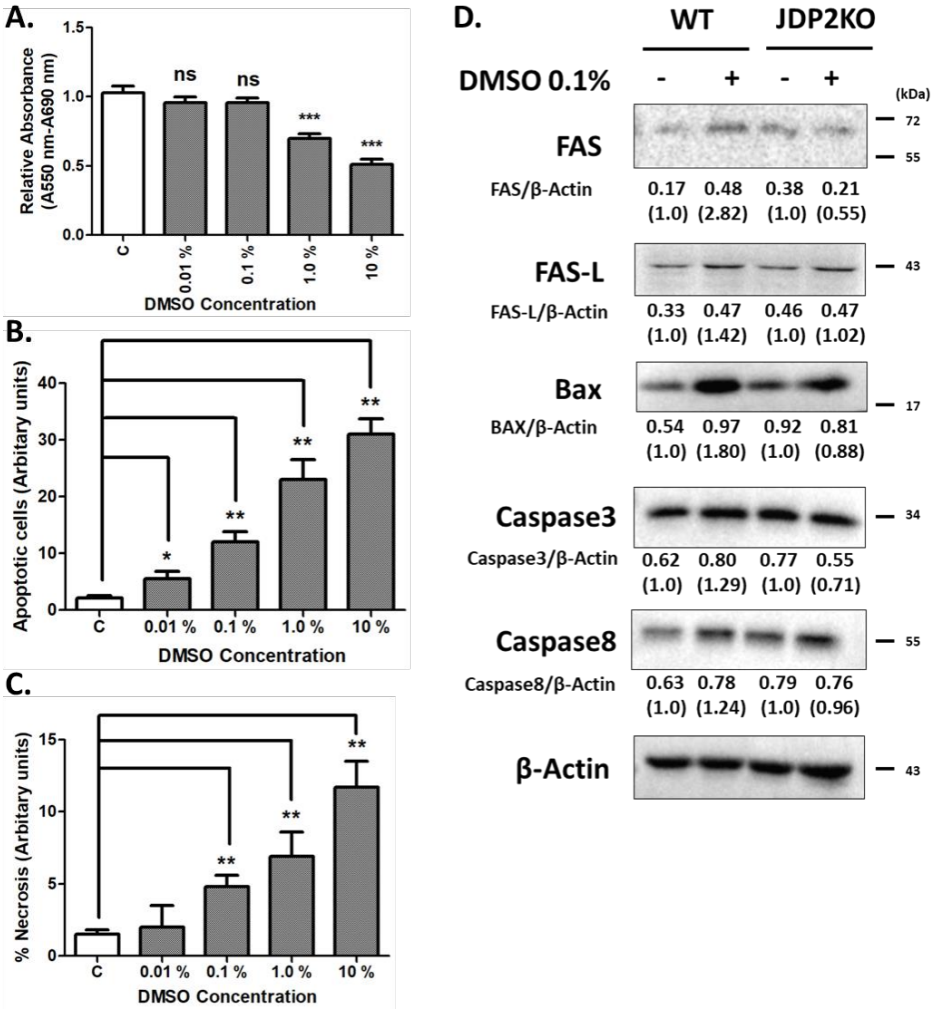

Fig. 3 Effect of DMSO concentration on the activity of NAD(P)H-dependent cellular oxidoreductase in 3-(4,5-dimethylthiazol-2-yl)-2,5-diphenyltetrazolium bromide (MTT) assay, necrosis, and apoptosis in WT MEFs . (**A**) Effect of 0%, 0.01%, 0.1%, 1.0%, and 10% DMSO on relative absorbance (A_{550} nm-A_{690} nm; NAD(P)H-dependent cellular oxidoreductase activity), (**B**) apoptosis, (**C**) necrosis. The signal of WT MEFs 100% activity to DMSO exposure free was set as shown in (**A**), and 1.0 (**B**, **C**). Results were shown as mean ± SEM (n = 5). Statistical analysis was calculated by using one-way ANOVA with Tukey's test (* $p< 0.01$, ** $p < 0.01$). (**D**) Expression of FAS/FAS-1 apoptosis related proteins in cell death signaling was detected in WT and *Jdp2*$^{-/-}$ MEFs with (+) or without (–) 0.1% DMSO; relative expression based on the beta-actin expression was shown in the parenthesis. Dimethyl sulfoxide stimulates the AhR-Jdp2 axis to control ROS accumulation in mouse embryonic fibroblasts © 2023 by Wuputra K is licensed under CC BY 4.0.

2.1.3 DMSO exposure effects AhR protein expression and ROS level

The effects of DMSO inducing apoptosis, necrosis, and metabolic activity were significant, and this suggested cellular oxidative stress was enhanced after MEFs exposed to DMSO. To understand the impact caused by DMSO, the level of ROS was being examined. Expose to 0.1%-10% DMSO can significantly increase ROS level (Fig.4A). 0.1% DMSO exposure in WT MEFs for 2 and 6 h showed 3.3-4.8-fold increase of AhR protein expression by compared with the control group, then a significant reduction of AhR expression was followed at 16 and 24 h (Fig. 4B). This result of AhR upregulation was not observed in *Jdp2*$^{-/-}$ MEFs in 2 and 6 h; the activation (1.9-fold) was delayed to 6 h after 0.1% DMSO exposure (Fig. 4B). Expression of AhR downstream genes were modulated by increasing ROS intracellular levels and AhR endogenous triggered by the detoxification phase I ligands as previous literature [18,56,57]. Higher ROS levels were observed in WT MEFs at the exposure of 2 h DMSO, in contrast *Jdp2*$^{-/-}$ MEFs showed insensitive response of ROS level (Fig. 4C, D).

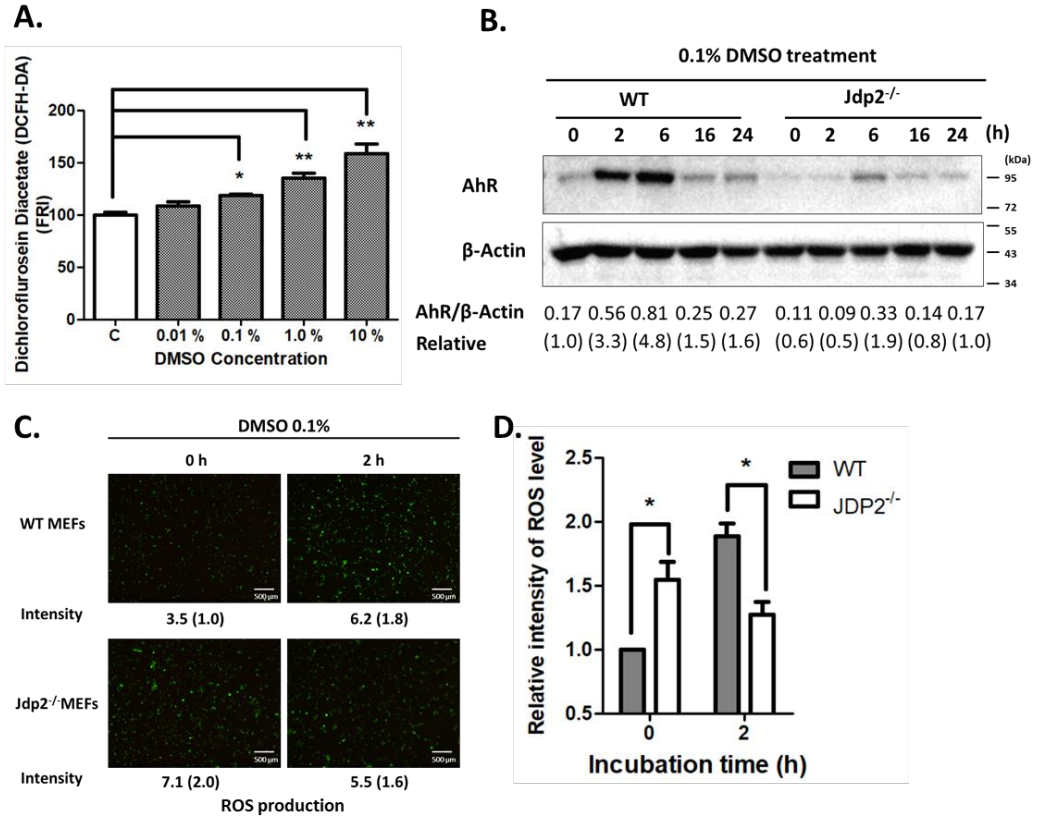

Fig. 4 Activity of WT MEFs ROS measured with the treatment of DMSO .

(**A**) 0%, 0.01%, 0.1%, 1.0%, and 10.0% of DMSO were cultured with MEFs for 2 h, labeled with 0.25 M CM-H2-DCFDA. Data collected from flow cytometry, presented as mean ± SEM (n = 5, triplicate experiments). Control incubation of ROS level without DMSO were set to 100 arbitrarily units. (* $P < 0.05$, ** $P < 0.01$). (**B**) AhR protein in WT and *Jdp2*$^{-/-}$ MEFs were compared after 0.1% DMSO incubation for indicated periods of time. (**C**) Activity of ROS measurements were compared between WT and *Jdp2*$^{-/-}$ MEFs with 2h treatment of 0.1% DMSO. CM-H2-DCFDA were used for the detection, representative results of ROS were shown. (**D**) CM-H2DCFDA detection of DMSO treatments. ImageJ were used to analyze ROS data. 0 h DMSO treatment WT MEFs was set as 1.0 value of fluorescence. Results were shown as mean ± SEM (n = 6). Statistical analysis calculated by using two-way ANOVA with *post hoc* Bonferroni analysis (*$P < 0.05$). Dimethyl sulfoxide stimulates the AhR-Jdp2 axis to control ROS accumulation in mouse embryonic fibroblasts © 2023 by Wuputra K is licensed under CC BY 4.0.

To further investigate this observation also found in other cells, 0.1% DMSO was added to NIH3T3 mouse fibroblast, diploid cells origin from human WI38, and human origin cells of hepatoblastoma HepG2. AhR protein expression level shown to increase after the treatment of 0.1% DMSO (Fig. 5A, B, C). Furthermore, the expression level of AhR downstream genes Cyp1a1 and Cyp1b1 were also being investigated in WT and *Jdp2*$^{-/-}$ MEFs. Cyp1a1 expression was enhanced (2-fold) exposed DMSO in WT MEFs (Fig. 4D), but this observation was not occurred in *Jdp2*$^{-/-}$ MEFs (data not shown).

Furthermore, TCDD (10nM) another phase I ligand was treated. AhR promoter also showed significant increase when compared with the control (Fig. 4E). Thus, TCDD effect on AhR was more pronounced than that of DMSO, and the increased AhR expression was higher in DMSO-treated condition when compared with control.

Taken these results together, deficiency of Jdp2 shows the potential to retard the effect of ROS levels when 2 h exposure to 0.1% DMSO was performed.

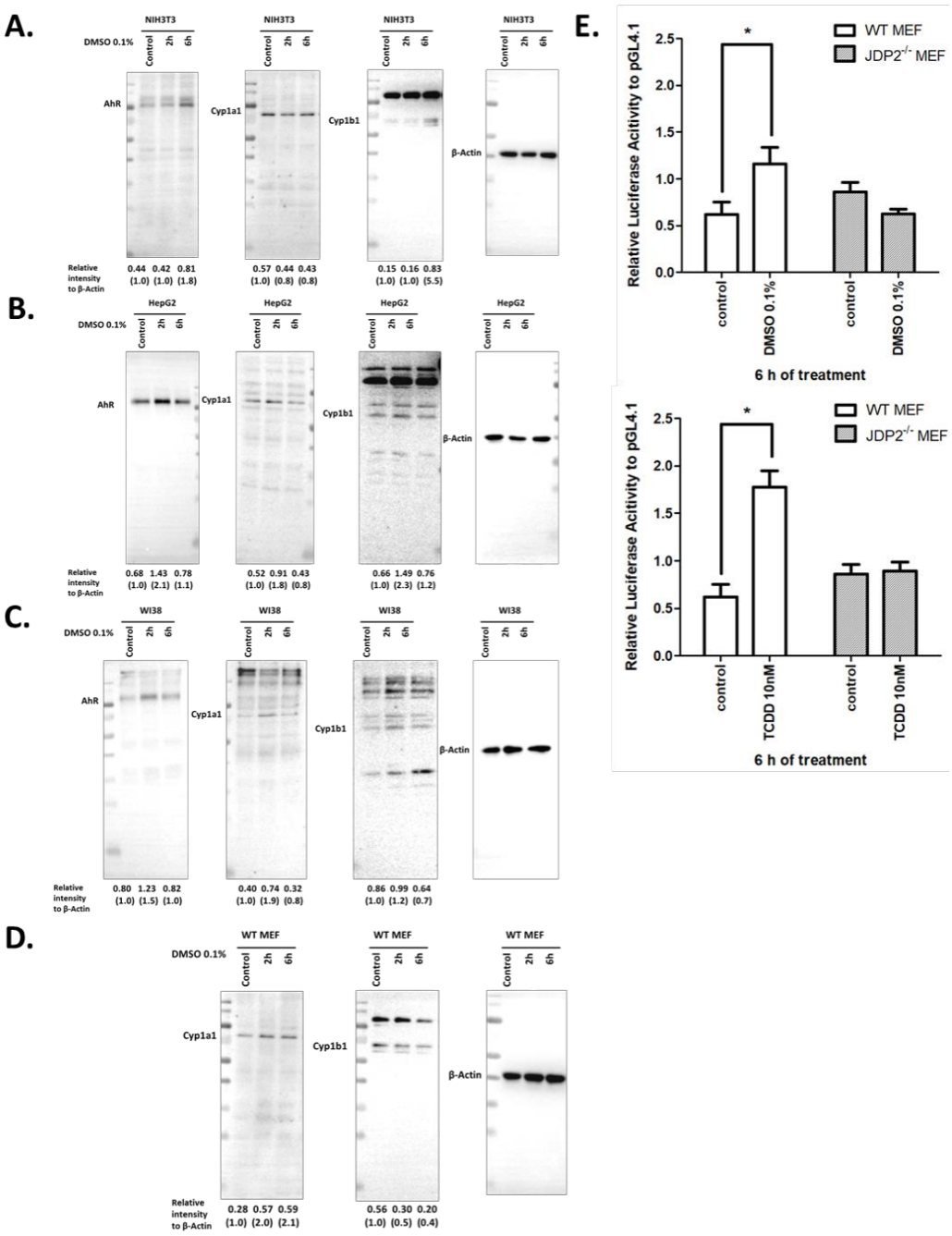

Fig. 5 Effect of 0.1% DMSO and TCDD on the expression of AhR, Cyp1a1, Cyp1b1. In mouse fibroblast cells–NIH3T3 (**A**), human hepatoblastoma cells-HepG2 (**B**) and human diploid lung fibroblast cells-WI38 (**C**) in the presence or absence of 0.1% DMSO. In MEFs (**D**), the expression levels of AhR target proteins Cyp1a1 and Cyp1b1 were shown and calculated based on the expression level of β-actin. The relative expression levels were shown in parentheses. (**E**) AhR-luciferase activities were quantified, activity relative to pGL*4*.1-*AhR*-luciferase were measured with 6 h

treatment of 10 nM TCDD (upper panel) or 0.1% DMSO (lower panel) in WT and *Jdp2*$^{-/-}$ MEFs. *AhR*-luciferase activity were analysis as the ratio over control pGL4.1. Results were shown as the mean ± SEM (n = 5, triplicate experiments). Statistical analysis was conducted by one-way ANOVA with *post hoc* Tukey's test (* $P < 0.01$, ** $P < 0.01$).

2.2 Transcription of *AhR* promoter and apoptosis event by Jdp2, AhR and Nrf2

From the result of previous studies, we examined the activity of AhR promoter. AhR promoter was being determined to contain three putative DRE elements and two putative ARE elements (Fig. 6A). Treatment of DMSO with concentration of 0.1% for 2 h, constructed promoter of *AhR* luciferase reporter (*pAhR-Luc*) observed activation in WT MEFs, but not activated in *Jdp2*$^{-/-}$ MEFs (Fig. 6B). Activity of AhR promoter induced by DMSO was observed gradually reduced at 14 h.

Both cis-elements DRE2 and DRE3 were critical for activation of *pAhR*-Luc since two of these *cis*-elements were shown to be significantly decreased (DRE2: 65%, and DRE3: 38%) in activity of *AhR* promoter when mutated in WT MEFs compared with the 0.1% DMSO in the absence of control (Fig. 6C). The 0.1% exposure of DMSO, mutation of DRE2 and DRE3 can result in the reduction activity of *AhR* promoter (Fig. 5E); this effect of mutation *DRE2 and DRE3 with th*e 0.1% treatment of DMSO was not observed in *Jdp2*$^{-/-}$ MEFs (Fig. 6D, F). Knockdown experiment of Arnt, AhR, Jdp2, and Nrf2 decreased the activity of AhR promoter with or without the DMSO of 0.1% treatment in WT MEFs (Fig. 6G).

Results of knockdown demonstrated AhR, Arnt, Nrf2, and Jdp2 can decrease ROS level (Fig.7 A, B) and apoptosis (Fig.7 E, F), but Ahrr and MafK showed no effect in 0.1% DMSO treatment of WT MEFs. Contrast to WT MEFs results, *Jdp2*$^{-/-}$ MEFs showed no significant effect of repression when introduced with mentioned siRNAs on the activity of *AhR* promoter, ROS level (Fig.7 C, D), and apoptosis [58]. Taken together, these findings suggested Jdp2, AhR-Arnt, and Nrf2 contributed to AhR promoter and regulated cell apoptosis, and ROS level.

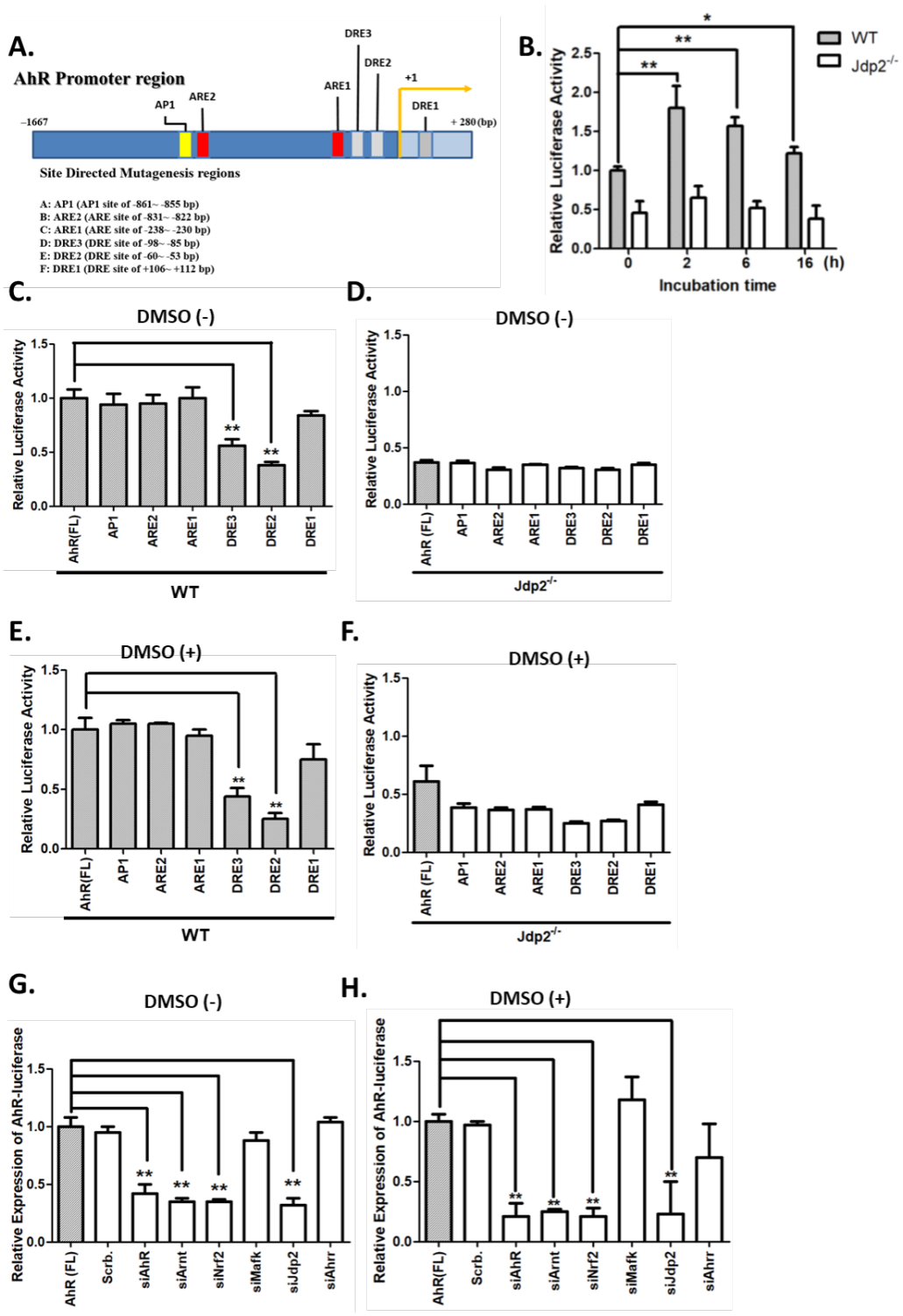

Fig. 6 The activity characterization of *AhR* promoter. (**A**) Illustration of mentioned DRE and ARE positions on promoter region of *AhR*. Individual *cis*-element was engineered to create the mutants of mentioned *cis*-elements, positions were shown from the transcription putative start site. (**B**) Treatment of 0.1% DMSO for 0, 2, 6, and 16 h

in WT MEFs and *Jdp2*$^{-/-}$ MEFs of pGL4.1-*AhR*-luciferase relative activity. *AhR*-luciferase activity ratio to the pGL4.1 control was analysis as relative activity of luciferase. Results were shown as mean ± SEM (n = 5, triplicate experiments). Statistical analysis was performed by two-way ANOVA with *post hoc* Bonferroni tests (* $P < 0.05$, ** $P < 0.01$). (**C-F**) Each *cis*-element mutation effects on the region of *AhR* promoter. Activity of luciferase in WT MEFs (**C**, **E**), *Jdp2*$^{-/-}$ MEFs (**D**, **F**) without the treatment (**C**, **D**) or with the 0.1% treatment of DMSO (**E, F)** was measured. Full length (FL) *AhR*-luciferase activity was arbitrarily set as 1.0. (**G**, **H**) Effect of transcription factors with siRNAs treatment in WT MEFs pGL4.1-*AhR*-luciferase activity with or without 0.1% DMSO. The activity of FL *AhR*-luciferase was set as 1.0 arbitrarily units. **(C-H)** Statistical analyses by one-way ANOVA with *post hoc* Tukey's test (** $P < 0.01$) shown as the mean ± SEM (n ≧ 3). Dimethyl sulfoxide stimulates the AhR-Jdp2 axis to control ROS accumulation in mouse embryonic fibroblasts

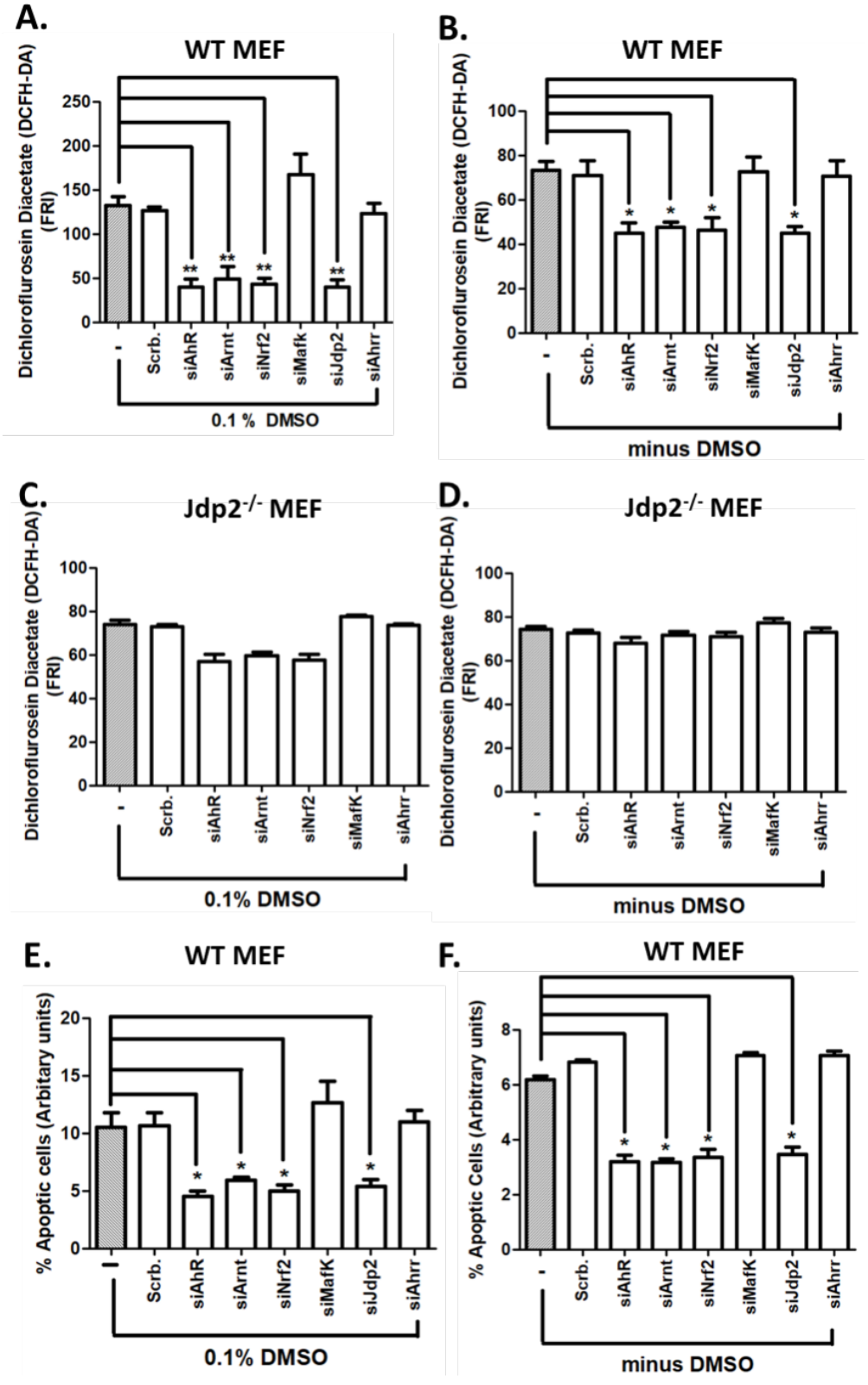
A.
WT MEF
Dichloroflurosein Diacetate (DCFH-DA) (FRI)
250
200
150
100
50
0
-
Scrb.
siAhR
siArnt
siNrf2
siMafk
siJdp2
siAhrr
0.1 % DMSO
B.
WT MEF
Dichloroflurosein Diacetate (DCFH-DA) (FRI)
100
80
60
40
20
0
-
Scrb.
siAhR
siArnt
siNrf2
siMafK
siJdp2
siAhrr
minus DMSO
C.
Jdp2-/- MEF
Dichloroflurosein Diacetate (DCFH-DA) (FRI)
100
80
60
40
20
0
-
Scrb.
siAhR
siArnt
siNrf2
siMafK
siAhrr
0.1% DMSO
D.
Jdp2-/- MEF
Dichloroflurosein Diacetate (DCFH-DA) (FRI)
100
80
60
40
20
0
-
Scrb.
siAhR
siArnt
siNrf2
siMafK
siAhrr
minus DMSO
E.
WT MEF
% Apoptic cells (Arbitary units)
20
15
10
5
0
-
Scrb.
siAhR
siArnt
siNrf2
siMafK
siJdp2
siAhrr
0.1% DMSO
F.
WT MEF
% Apoptic Cells (Arbitrary units)
8
6
4
2
0
-
Scrb.
siAhR
siArnt
siNrf2
siMafK
siJdp2
siAhrr
minus DMSO

Fig. 7 Regulation of apoptotic activity and ROS production in WT and *Jdp2*$^{-/-}$ MEFs. Treatment of siRNAs targets Arnt, AhR, Nrf2, Jdp2, MafK, and Ahrr in WT MEFs (**A**, **B**) and *Jdp2*$^{-/-}$ MEFs (**C**, **D**) with or without 0.1% DMSO exposure. Cells were labeled with 0.25 M CM-H2DCFDA and detected by FACs (* $P < 0.05$, ** $P < 0.01$). (**E**, **F**) The siRNA targets mentioned transcription factors, on the activity of apoptosis in WT MEFs with (**E**) or without (**F**) the treatment of 0.1% DMSO. All above results were shown as the mean ± SEM (n = 3, in triplicate), and statistical analysis by one-way ANOVA with *post hoc* Tukey's test (* $P < 0.05$, ** $P < 0.01$). Dimethyl sulfoxide stimulates the AhR-Jdp2 axis to control ROS accumulation in mouse embryonic fibroblasts © 2023 by Wuputra K is licensed under CC BY 4.0.

2.3 AhR promoter recruit Jdp2 and trans factors to the DRE and ARE sites

In order to clarify the identified *trans* acting factors (Arnt, AhR, MafK, Jdp2, and Nrf2) the interaction with the *AhR* promoter *cis*-elements (DRE and ARE), the chromatin immunoprecipitation (ChIP)-qPCR assays were performed. Four pairs primers were designed to identify the mentioned *trans* acting factors recruitment interacting with AhR promoter (Fig. 8A). From the observation of WT MEFs 0.1% treatment with 2 h DMSO, ARE1, ARE2, and the DRE1 sites did not possess function (Fig. 7B-D). In contrast, the recruitment of Nrf2, Jdp2, Arnt, and AhR were detected on DRE2/3 sites (Fig. 8E), it is crucial for activity induced by DMSO on *AhR* promoter. None of the results was observed in *Jdp2*$^{-/-}$ MEFs, transcription factors mentioned earlier were not recruited to the AhR promoter DRE and ARE locations (Fig. 8F-I).

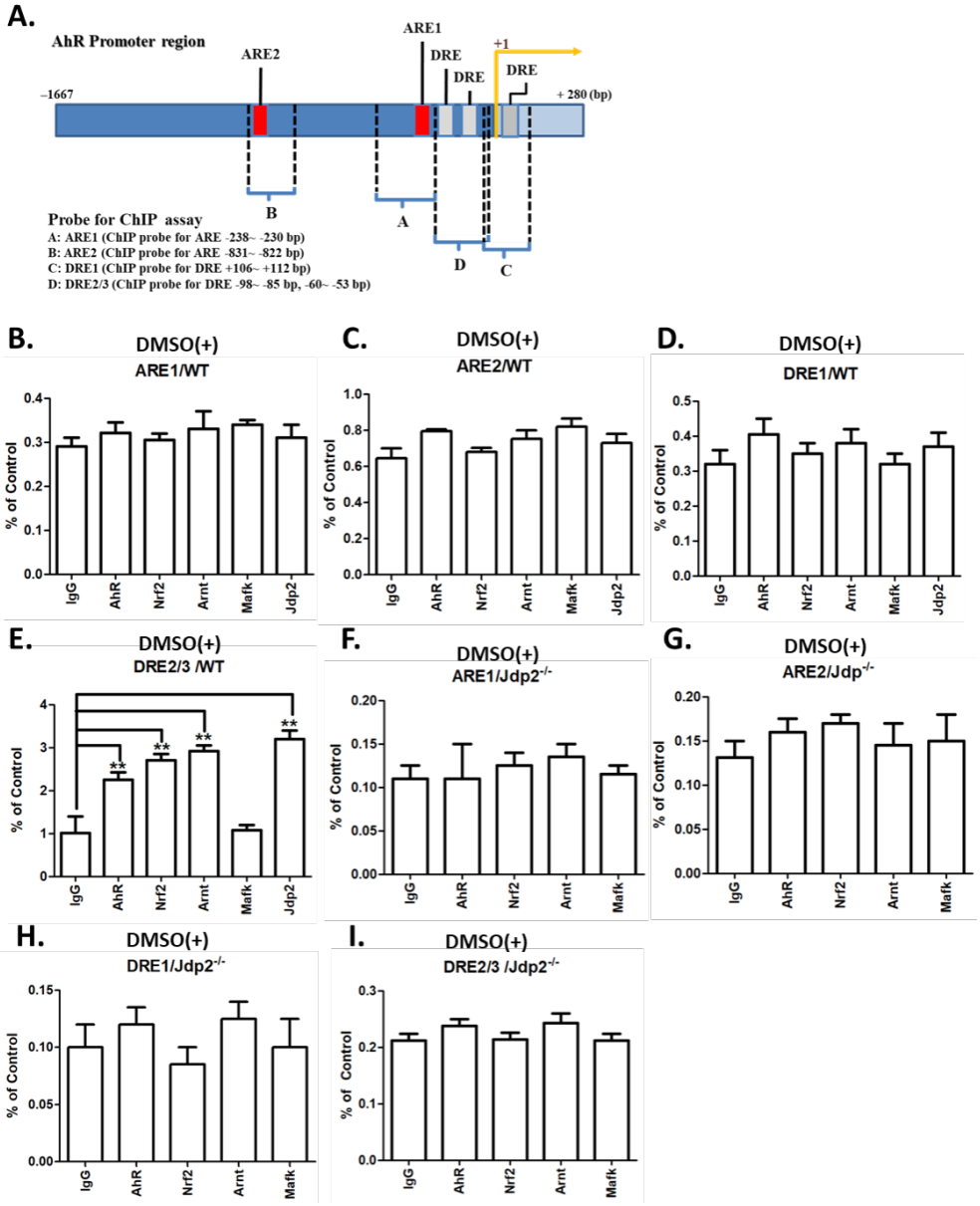

Fig. 8 Recruitments of transcription factors binding to DRE and ARE sites in WT MEF differs from *Jdp2*$^{-/-}$ MEFs. (**A**) Illustration for the position of *cis*-elements in mouse *AhR* promoter for ChIP assay. (**A–D**; **F-H**) Specific primers (ARE2, ARE1 and DRE1) were used to detect regions amplified by qPCR (**E**, **I**) and the primer pairs that detects *cis*-elements DRE 2 and 3 were shown. Results are shown with or without the treatment of 0.1% DMSO, as mean ± SEM (n = 5). Statistical analysis was done by using one-way ANOVA with *post hoc* Tukey's test (** $P < 0.01$). Dimethyl sulfoxide stimulates the AhR-Jdp2 axis to control ROS accumulation in mouse embryonic fibroblasts © 2023 by Wuputra K is licensed under CC BY 4.0.

2.3.1 AhR-luciferase activity was affected through DRE2 and DRE3 by Jdp2, MafK, and Nrf2 in *Jdp2*$^{-/-}$ MEFs

According to previous results, Nrf2, MafK, and Jdp2 play important roles on AhR promoter modulation through interacting with DRE3 and DRE2 *cis*-elements, these properties were further examined. Overexpression protein of Jdp2 (Fig. 9A) or Nrf2 (Fig. 9B) shown significant elevated activity of *AhR* promoter in *Jdp2*$^{-/-}$ MEFs with the presence of DMSO. By contrast, no signs of AhR promoter activation in the sites of mutation DRE2 and DRE3 were detected through Jdp2 overexpression (Fig. 9A) or Nrf2 overexpression (Fig. 9B). However, the expression of ectopic MafK reduced activity of AhR promoter, which mutation of DRE3 and DRE2 showed no response (Fig. 9C).

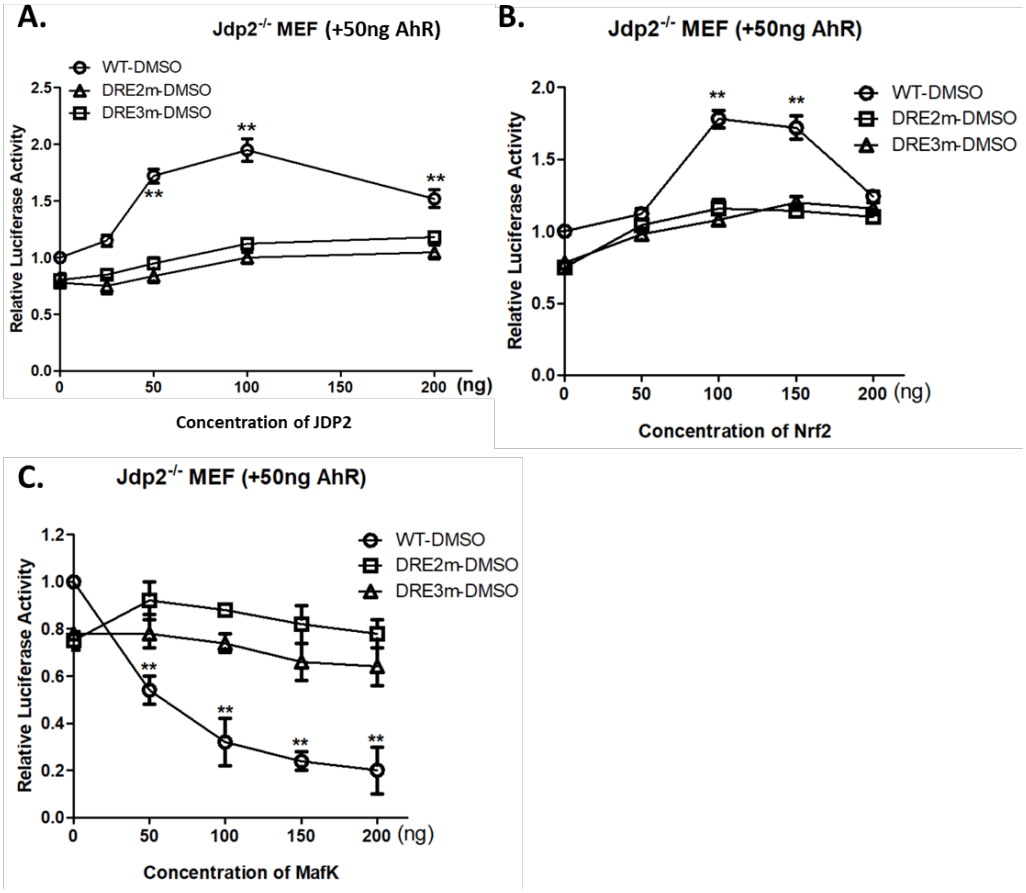

Fig. 9 DRE2 and DRE3 activation of AhR-luciferase in *Jdp2*$^{-/-}$ MEFs.

The reporter activity was detected by using mutant of DRE2 luciferase, AhR-luciferase, and mutant of DRE3 luciferase reporter (50 ng), with 0–200 ng of *pcDNA-Jdp2* (**A**), *pcDNA-Nrf2* (**B**), *pcDNA-MafK* (**C**) transfected into *Jdp2*$^{-/-}$ MEFs. Statistical analysis

by two-way ANOVA with *post hoc* Bonferroni tests (* $P < 0.05$, ** $P < 0.01$). Dimethyl sulfoxide stimulates the AhR-Jdp2 axis to control ROS accumulation in mouse embryonic fibroblasts © 2023 by Wuputra K is licensed under CC BY 4.0.

2.3.2 Jdp2 association with Nrf2 and AhR *in vitro*

In order to clarify the interaction potential between mentioned *trans* factors, the AhR interactions with Nrf2 or Jdp2 was investigated by western blotting and coimmunoprecipitation assays. Judging from the result, by using anti-AhR antibody in the nucleus Nrf2 was being coimmunoprecipitated in both WT and *Jdp2*$^{-/-}$ MEFs (Fig. 10A). The detected levels of AhR–Arnt and AhR–Nrf2 complexes in *Jdp2*$^{-/-}$ MEFs were 5- to 7-fold lower than those in WT MEFs. Anti-Jdp2 antibody was able to coprecipitate Nrf2 and AhR proteins (Fig. 10B). The AhR–Jdp2 colocalization was observed by immunofluorescence staining (Fig. 10G). AhR and Jdp2 colocalization was detected, regardless the treatment of DMSO. Furthermore, the signals of Ahr and Arnt colocalization was detected as a control (Fig. 10H). This colocalization was also observed in the presence of 0.1% DMSO (data not shown). Moreover, AhR protein was enhanced in the nuclear localization by treatment of 2 h to TCDD or 0.1% DMSO (data not shown).

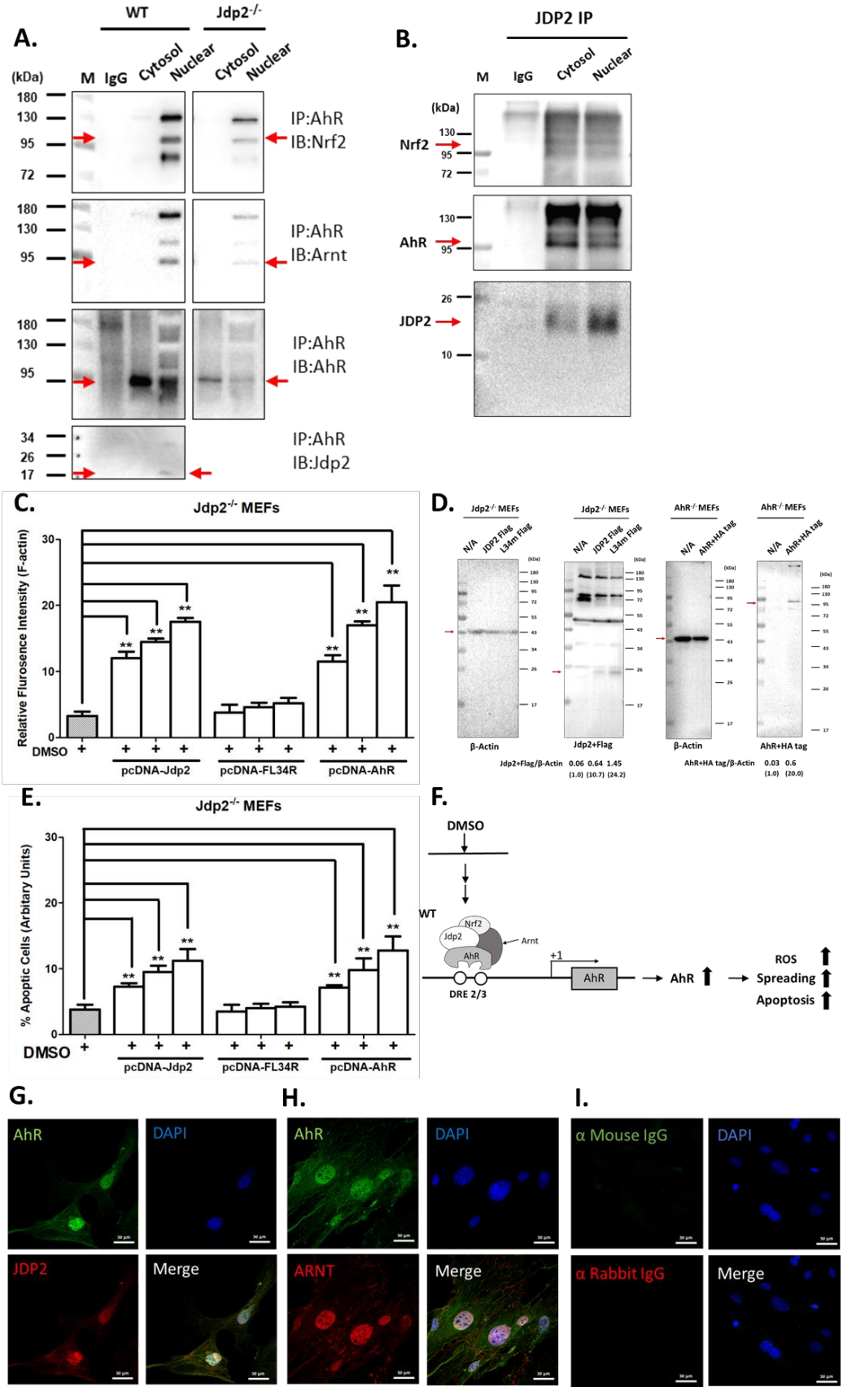
A.
WT
Jdp2-/-
(kDa)
M IgG Cytosol Nuclear Cytosol Nuclear
180
130
95
72
IP:AhR
IB:Nrf2
IP:AhR
IB:Arnt
IP:AhR
IB:AhR
34
26
17
IP:AhR
IB:Jdp2
B.
JDP2 IP
M IgG Cytosol Nuclear
(kDa)
Nrf2
AhR
JDP2
26
10
C.
Jdp2-/- MEFs
Relative Flurosence Intensity (F-actin)
DMSO
pcDNA-Jdp2
pcDNA-FL34R
pcDNA-AhR
D.
Jdp2-/- MEFs
Jdp2-/- MEFs
AhR-/- MEFs
AhR-/- MEFs
N/A
JDP2 Flag
L34m Flag
AhR+HA tag
β-Actin
Jdp2+Flag
Jdp2+Flag/β-Actin 0.06 0.64 1.45
(1.0) (10.7) (24.2)
AhR+HA tag
AhR+HA tag/β-Actin 0.03 0.6
(1.0) (20.0)
E.
Jdp2-/- MEFs
% Apoptic Cells (Arbitary Units)
DMSO
pcDNA-Jdp2
pcDNA-FL34R
pcDNA-AhR
F.
DMSO
WT
Nrf2
Jdp2
AhR
Arnt
+1
AhR
DRE 2/3
AhR
ROS
Spreading
Apoptosis
G.
AhR
DAPI
JDP2
Merge
H.
AhR
DAPI
ARNT
Merge
I.
α Mouse IgG
DAPI
α Rabbit IgG
Merge

Fig. 10 Rescue of *JdP2*$^{-/-}$ MEFs require Jdp2 interaction in nuclei with AhR and Nrf2.

(**A**) Cytosolic and nuclear fractions of cell lysate (300 μg) immunoprecipitated from WT and *Jdp2*$^{-/-}$ MEFs with antibodies to detect bounded proteins by western blotting. IgG indicated the control. (**B**) Cytosolic and nuclear fractions of cell lysate (300 μg) from WT MEFs were immunoprecipitated with antibody against Jdp2 and target proteins. (**C**) Spreading of cell structure elevated by DMSO through overexpression of Jdp2 were rescued. 2 h treatment of DMSO-induced spreading of cell structure (**C**) and cell apoptosis (**E**) Demonstrated doses of mentioned plasmids were treated in *Jdp2*$^{-/-}$ MEFs. The signals of fluorescence in *Jdp2*$^{-/-}$ MEFs in the absence of DMSO treatment was set as 1.0. Results were shown as the mean ± SEM (n = 5; ** $P < 0.01$). (**D**) Overexpressed plasmid detected by western blots of tagged proteins Jdp2 and AhR. (**F**) Schematic figure of *AhR* activation through DMSO-induced the complex of AhR, Nrf2, and Jdp2 to upregulate ROS production, apoptosis, and cell spreading in WT MEFs. In the other hand, *Jdp2*$^{-/-}$ MEFs only recruited a small amount of AhR-Arnt complex to the *cis*-elements DRE2 and DRE3 of the *AhR* promoter. (**G**) JDP2 and AhR colocalization. WT MEFs were labeled with rabbit anti-Jdp2 (Santa Cruz Biotechnology) and anti-AhR (Clone A-3; Santa Cruz Biotechnology) antibodies. (**H**) AhR with Arnt colocalization. MEFs were labeled with mouse anti-AhR antibody (GeneTex) and rabbit anti-mouse Arnt (GeneTex). (**I**) Immunostaining with normal mouse IgG with anti-mouse 488. Scale bars, 30 μm.

2.3.3 Reduction of cell spreading and Jdp2-mediated apoptosis by Jdp2 deficiency can be rescued by AhR

Expression of AhR and deficiency of Jdp2 effects the response of cell to 0.1% DMSO in the result of apoptosis and spreading of cell structure. Fluorescence of F-actin intensity and the expression of pMLC2 were measured to observe spreading activity by was reduced in *Jdp2*$^{-/-}$ MEFs compared to WT MEFs, in the presence or absence of 0.1% DMSO (Fig.11).

To investigate the rescue effect of AhR in *Jdp2*$^{-/-}$ MEFs, AhR and Jdp2 overexpression was performed, the enhanced of cell spreading activity was observed in *Jdp2*$^{-/-}$ MEFs (Fig. 10C, D). As expected, the activity of cell spreading was not increased by the overexpression of Jdp2 mutant Jdp2FL34R, which did not possess the ability to bind on the AP1/ATF *cis*-regulatory elements [59] and DRE *cis* regulatory elements *in vitro* (Fig. 11E). Likewise, the overexpression of Jdp2, AhR, and DMSO treatment increased apoptosis in a dose dependent pattern; nonetheless, Jdp2FL34R shown no reduction of apoptotic activity induced by DMSO (Fig. 10E). These results suggested the AhR protein was one of the downstream protein targets of Jdp2, and DMSO-induced apoptosis, and cell spreading were involved with Jdp-AhR axis.

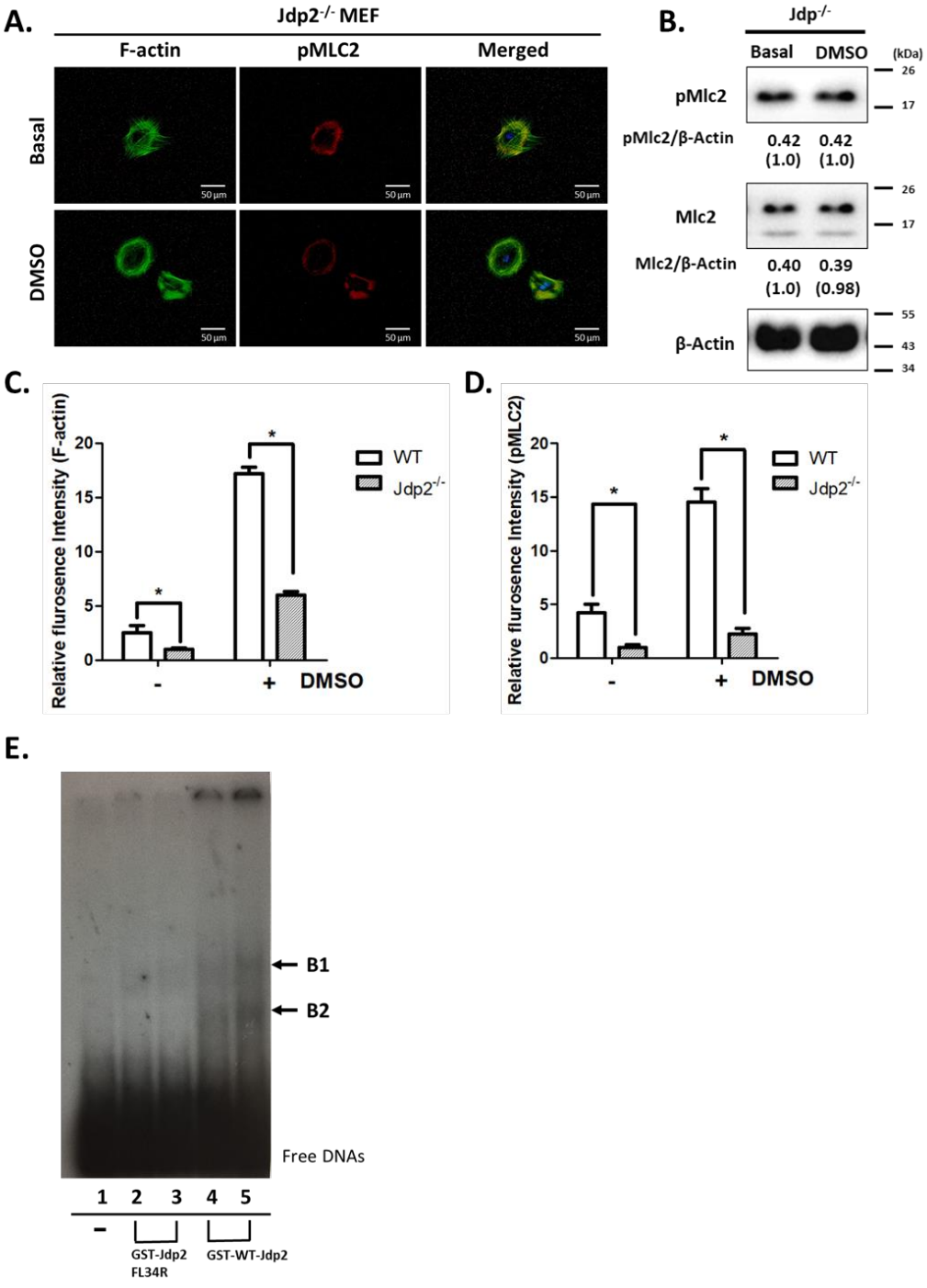

Fig. 11 DMSO exposure of WT and *Jdp2*$^{-/-}$ MEFs results in different extension of cell spreading .

(**A**) *Jdp2*$^{-/-}$ MEFs were starved for 24 h of low serum before treatment to 0.1% DMSO for 2 h, F-actin and phosphorylated myosin light chain (pMLC2) were stained. (**B**)Western blotting of pMLC2, and MLC2 in basal and 0.1% DMSO-treated 2 h

Jdp2$^{-/-}$ MEFs. (**C**) Quantification of F-actin staining results for cells harvested at 2 h after 0.1% DMSO treatment. (**D**) Quantification of signaling of phosphorylated myosin light chain. Data represent the mean ± SEM (n = 5), **P* < 0.05. Results were shown for cells harvested at 2 h treatment of 0.1% DMSO. (**E**) Electrophoretic mobility-shift assays (EMSAs) with in vitro recombinant GST-Jdp2 mutant and WT proteins. Interaction of Jdp2 and AhR *in vivo* and Jdp2 leucine zipper mutant did not interact with the DRE *cis*-element. Recombinant GST fusion proteins from WT GST-Jdp2 and mutant GST-Jdp2LZ3,4, were incubated with 0.1 pmol of mouse AhR oligodeoxynucleotide probes and 400 ng. Lane 1, no protein; lanes 2 and 3, 200 ng of Jdp2 LZ34; and lanes 5 and 6, 200 ng of WT Jdp2.

2.4 Materials and Methods

2.4.1 Animals, reagents, and cell culture

Animal welfare approved guidelines were followed in all of the experiments were proceeded. The animals care in laboratory followed by the Animal Care Committee of RIKEN Bioresource Research Center (BRC) in Japan, Kaohsiung Medical University, and National Laboratory Animal Center in Taiwan. The generation of *Jdp2*$^{-/-}$ mice strategy used was as described elsewhere [58,60]. MEFs were cultivated as primary culture in Dulbecco's modified Eagle's medium (Hyclone, high glucose; GE-Healthcare, Pittsburg, PA, USA), additives with fetal bovine serum 10% (FBS; Invitrogen, Grand Island, NY, USA), as described in previously literature [58,60]. NIH3T3, HepG2, WI38, and 293T were bought from RIKEN BRC (Tsukuba, Japan). DMSO was purchased from Sigma-Aldrich (St. Louis, MO, USA).

2.4.2 Construction of plasmids, and antibodies used

pcDNA-Jdp2, pcDNA-MafK, and *pcDNA-Nrf2* were purchased from RIKEN BRC (Tanigawa et al. 2013). *pQCXIN-CA-AhR-EGFP* was given as a gift from Dr. Y. F-Kuriyama, Tsukuba University (Tsukuba, Japan). DRE-luciferase was a gift from Dr. Y. H. Cheng, (China Medical University, Taiwan [61]) and ARE-luciferase (*pGL4-hQR25*-firefly luciferase) was obtained as shown in literature [24]. All the antibodies used in this study are listed in **Material Table 1**.

2.4.3 Luciferase reporter assay and cell transfection

MEFs were cultivated in 24-well plates (4×10^5 cells) for 24 h, then co-transfected with 10 ng of pRL-CMV plasmid (encoding *Renilla* luciferase) and 500 ng of AhR-luciferase plasmid using polyethylenimine (PEI; linear, MW25,000, cat. no. 23966; Polysciences, Warrington, PA, USA) or Lipofectamine 2000 (Invitrogen). Overexpression studies cells were co-transfected with pcDNA3 plasmid backbone encoding MafK, Nrf2, Jdp2, or AhR. DNA was prepared at the amount of 1 μg/well with fillers of pBluescript plasmid for transfection. DMSO treatment for the transfected cells were as the indicated time and cells were collected at 48 h after the transfection. GloMax20/20 Luminometer were used to determine the luciferase activity, using a dual-luciferase reporter assay by following its protocol (Promega, Madison, WA, USA). Relative luciferase activity (*Firefly* luciferase/*Renilla* luciferase) was analyzed and

compared with induction over the empty vector in wild-type (WT) MEFs. Data were obtained in triplicate, values are demonstrated as means ± standard error of the mean (SEM) at least three independent experiments.

2.4.4 Immunocytochemistry

Cells of MEFs were fixed for 10 min with 4% formaldehyde, then washed twice with 4°C phosphate-buffered saline (PBS). Fixed MEFs were incubated in a blocking solution consisted of 10% FBS and 0.1% Triton X-100 in PBS for 15 min to block the nonspecific interactions, primary antibodies were incubated for overnight incubation with the fixed MEFs. After the incubation cells were washed twice with 4°C PBS-T, then cells were treated with specific secondary antibodies for 90 min, followed by nuclei staining through using 4′,6′-diamino-2-phenylindole (DAPI) (1:3000; 5 mg/mL in DMSO; Merck, Darmstadt, Germany). Using ProLong Gold antifade mounting medium (Molecular Probes, P36034; Thermo Fisher Scientific) cells were mounted on slides, and immunofluorescence was detected by using Olympus FV1000 confocal laser scanning microscope (Olympus, Tokyo, Japan).

2.4.5 Immunoprecipitation, SDS–polyacrylamide gel electrophoresis (SDS–PAGE), and western blotting

The experiments of immunoprecipitation, SDS–PAGE, and western blot assays were carried out as mentioned in previous literature [24,58]. In general, 500 ×*g* for 5 min at 4°C were used to separate cell lysates into nucleic and cytosolic fraction, by stepwise separation and preparation of cytoplasmic and nuclear extracts (NE-PER; 78833; Thermo Fisher Scientific). Fractionated cell lysates are loaded into 10% SDS–PAGE and transferred to Immobilon-P polyvinylidene difluoride (PVDF) membranes (0.45 μm IPVH00010; Merck) for 100 V (fixed) 1 h at 10°C using a blotting equivalent Mini Trans-blot transfer system (Bio-Rad Laboratories, Hercules, CA, USA). Membranes of PVDF were then incubated with primary and secondary antibodies listed (**Material Table 1**). ChemiDoc XRS Plus detection system (Bio-Rad) were used to obtain the results. Protein A/G beads immunoprecipitation was conducted by coated with specific antibodies [24,58] for detection.

2.4.6 Chromatin immunoprecipitation

Cells of MEFs were collected in room temperature, fixed 8 min in 1% formaldehyde in PBS. Glycine (0.125M) was added to deblock the cross-linking, incubated 5 min at room temperature. 4℃ of cool PBS with protease inhibitors were used to harvest the cells, and three times washed at 4℃, with 5 min each of 120 rpm rotation. Cells were then collected and lysed with 750 μL of SDS lysis buffer (50 nM Tris-HCl pH 8.0, 10 mM EDTA, and 1% SDS) with proteinase inhibitors by pipetting the pellet, then incubation 30 min on ice. Lysate of the were then sonicated by sonicator Sonics VC50 instrument as condition: 10 min of 10 s on/10 s off on ice, to shear DNA into 350 bp average length. The primary antibodies (4 μg) or an IgG control were used to incubate overnight. Protein A/G-agarose beads (1:1; Millipore, Billerica, MA, USA) were precleared before blended into samples, mixture of beads and samples were rotated for 2 h at 4℃. Target bounded beads were then cleaned by following buffers: low-NaCl buffer (20 mM Tris-HCl, pH 8.0, 0.1% SDS, 0.1% TritonX-100, 150 mM NaCl, 2mM EDTA); high-NaCl buffer (20 mM Tris-HCl, pH 8.0, 0.1% SDS, 0.1% TritonX-100, 500 mM NaCl, 2mM EDTA); Washing buffer (100 mM Tris-HCl, pH 9.0, 1% NP-40, 0.5 M LiCl, and 1% deoxycholic acid); and Tris-EDTA buffer (10 mM Tris-HCl pH 8.0, and 1 mM EDTA). Samples were disassociated from beads then reverse cross-linked by using 0.3 M NaCl at 65℃ of incubation overnight. DNA were released by the treatment of proteinase K, phenol/chloroform/isoamyl alcohol (25:24:1) was used to isolate DNA fragments. Data were obtained by using real-time PCR assay. The antibodies used in the study were listed as below: anti-Nrf2 (1:1000, sc-722), anti-Arnt (1:1000, NB100-124), anti-AhR (1:1000, sc-8088), anti-MafK (1:2000, ab229766), anti-Jdp2 (1:500, from Dr. Aronheim), and IgG (1:1000, C15400001015). The primer pairs used to detect each fragment are listed in **Material Table 2**.

2.4.7 AhR promoter plasmids and site-directed mutagenesis plasmid construction

The promoter region of AhR was cloned from C57BL/6J *Mus musculus* strain in chromosome 12 (GRCm38.p4 C57BL/6J 35535598 to 35536615) using a KAPA HiFi PCR kit (Kapa Biosystem, Roche Sequencing Solutions, Pleasanton, CA, USA) with the primers listed: 5′–ATAGGTACCGGATCCCCTCTTCTCCTTCT–3′, 5′–ATACTCGAGGCTGCTCATGGTG–3′, added *Kpn*I or *Xho*I at the 5′ end for the purpose of insertion. Total length of 1947 bp promoter region of AhR were cloned into

the pGL4.1 plasmid back bone (Promega). To confirmed the construction, restriction endonuclease analysis and new generation sequencing were used, to confirm the orientation and location of the region of DNA fragment. Binding sites were predicted using ALGGEN-PROMO (http://alggen.lsi.upc.edu) on the AhR promoter region. Individual sites of the AhR promoter region were changed by using Quick Change Lightning Site-Directed Mutagenesis Kits (Agilent Technologies, Santa Clara, CA, USA) as listed in **Material Table 3.**

2.4.8 Expression suppression by small interfering RNA- and short hairpin RNA-mediated gene knockdown

Lentiviruses against mouse Nrf2, AhR, MafK, GFP, Jdp2, and Arnt recombinant short hairpin RNA (shRNA)were obtained from the small interfering RNA (siRNA) Core Center of Academia Sinica (Taipei, Taiwan). ON-TARGETplus SMARTpool siRNAs against mouse Nrf2, AhR, MafK, Ahrr, and ARNT were predesigned with a control scrambled siRNA were purchased from GE Dharmacon (Austin, TX, USA). Either siRNA or control RNA 20-40 nM in 0.5 mL of 6-well (Western blotting) or 0.2 mL of 24-well (Luciferase) were transfected into MEFs by OPTI-MEM (Invitrogen) and Lipofectamine RNAiMAX (Invitrogen). On condition of shRNAs, multiplicity of infection of 10 were infected into MEFs. Cells were then collected after 24 h treatment, washed with fresh medium including 10% FBS, introduced into cells by indicated target luciferase constructs, and analyzed their luciferase activities. The efficiency of knockdown siRNAs and shRNAs were analyzed by collected cells at 48 h and 72 h after siRNA transfection and shRNA infection, respectively. Data were analyzed by immunoblotting and correlated assays. The siRNAs used are listed in **Material Table 4.**

2.4.9 Chloromethyl-2′,7′-dichlorofluorescein diacetate fluorescence detection of flow cytometry and ROS in target cells

Petri dishes of 3 cm with 0.1% gelatin-coated were used to culture MEFs. Cells were treated with 0.1% DMSO for the indicated time, warm Hank's balanced salts solution (HBSS: Gibco-Thermo Fisher Scientific) were used to wash the cells, then incubated with 5 μM chloromethyl-2′,7′-dichlorofluorescein diacetate (CM-H_2DCFDA; C-6827, Life Technologies) in the dark with complete growth medium for 10 min at

37℃. After the incubation, HBSS were used to wash the cells twice, then observed by a Nikon inverted fluorescence microscope. Several fields were captured for imaging data with a 10× objective lens and quantified the results by ImageJ (National Institutes of Health, Bethesda, MD, USA). WT MEFs basal value set as 1.0 for normalize.

2.4.10 Cellular accumulation of ROS analysis

Analysis was done by using the ROS-Glo H_2O_2 assay (Promega) for the level of cellular ROS. Antioxidants and H_2O_2 was treated for 2 h, then followed with twice HBSS wash, cells were then incubated for 20 min in the ROS-Glo detection solution. GloMax fluorometer (Promega) were used to detect fluorescence. In certain cases, net accumulation of intracellular ROS was measured using the dihydrorhodamine 123 (DHR 123; Molecular Probes, Eugene, OR, USA) oxidation product. DMSO were treated for 2 h, HBSS solution were used to wash the cells twice, and loaded with 10 mmol/l of H_2DCFDA or DHR 123 in a 5% CO_2 incubator kept at 37°C for 5-min. After the incubation cells were washed twice with HBSS (Gibco), then suspended in complete medium to examined under fluoresce microscope. The number of DCF-stained cells was measured in an area of 8.75 mm^2 as described [24].

2.4.11 MTT [3-(4,5-Dimethylthiazol-2-yl)-2,5-diphenyltetrazolium bromide] assay

MTT [3-(4,5 dimethyldiazol-2-yl)-2,5-diphenyltetrazolium bromide; Merck Promega] colorimetric assays were performed to determine DMSO effect on the MEFs viability. Density of 5000 cells/well were seeded into 96-well plates with 100 μL of 10% FBS included DMEM medium. Viability of cells was determined at 24 h of DMSO treatment with various concentrations with 10% MTT dye added to each well. Incubation of plates were done in 37℃ for 4 h, in order to allow generation of formazan crystals by enzymes of mitochondrial dehydrogenase in living cells from MTT. After the incubation crystals were washed twice with PBS, crystals were dissolved by adding DMSO. Solution of crystals were incubated in the dark for 10 min with gentle horizontal rotations, 550 nm (A550) and 690 nm (A690) absorbance were measured to detect the percentage of the viable cells.

2.4.12 Necrosis and apoptosis detection by flow cytometry assay

The staining of cells with annexin V (AnnV) and propidium iodine (PI) were

performed to measure the number of necrotic and apoptotic cells. After specific treatment, cells were detached by trypsin/EDTA incubation, washed twice with warm PBS, and resuspended in binding buffer of AnnV (BD Biosciences, Franklin Lakes, NJ, USA). 15 min of incubation were done with fluorescein isothiocyanate (FITC)-labeled AnnV and PI (Cat. No. 556547, BD Biosciences) added to cells. The quantification of $AnnV^+/PI^-$ and $AnnV^+/PI^+$ events/μL were done by using a Micro-Plus Flow cytometer (Apogee Flow, Hemel Hempstead, UK). By recording the AnnV positive cells percentage in at least 500 cells, the apoptotic index was determined. Combining the Annexin V-FITC and PI (ab14085; Abcam, Cambridge, UK) cell death was visualized, both dyes were treated in the dark for five minutes, followed by fixation, and stained with DAPI or 0.8 μg/mL Hoechst 33342. The necrotic and apoptotic cells percentage was quantified by flow cytometry.

2.4.13 Assessment of actin stress fibers and pMLC2 immunofluorescence staining with the cell area measurement

Glass cover slips precoated with 0.1% gelatin were seeded with MEFs, allowed the cells incubate for 2 h at 37°C in DMSO (0.1%) with complete medium. Cell were fixed by 4% formaldehyde for 30 min and treated with 0.2% TritonX/PBS for 15 min at room temperature to permeabilized. Cells were then blocked with 5% FBS in PBS for 10 min, washed twice with cool PBS, then labeled with anti-pMLC2 antibody (1:50, Cell Signaling Technology, Danvers, MA, USA) at 4℃ overnight. After the antibody incubation, cells were washed twice with cool PBS, incubated with Alexa Fluor-594 anti-goat secondary antibody (1:400; Invitrogen) 60 min at room temperature. The actin stress fibers were labeled by Alexa Fluor 488-labeled phalloidin (1:80; Invitrogen), and detected green fluorescence. Cell nuclei were labeled with blue fluorescence by using DAPI. Five fields per treatment was visualized by fluorescence and taken respective images by Nikon epifluorescence microscope (Nikon Instruments, Melville, NY, USA). Area and fluorescence intensity of cells were calculated using ImageJ software. DAPI signals was set at 1.0 to determine the relative intensity, which was then divided by the value of pMLC2 or phalloidin fluorescence to obtain the relative intensities.

2.4.14 Statistical analyses

All results were presented as the mean ± SEM. Statistical comparisons between

experimental treatments were demonstrated by using GraphPad Prism 5.0 (GraphPad Software, San Diego, CA, USA). One-way ANOVA followed by a Tukey *post hoc* test or a two-way ANOVA with a Bonferroni *post hoc* test were used for multiple comparisons. Unpaired, two-tailed Student *t* test was used for the control and treatment groups comparison. To determine the effect of each site-directed mutagenesis on the *AhR* promoter, paired, one-tailed Student *t* test was used. For analyses of cell areas, Mann–Whitney nonparametric median statistical test was used. All differences were estimated statistically significant at $P < 0.05$.

2.4.15 Material Tables

Table1. Antibodies used in this study

Antibody name	Company	Cat. No.	RRIDs
Arnt	Cell Signaling Technology	CST#5537	AB_10694232
HIF-1beta	Gene Tex	GTX128795	AB_2861418
AhR	Santa Cruz Biotechnology	SC-8088	AB_2223957
AhR	Santa Cruz Biotechnology	SC-133088	AB_2273721
Nrf2	Santa Cruz Biotechnology	SC-722	AB_2108502
Nrf2	Gene Tex	GTX103322	AB_1950993
Mafk (NF-E2p18)	Santa Cruz Biotechnology	SC-477	AB_2137821
Jdp2	A gift from Dr. A. Aronheim		
Jdp2	Santa Cruz Biotechnology	SC-517133	AB_2861419
Ahrr	Sigma-Aldrich	HpA019614	AB_1855109
β-actin	Santa Cruz Biotechnology	SC-47778	AB_2714189
FLAG-M2	Merck Millipore	F1804	AB_262044
MLC2	Cell Signaling Technology	CST#3672	AB_10692513
pMLC2	Cell Signaling Technology	CST#3671	AB_330248
GAPDH	Millipore	MAB374	AB_2107445
Phalloidin (=F-actin) Alexa-Fluor488-Phalloidin	Thermo Fisher Scientific	A12379	N/A
Normal Rabbit IgG	Cell Signaling	CST#2729	AB_1031062

	Technology		
Normal Mouse IgG	Merck Millipore	12-371	AB_145840
Anti-Rabbit IgG HRP	Cell Signaling Technology	CST#7074	AB_2099233
Anti-Mouse IgG HRP	Cell Signaling Technology	CST#7076	AB_330924
Anti-Goat IgG HRP	Santa Cruz Biotechnology	SC-2020	AB_631728
Alexa-Fluor ® 488 conjugated Goat anti-Mouse IgG	Thermo Fisher Scientific	A-11029	AB_138404
Alexa-Fluor® 488 conjugated Goat anti-Rabbit IgG	Thermo Fisher Scientific	A-11034	AB_2576217
Alexa-Fluor ® 594 conjugated Goat anti-Mouse IgG	Thermo Fisher Scientific	A-11032	AB_2534091
Alexa-Fluor ® 594 conjugated Goat anti-Rabbit IgG	Thermo Fisher Scientific	A-11037	AB_2534095

Table2. Primer sequence of Probes ARE1, ARE2, DRE1 and DRE2/3 in ChIP assay

Regions	**Primer sequences**	**Amplified size (bp)**
ARE1	Sense 5'-CCTGGTAAATCTTGATGTCTGGG-3' Antisense 5'-ATGACGCAGGACGTAGTGAC-3'	159
ARE2	Sense 5'- CAGAATTTCCACCTTTTCCCACA-3' Antisense 5'-AGGAAAGAACACAGGAGTGC-3'	223
DRE1	Sensei 5'- ACTGCGCGGGGTCG-3' Antisense 5'-GTCCACCAGTTCGTCCTCC-3'	139
DRE2/3	Sense 5'- GACGAACTGGTGGACGGA-3' Antisense 5'- GGAGAAACCCGCACGCTA-3'	145

Table3. ARE1, ARE2, DRE1, DRE2, and DRE3 mutation primers in AhR promoter

Site	Primer sequences for mutation cis-element
ARE1	5'- GGGAGTCACTACGTCCTCTTCCGCACCGTGCTGCGAAGAGGGTG-3'
ARE2	5'- TTCCACCTTTTCCCACAACAGTCCCTTCAAGAAAGATGGAACATC-3'
DRE1	5'- GGACCGGGCGCGGCGCTACATCGGGTTTCTCCTC-3'
DRE2	5'-CTCGGTGCCCCACTTCCACGGCGGAGAGGCTCAGC-3'
DRE3	5'- CGCGGCGGGCGGCACGTACACTGCCACCTCCCTTTGACGCTC-3'
AP-1	5'- CTTCCATCTGTTTTGTTCCCGTACACCAGAATTTCCACCTTTTC-3'

Table4. siRNAs used in this study

siRNA	Santa Cruz Co.	Other company
Control siRNA	SC-44234	
Negative control	#01 siRNA	Ambion ®. Thermo Fisher Scientific
AhR	SC-29658	
AhRR	SC-140918	
Nrf2	SC-37049	
Arnt	SC-29734	
Mafk	SC-38104	
Jdp2	SC-38018	

Chapter III Spatiotemporal transcription control of aryl hydrocarbon receptor by JDP2 and antioxidation complex in response to phase I ligand

From our previous research, we established that the AhR response to aromatic hydrocarbons requires the regulation of the AP-1 transcriptional regulator Jdp2 [27]. The expression of phase II enzymes for example, UDP-glucuronosyltransferases (UGTs) and glutathione S-transferases (GSTs) are known to be recruited to AREs (5′-G/ATGACNNNGC-3′) as AhR-dependent regulation. As a master regulator of antioxidation response, Nrf2 can recognize these cis-elements [16]. When exposed to oxidative stress, Nrf2 can disassociate from the Keap1 complex and shuttle into the nucleus, where it forms a transcriptional complex with members of the small Maf protein family (MafK, MafF, and MafG) to induce an ARE-dependent response [17,18,62,63]. This antioxidative response process induce by phase II enzymes activating that are responsible for the suppression of ROS production [18]. Both AhR and Nrf2 coordinated regulation of the detoxification pathway and were named "AhR–Nrf2 gene battery" [20,64,65].

The Nrf2 and AhR signaling pathways interaction is used for protection against environment toxic materials. The detoxification of AhR-dependent reaction is crucial to maintain the balance of ROS. Aerobic metabolism created ROS can result in inducing cell senescence, DNA damage, or cell death [20,66]. ROS generation can be reversed through antioxidation reactions including Nrf2 signaling, which is necessary for reducing ROS and maintaining ROS homeostasis [56,57]. The control of ROS regulated by AhR and Nrf2 against exogenous and endogenous toxicants provides an important cellular defense mechanism [67]. However, the mechanism that links these two signaling pathways with mediators controlling both detoxification phase I and phase II enzyme systems has not been determined.

3.1 TCDD response abolished through depletion of Cyp1b1 promoter activity by Jdp2 deficiency

TCDD, one of the ligands of AhR, is well known to induce the expression of Cyp1a1, and Cyp1b1 in human and mouse cells [68,69]. By using real-time PCR (qPCR) and western blotting analysis, target genes of AhR activation pathway as example *Cyp1b1* and *Cyp1a1* in wild type mouse embryonic fibroblasts (WT MEFs) and Jdp2-deleted mouse embryonic fibroblasts (*Jdp2*$^{-/-}$ MEFs) were examined (Fig. 12A, B). Although Cyp1a1 did not show significant difference between WT and *Jdp2*$^{-/-}$ MEFs, but we observed Cyp1b1 were significantly elevated in WT MEFs than that in *Jdp2*$^{-/-}$ MEFs.

In order to investigate if Jdp2 can affect the activation of an AhR endogenous target gene Cyp1b1 transcription, luciferase reporter assay on Cyp1b1 promoter was conducted on WT and *Jdp2*$^{-/-}$ MEFs. 16-fold higher activation of Cyp1b1 reporter was observed on avarage with the treatment of TCDD for 6 h in WT MEFs (Fig. 12C), the difference was observed until 24 h. Homogeneous pattern was detected after 6 h treatment of TCDD in *Jdp2*$^{-/-}$ MEFs, but the intensity was about 0.16 fold of WT MEFs (Fig. 12D). The *Cyp1b1* promoter activity was being measured maximal at 10-200 nM treatment of TCDD in WT MEFs. Here, we also observe the increased activity of *Cyp1b1* promoter in *Jdp2*$^{-/-}$ MEFs, but the intensity is only 50-60% of the counterpart in WT MEFs (Fig. 12E).

Intriguingly, compared with scrambled control, Nrf2 silencing also supressed TCDD induced activation of luciferase in *Cyp1b1* reporter. Moreover, knockdown of MafK elevated the activity of luciferase promoter in *Cyp1b1* reporter. These results suggested that MafK had a supression effect on the of *Cyp1b1* promoter activation in WT MEFs (Fig. 12F). In order to study the role of Jdp2, 50 ng of Jdp2 was provided to *Jdp2*$^{-/-}$ MEFs with the dosage of TCDD and significant activaton of *Cyp1b1* promoter was observed (Fig. 12G).

These *Jdp2*$^{-/-}$ MEFs experiments combined with knockdown of small interfering RNA (siRNA) suggested that Jdp2 and Nrf2 functioned as a complex binding on ARE *cis* element, this required AhR promoter activation; on the other hand, MafK depletion increased *AhR* promoter activition. These results agreed with the earlier report of Nrf2 regulating *AhR* transcription, and modulating downstream event of *AhR* signalling cascade including xenobolic metabolism gene *Cyp1b1* [19].

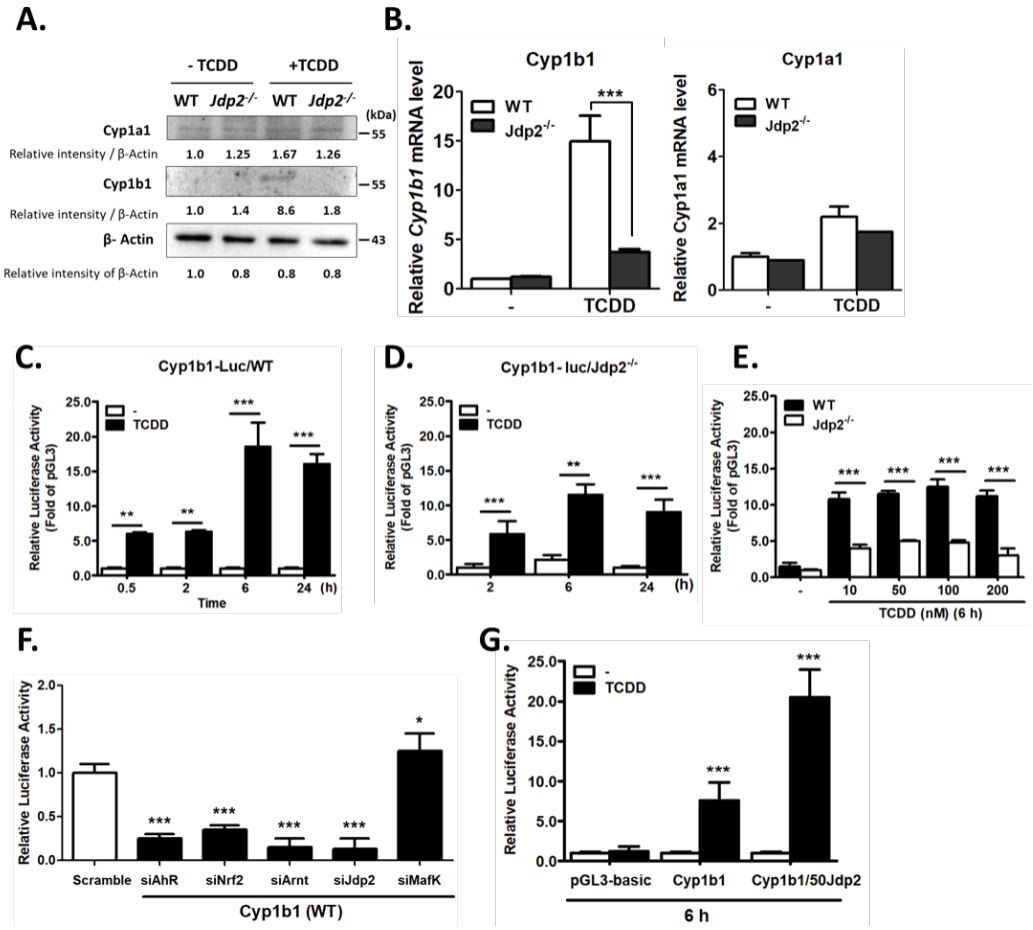

Fig. 12 *Cyp1b1* promoter luciferase activity in response to TCDD.

(**A**) Expression of Cyp1a1 and Cyp1b1 proteins in WT and *Jdp2*$^{-/-}$ MEFs with or without the treatment of TCDD. The relative expression ratio was calculated based on β-actin expression. The intensity of each event was measured, relative value was shown in ratio and normalized to β-Actin. (**B**) *Cyp1b1* and *Cyp1a1* mRNAs expression in WT and *Jdp2*$^{-/-}$ MEFs. The promoter activity is expressed as a relative value (fold) to the pGL3 basic vector (***p < 0.001). (**C, D**) Effects of time of TCDD exposure on promoter activity in WT (**C**) and *Jdp2*$^{-/-}$ MEFs (**D**) cells. *pGL3-CYP1B1* luciferase (0.5 μg) and *pRL-CMV-Renilla* (0.01 μg) plasmids were co-transfected into MEFs. (**E**) Luciferase plasmid-transfected MEFs were treated with different doses of TCDD or 0.1% DMSO for 6 h. (**F**) Effects of siRNA against *AhR*, *Nrf2*, *Arnt*, *Jdp2*, and *MafK,* and the scrambled control on *Cyp1b* promoter luciferase activity was examined. The value for the scrambled control was set at 1.0. (**G**) Jdp2 increased the *Cyp1b1* promoter luciferase activity with the treatment of 10 nM TCDD. The promoter activity was expressed as relative value (fold) to the *pGL3* basic vector. The above data are mean ±

SEM from four independent measurements, analyzed using two-way ANOVA with the Bonferroni *post hoc* test for multiple comparisons (*p < 0.05, **p < 0.01, ***p < 0.001).

3.2 AhR promoter activity was affected by the existence of Jdp2

Since the transcriptional regulation of *Cyp1b1* involved *Nrf2* and *Jdp2* regulations, we further examin the AhR expression in WT and *Jdp2*$^{-/-}$ MEFs (Fig. 13A). The protein of AhR expression was significantly elevated in WT MEFs than that in *Jdp2*$^{-/-}$ MEFs. This lowered AhR protein expression in *Jdp2*$^{-/-}$ MEFs can be rescued through gene forced expression of *Jdp2* protein position 139 alanine mutant or WT *Jdp2* (Fig. 13B). To clarify if Jdp2 is regulating the AhR expression, TCDD treatment on MEFs as stimulation of DRE binding by AhR [70]. Time dependent experiments of AhR expression shown upregulated pattern of AhR at 60 to 120 min in both WT and *Jdp2*$^{-/-}$ MEFs, with 2-fold higher expression of AhR in WT than *Jdp2*$^{-/-}$ MEFs with TCDD (Fig. 13C).

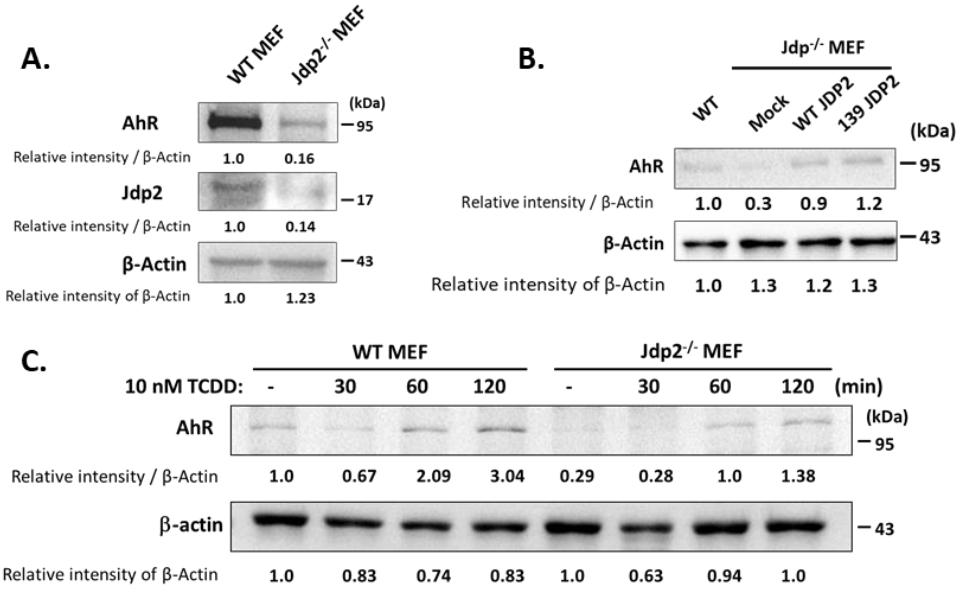

Fig. 13 Deletion of Jdp2 results in AhR expression and reduction of promoter activity. (**A**) The protein level of AhR expressed in WT was compared with *Jdp2*$^{-/-}$ MEFs. (**B**) The expression of AhR protein was rescued by transfection WT *Jdp2* into *Jdp2*$^{-/-}$ MEFs. Plasmid of139Jdp2 (C139AJdp2): alanine-mutated Jdp2 at position 139 [59], and WT Jdp2: wild-type Jdp2 were selected with G418 and harvested for the

examination of AhR expression. (**C**) Protein levels of AhR in WT was compared with *Jdp2*$^{-/-}$ MEFs treated with 10 nM TCDD for mentioned periods of time. The intensity of each band was then calculated, β-actin was divided for the relative value normalization. Jdp2 is a spatiotemporal transcriptional activator of the AhR via the Nrf2 gene battery

Using a proteasome inhibitor at the concentration of 10 μM MG132, changes of AhR expression were observed. At 120 min with treatment of TCDD the highest AhR protein expression of was observed in WT MEFs without the treatment of MG132, but in the presence of MG132 only 30-60 min was required to reach the maximum expression. Nevertheless, the level of AhR protein expression did not showed significant difference with or without the treatment of MG132 (Fig. 14A). By contrast, in *Jdp2*$^{-/-}$ MEFs, the AhR protein expression pattern and level (Fig. 13 C) was very similar in both with or without MG132 (Fig. 14B). These results suggested that the response to TCDD, the level of AhR protein was not notably affected by MG132 between WT and *Jdp2*$^{-/-}$ MEFs. Nevertheless, the AhR expression with or without TCDD treatment in the presence or absence of MG132 showed significant difference between WT and *Jdp2*$^{-/-}$ MEFs (Fig. 14B, C). These findings suggested Jdp2 did not change the AhR protein expression through protease degradation significantly. We further focused on the transcriptional changes of *AhR*.

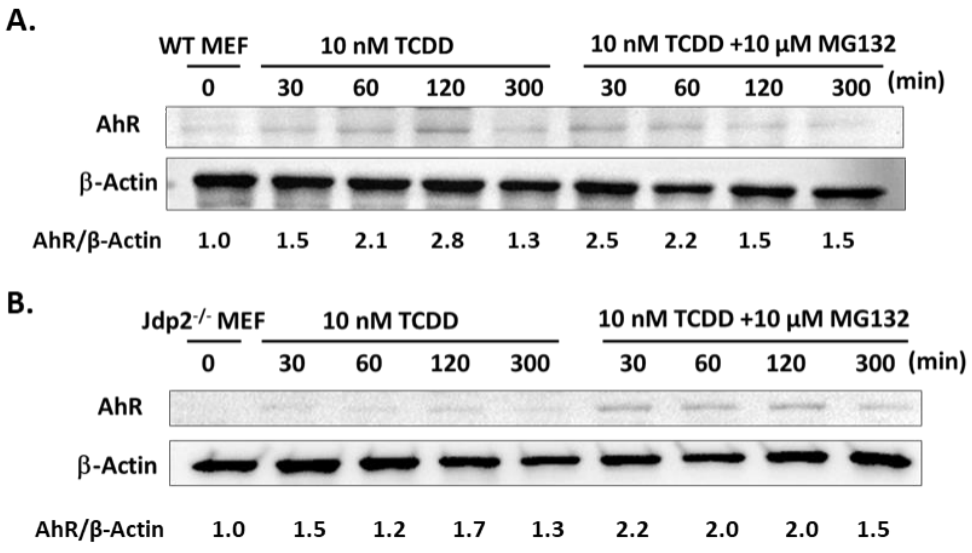

Fig. 14 The protein expression of AhR and characteristics of AhR expression effected by Jdp2. (**A, B**) Effects of MG132 on AhR expression affected by TCDD treatment in WT (**A**) and *Jdp2*$^{-/-}$ MEFs (**B**). The result in WT and *Jdp2*$^{-/-}$ MEFs was induced with TCDD at the concentration of 10 nM as mentioned periods of time with with or without 10 μM MG132. Expression of the AhR relative to that of β-actin was calculated. Jdp2 is a spatiotemporal transcriptional activator of the AhR via the Nrf2 gene battery

3.2.1 Exposure to TCDD effected the activity of AhR, ARE and DRE luciferase in a time dependent manner.

The region of promoter in AhR contained DRE and ARE sequences, and the activation of DRE and ARE luciferase activity stimulation by TCDD treatment response in WT and *Jdp2*$^{-/-}$ MEFs were examined. At the exposure of TCDD of 2–6 h, activity of DRE luciferase was 6-fold elevated in WT MEFs than that in *Jdp2*$^{-/-}$ MEFs (Fig. 15A). At TCDD exposure of 6-24 h, ARE luciferase activity was 5–6-fold elevated in *Jdp2*$^{-/-}$ MEFs than in WT MEFs (Fig. 15B). These results were consistent with previous studies [71,72].

Phase I metabolizing enzyme signaling response first, then followed by the phase II metabolizing enzyme; this is a portion of detoxification and antioxidation general response [71,72]. For DRE and ARE luciferease, *Jdp2*$^{-/-}$ MEFs had significant lesser activity than that in WT MEFs presence or absence of TCDD treatment. These findings suggested Jdp2 played an important role to elevate the activity of both systems (Fig. 15A, B).

To further investigate the modulation of transcriptional change in AhR, *AhR* promoter full-length construct (1947 base pairs) was used in later experiments to investigate the effect of elements DRE, ARE, and AP-1. The characterization of TCDD -induced AhR response , TCDD exposure with mentioned time effect of *AhR* pormoter activity was being evaluated (Fig. 15C, D). When WT and *Jdp2*$^{-/-}$ MEFs were treated with TCDD at 2-6 h, *AhR* promoter activity showed 2-fold difference and that lasted for 24 h of TCDD exposure. In summary, *AhR* promoter shown significantly higher activity inWT MEFs than that in *Jdp2*$^{-/-}$ MEFs.

We further study the effect of Jdp2 in activation of *AhR* promoter. Short hairpin

RNA (shRNA) –*Jdp2* target recombinant constructions were purchased from Merck & Co., Inc. (Darmstadt, Germany). Four segments out of five vectors showed reduction significantly in activity of AhR reporter (Fig. 15E). Moreover, pcDNA3–*Jdp2* overexpression in *Jdp2*$^{-/-}$ MEFs can result in elevation of *AhR* promoter activity and expression in the presence and absence of TCDD (Fig. 15F). From these findings, we concluded that *Jdp2* is crucial for inducing the activity of *AhR* promoter report.

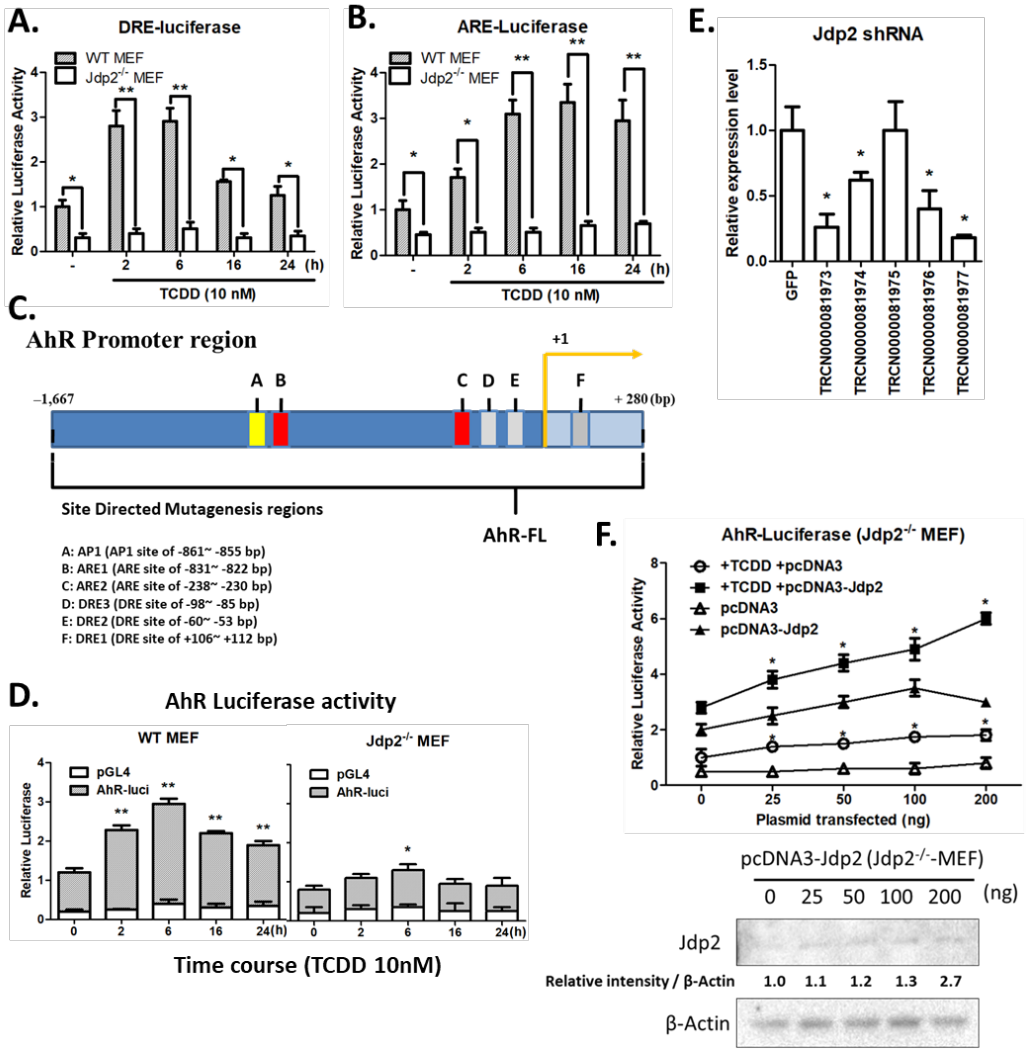

Fig. 15 The activity of *AhR* promoter properties and characterization of transcription factors.

(**A**) Relative luciferase activity of *DRE* promoter (**B**) *ARE* promoter in WT and *Jdp2*$^{-/-}$ MEFs in the treatment to 10 nM TCDD for the mentioned periods of time. WT MEFs luciferase activity at 0 h was set as 1.0. Results were shown as the mean ± SEM (n = 3). Results were calculated by one-way ANOVA with *post hoc* Tukey test (*$p < 0.05$;

$p < 0.01$). (C**) Illustration of each ARE and DRE positions in the region of *AhR* promoter regions mentioned were used to generate ARE and DRE mutants. (**D**) Activity in WT and *Jdp2*$^{-/-}$ MEFs of *pGL4.1-AhR* luciferase was treated with 10 nM TCDD for mentioned periods of time. (**E**) Effects of various constructions of shJdp2 on *Jdp2* mRNA expression were examined in WT MEFs. (**F**) Effects of increased dose of *pcDNA3-Jdp2* on *AhR* promoter luciferase activity with or without TCDD (10 nM) in *Jdp2*$^{-/-}$ MEFs. Expression of Jdp2 was examined by western blotting with anti-Jdp2 antibodies; β-actin was normalized to relative value and shown as ratio. Above data represent the mean ± SEM ($n = 5$) (*$p < 0.05$) as indicated by two-way ANOVA with the Bonferroni *post hoc* test for multiple comparisons. Jdp2 is a spatiotemporal transcriptional activator of the AhR via the Nrf2 gene battery

In order to investigate the activation of phase I ligands by AhR promoter, we performed an experiment using the phase I endogenous ligand kynurenine, and 6-formylindolo [3,2-*b*] carbazoleand benzo[*a*]pyrene (BaP). By dosing these phase I ligands, the activity of *AhR* promoter increased, but Jdp2 depleation repressed AhR promoter by 50 – 60% activity in *Jdp2*$^{-/-}$ MEFs than that in WT MEFs (Fig. 16A). These results were also confirmed in 293T and HeLa cells (data not shown).

To confirm the response of phase II ligands as examples, cinnamaldehyde, L-sulforphane, perillaldehyde, and *tert*-butylhydroquinone (tBHQ) [64,66,73-75] (Fig. 16 B-D) were dosed to WT and *Jdp2*$^{-/-}$ MEFs. Perillaldehyde was reporterd to induce Nrf2-related response without AhR activation [22], while AhR signaling was inhibited by cinnamaldehyde and promote antioxidative activity mediated by Nrf2 in human keratinocytes [76]. AhR promoter activity was not observed significantly induction in response to the majority of phase II reagents other than tBHQ treatment in WT MEFs (Fig. 16B-D). By contrast, *AhR* promoter activity increased significantly by treatment of phase II reagents in *Jdp2*$^{-/-}$ MEFs. Apparently, in WT MEFs Jdp2 functioned as a negative regulator of *AhR* promoter. Absence of Jdp2 resulted in increase of ROS production, which then stimulated *AhR* promoter activity; the observation was similar to previous report [24]. Our findings suggested that Jdp2 is crucial in AhR repression response subsequently stimulation reactions of Nrf2-dependent phase II enzymes.

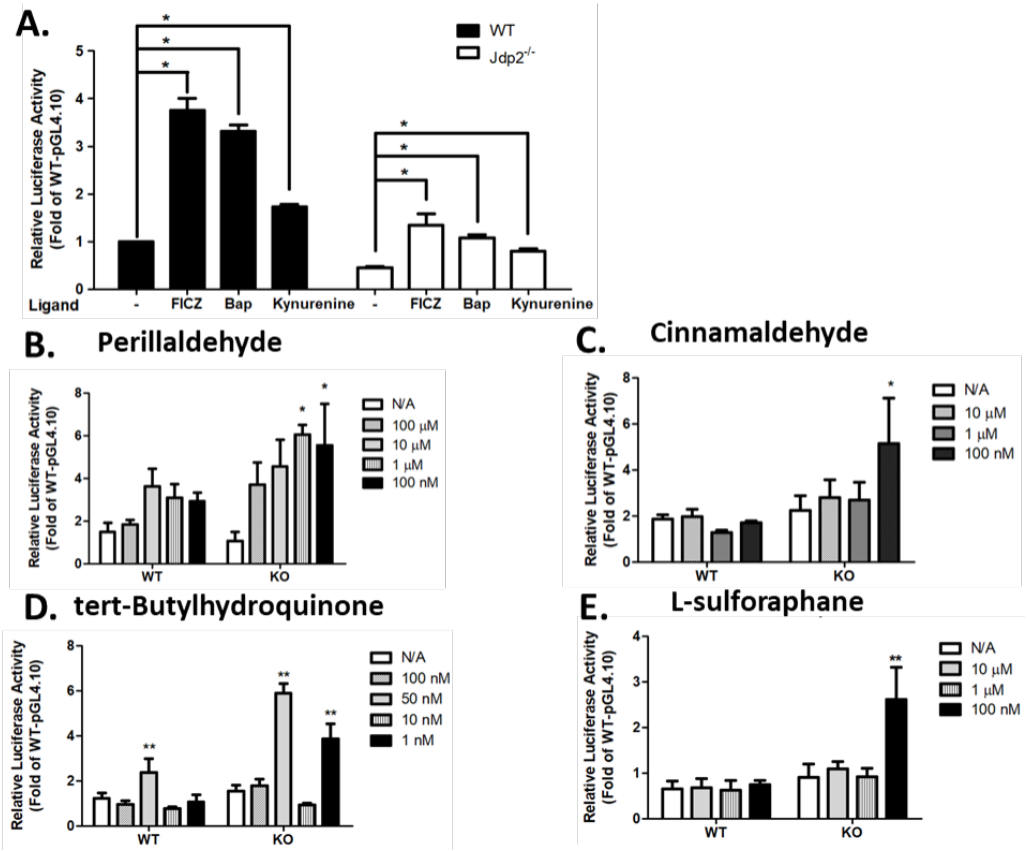

Fig. 16 Characteristics of phase I and phase II reagents response in activity of *AhR* promoter. (**A**) Effects of phase I reagents on luciferase activity of *AhR* promoter in WT and *Jdp2*$^{-/-}$ MEFs. Kynurenine, benzo[*a*]pyrene (BaP), and 6-Formylindolo[3,2-*b*]carbazole (FICZ) were added to WT and *Jdp2*$^{-/-}$ MEFs at a concentration of 100 nM for each, and the cells were incubated for 2 h and harvested for the luciferase assay of the *AhR* promoter (*p < 0.05). (**B-E**) Effects of phase II reagents in WT and *Jdp2*$^{-/-}$ MEFs. Cells were exposed for 2 h to perillaldehyde (**B**), cinnamaldehyde (**C**), tert-butylhydroquinone (**D**), or l-sulforaphane (**E**) at the indicated doses, and the *AhR* promoter luciferase activity was measured and expressed relative to the pGAL4.10 luciferase control (*p < 0.05, **p < 0.01). Jdp2 is a spatiotemporal transcriptional activator of the AhR via the Nrf2 gene battery

3.2.2 TCDD induced AhR promoter activaty require *cis*-Elements response

To inspect *cis*-elements role in *AhR* promoter inducing AhR upregulation by TCDD treatment, experiments of site-directed mutagenesis performed to each individual ARE and DRE sites in order to substitute *cis*-elements were conducted on *AhR* promoter by using irrelevant sequence of DNA (Fig. 15C). WT MEFs were dosed with TCDD after transfection for 2 h, 6 h, or 24 h, the responses of mentioned durations were evaluate. For incubation 2 h of TCDD exposure, DRE2 and DRE3 were active, but not DRE1. 6 h exposure to TCDD gave rise to ARE1 and ARE2 activity, while at 24 h exposure AP-1 was the only required *cis*-element for activation promoter of AhR (Fig. 17A). These findings suggested the individual *cis*-elements in *AhR* promoter activation was dependent on the duration of TCDD treatment. Time dependent manner was shown in AhR activation, and the order of responding to TCDD involved the DRE subsequently activation of ARE, then followed by AP-1. From these results Nrf2 and Jdp2 may play a crucial role of regulation activity in *AhR* promoter.

In order to identify the molecule components that interact with DRE and ARE elements, siRNA against *Arnt*, *AhR*, *Nrf2,* and *Ahrr* were used to knock down each gene product (Fig. 17B) [77]. *AhR* promoter activity was significantly repressed with siRNA against *Arnt*, *AhR*, and *Nrf2* in the presence or absence of TCDD (Fig. 17C, D). Nevertheless, *MafK* and *Ahrr* siRNA did not supress the activity of *AhR* promoter. As previously mentioned, these results indicated both ARE2 and ARE1 *cis*-elements appeared to be critical for activating the response of AhR promoter to treatment of TCDD (Fig. 17A).

In order to characterize *Jdp2* and *Nrf2* in *AhR* promoter, induction of activity were investigated in *Jdp2*$^{-/-}$ MEFs. 50 – 200 ng of pcDNA-*Jdp2* was transfected with the luciferase plasmid of *AhR* promoter, 1.9–2.5-fold of luciferase activity was found to increase with the treatment of TCDD. *Jdp2* expression increased activity in *AhR* promoter by 1.4–1.6-fold in cells cultured with DMSO (Fig. 17E). Therefore, additional TCDD shown higher upregulated activity of *AhR* promoter than that in DMSO induction.

From our results, *AhR* promoter was positively autoregulated by AhR in WT MEFs, but in *Jdp2*$^{-/-}$ MEFs shown opposite results. AhR alone seemed to be crucial for activation of *AhR* promoter (Fig. 17F).

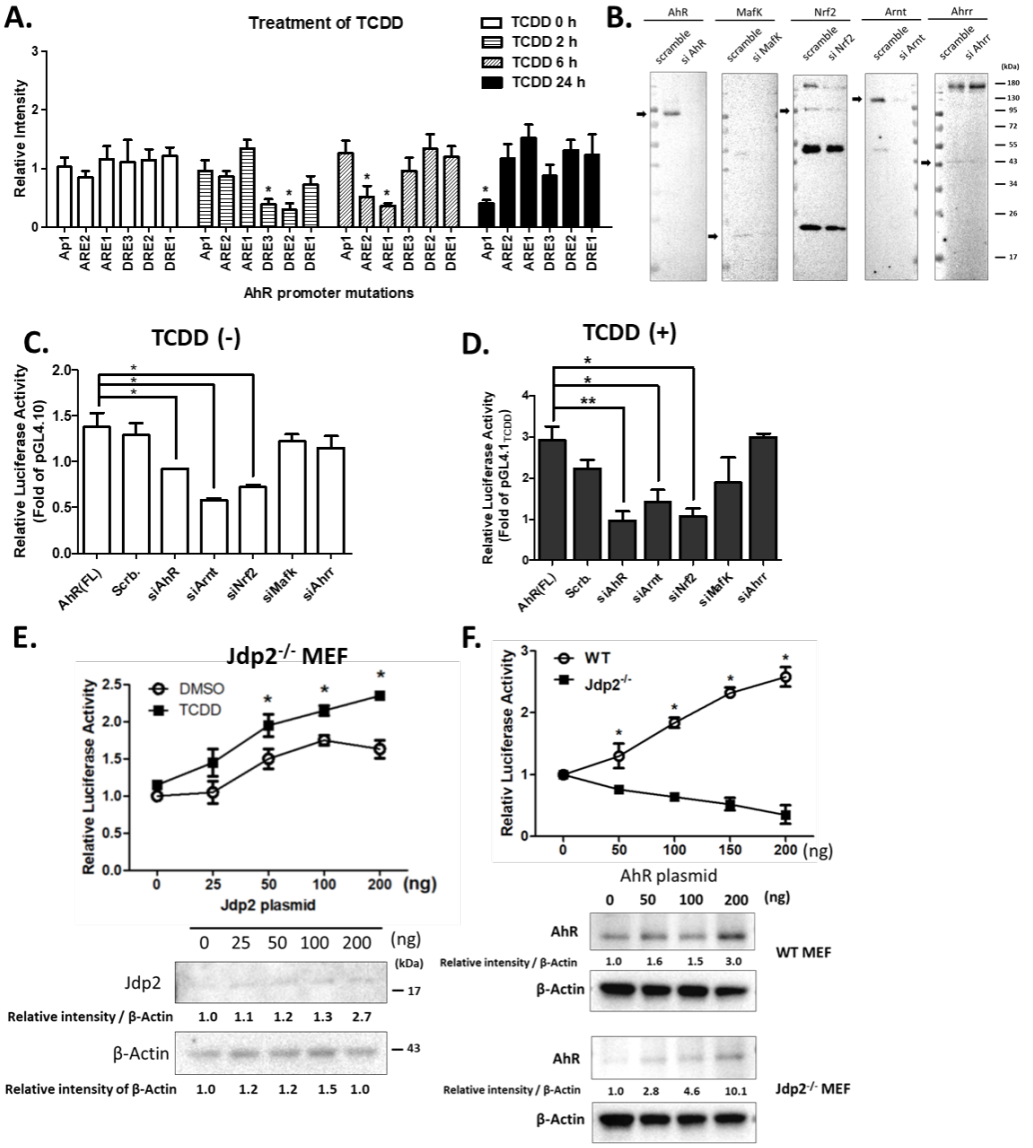

Fig. 17 Properties of full *AhR* promoter and transcription factors recruited. (**A**) Mutation of DRE1, ARE1, DRE2, ARE2, and DRE3 *cis*-element effects on the region of *AhR* promoter. Activity of was WT MEFs luciferase was measured with the treatment of 10 nM TCDD at the mentioned durations of time. The luciferase activity of *pGL4.1-AhR* luciferase was set as arbitrarily unit 1.0. (**B**) siRNA against *MafK, Ahrr, Arnt, AhR, Arnt, and Nrf2* in WT-MEFs. (**C**, **D**) Mentioned siRNA on *pGL4.1-AhR* activity of luciferase in WT MEFs with (**C**) or without (**D**) 10 nM treatment of TCDD. Activity of *pGL4.1* luciferase was set as arbitrarily unit 1.0. (**E**) Effects of increased dose of pcDNA3-Jdp2 (0, 25, 50, 100 and 200 ng) on AhR-luciferase activities (pGL4.1-AhR promoter-luciferase) in 10 nM TCDD or 0.1% DMSO treated Jdp2$^{-/-}$ MEFs. (**F**) Effects of increased doses of AhR on activity of *AhR* promoter luciferase in WT and *Jdp2*$^{-/-}$

MEFs. The AhR dose was 50, 100, 50, or 200 ng. The intensity of band was normalized to β-actin as relative value demonstrated in ratio. Above statistical results were analyzed by one-way ANOVA with *post hoc* Tukey test (*$p < 0.05$; **$p < 0.01$, $n \geqq 3$). Jdp2 is a spatiotemporal transcriptional activator of the AhR via the Nrf2 gene battery

3.2.3 ARE and DRE are crucial *cis*-elements for regulation of *AhR* promoter

In order to confirm the interaction of Arnt, Mafk, AhR, Nrf2, and Jdp2 with ARE and DRE *cis*-elements, chromatin immunoprecipitation (ChIP) was conducted in the promoter of AhR (Fig. 18A). Primers pairing to cover these cis-elements were designed to be detected individually except that DRE2/3 was in the same primer pairs; DRE2 and DRE3 *cis*-elements were too near to be separated by PCR.

10 nM of TCDD were treated in MEFs for 2 or 6 h for the activation of AhR-Arnt complex. After exposure for 2 h, majority of complexes included Arnt, AhR, Mafk, Nrf2, and Jdp2 were recruited to region of DRE2/3 (Fig. 18B), but Jdp2, MafK, and AhR were the only components recruited to DRE1 site(Fig. 18C). Site of DRE1 on *AhR* promoter shown unfunctional after 2 h treatment of TCDD (Fig. 18A, B); the same results were also observed on ARE1 and ARE2 elements (Fig. 18D, E). Howerver, after 6 h treatment of TCDD, complexes of Nrf2 involving MafK, Arnt, Nrf2, and Jdp2 were observed to form on ARE1 without AhR (Fig. 18I). These complexes were not observed on DRE1, ARE2, or DRE2/3 (Fig. 18F –H). These observations suggested Jdp2 was critical for DRE-dependent activation of ARE complex involving Nrf2 with MafK during 2 h treatment of TCDD, and AhR-Arnt and Jdp2 may be required for sequence-specific recruitment. Nevertheless, phase I promoter genes of AhR by phase I ligands early activation may be firstly modulated by their DRE *cis*-elements respectively. The activation of ARE recruited by phase I complex AhR–Arnt [11] was followed, subsequently the phase II complex of Nrf2-Jdp2-MafK [24].

In order to validate these results, immunocolocalization assay with antibody specific against AhR, Jdp2, and Nrf2 was performend. Signals of AhR, Nrf2, and Jdp2 were detected in all nucleus (Fig. 18J), no signals were detected in the control image (data not shown). In most of the regions, AhR, Nrf2, and Jdp2 signals are colocalized. Thus, the complex include Jdp2, Nrf2, and AhR seems to exist in the nucleus of WT MEFs without TCDD induction.

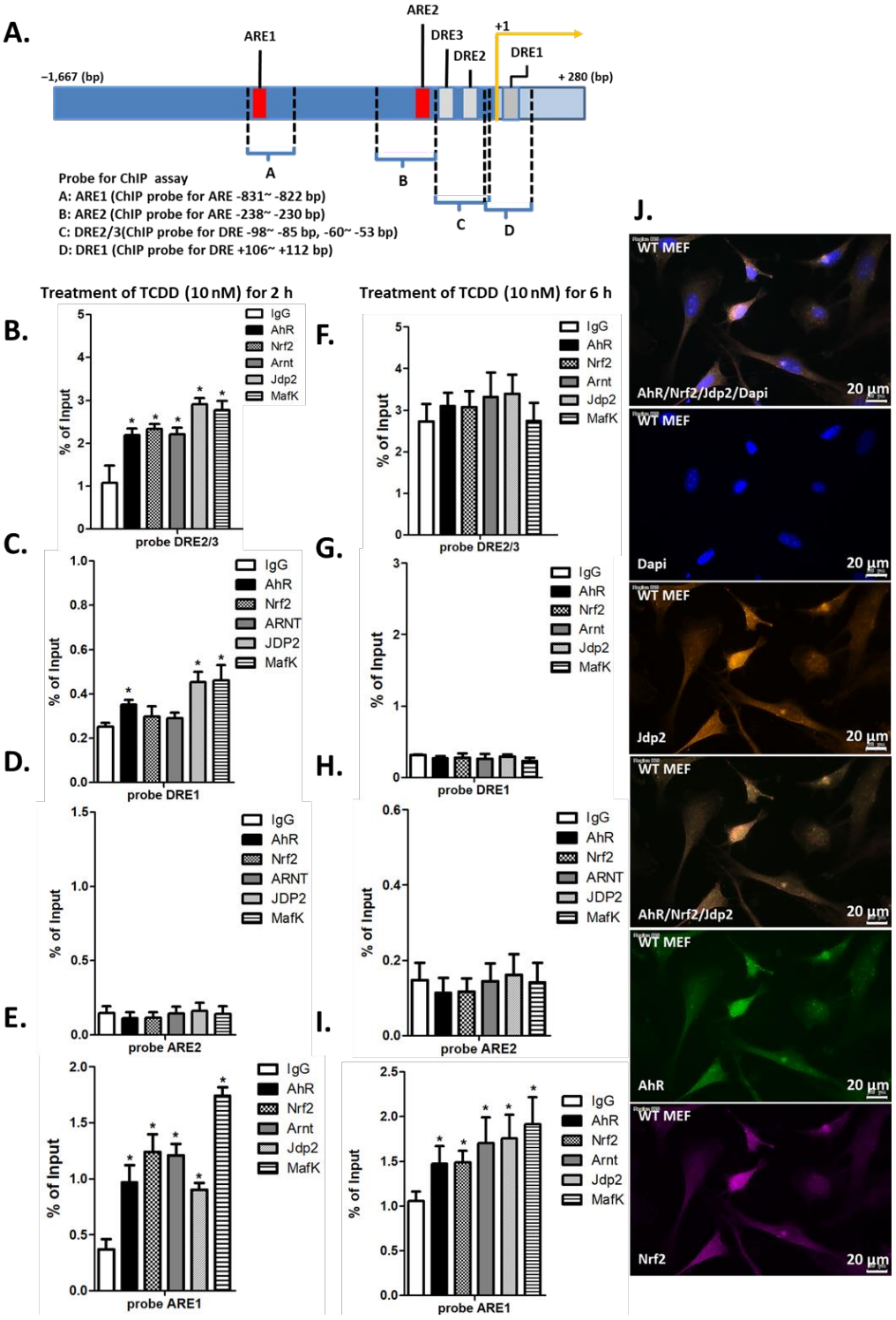

Fig. 18 Colocalization of AhR–Jdp2–Nrf2 axis by using chromatin immunoprecipitation (ChIP) assay. (**A**) Illustration promoter of *AhR* schematic figure and the positions of *cis*-elements, DRE1, DRE2/3, ARE1, and ARE2. (**B–I**) PCR amplified fragments in WT MEFs by the corresponding primer probes of DRE1, ARE1, and ARE2, or with primer pairs detectes DRE2 and DRE3 *cis*-elements. ChIP–qPCR

assay were performed by applying chromatin extract exposure for 2 h of TCDD (**B–E**) or 6 h (**F–I**) with the specific antibodies or negative control normal IgG. Probes are shown with the exposure of 10 nM TCDD for ARE1 (**E**, **I)**, ARE2 (**D**, **E**), DRE1 (**C**, **G**), and DRE2/3 (**B**, **F**). Values demonstrated as mean ± SEM (n = 5). Results were claculated with one-way ANOVA followed by *post hoc* Tukey test (*$p < 0.05$). (**J**) Nrf2, AhR, and Jdp2 colocalization. Goat anti-AhR (Clone N-19; Santa Cruz Biotechnology Inc., Dallas, TX, USA), anti-mouse Jdp2 (Clone A-3; Santa Cruz Biotechnology Inc., Dallas, TX, USA), anti-mouse Nrf2 (Santa Cruz Biotechnology) were stained, scale bars shown as 30 μm. Jdp2 is a spatiotemporal transcriptional activator of the AhR via the Nrf2 gene battery

3.3 The interaction of Nrf2, Jdp2,and AhR in nucleus

To futhur investigate the locations of AhR, Nrf2, and Jdp2 associate, coimmunoprecipitated using highly specific antibodies for endogenous proteins were performed. By contrast of overexpressing proteins, endogenous AhR were percipitated and followed by high-quality antibodies for western blotting used to identify the molecule interactions with AhR in WT and *Jdp2*$^{-/-}$ MEFs. AhR were precipitated with Nrf2 in nucleus fraction by immunoprecipitation (Fig. 19A–D). The nuclear expression of AhR-associated Nrf2 was higher with 2 h DMSO treatment in WT MEFs than TCDD. In contrast, nuclear AhR-associated Nrf2 shown lower expression in *Jdp2*$^{-/-}$ MEFs with 2 h of DMSO than treatment of TCDD. Our results demonstrated the absence of Jdp2 in the presence of TCDD treatment can enforce the AhR–Nrf2 interaction when compared with DMSO (Fig. 19A).

In addition, we also examined the interaction of AhR with Arnt. The increase of nuclear Arnt and AhR with TCDD incubation for 2 h, and 6 h was observed in WT and *Jdp2*$^{-/-}$ MEFs (Fig. 19B, C). These results suggested Nrf2 is one of the components in AhR–Arnt complex. Nrf2 binding with AhR occored at the treatment of TCDD 2 and 6 h in WT MEFs, but the complex of AhR–Nrf2 was not detected 24 h after the treatment of TCDD (Fig. 19B); this observation can be the result of endogenous AhR degradation [78]. The accumulation of AhR–Nrf2 complex in nucleus was observed with the treatment of TCDD for 2 h in *Jdp2*$^{-/-}$ MEFs. Nevertheless, complex of AhR–Nrf2 was not detected at the treatment of TCDD for 6 and 24 h even though AhR was being immunoprecipitated (Fig. 19B, C).

The AhR–Arnt maximum interaction of was observed at the treatment of TCDD for 6 h in WT MEFs, while the maximum for *Jdp2*$^{-/-}$ MEFs was at 2 to 6 h. Jdp2–Nrf2 interaction was observed in 2, 6, and 24 h in the WT MEFs, the interaction reached maximum at 6 h treatment, but the Jdp2–AhR interaction was observed at the treatment of TCDD for 2 and 6 h, not after 24 h (Fig. 19D). These results demonstrated in nucleus Jdp2 possess the ability to interact with Nrf2 and AhR, this multiprotein complex can be induced by TCDD in order to mediate the AhR-Arnt and Nrf2 cross-interaction pathways.

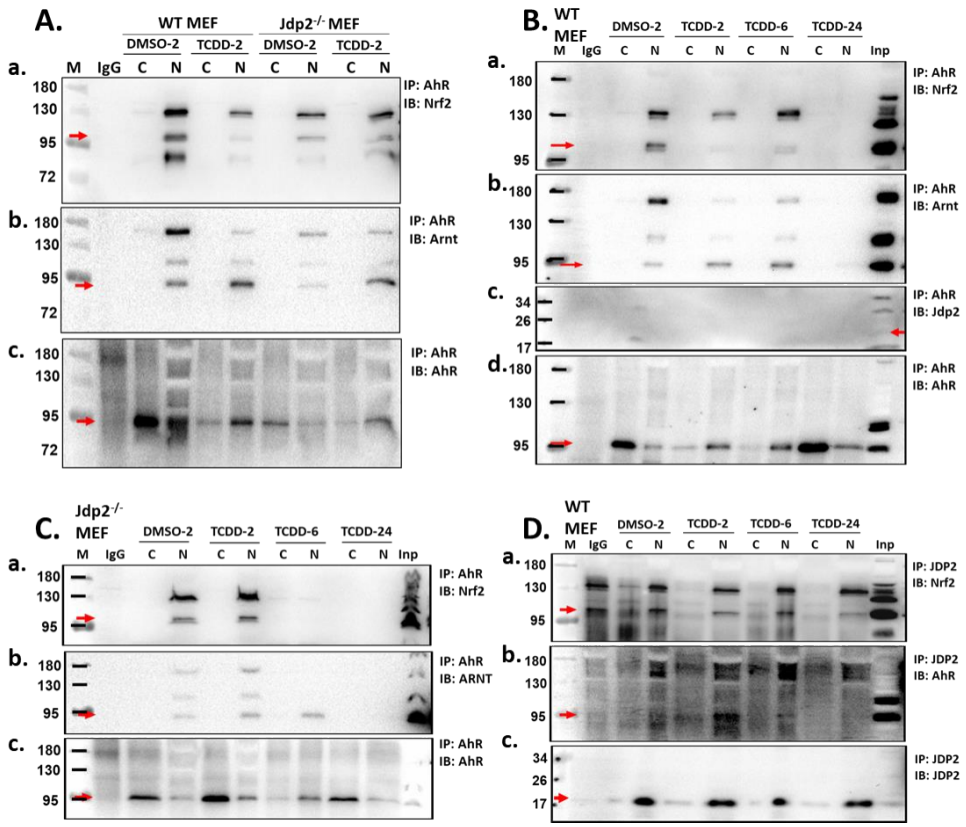

Fig. 19 Response of AhR–Jdp2–Nrf2 axis to the treatment of TCDD interact in WT MEFs and *Jdp2*$^{-/-}$ MEFs cytoplasm and nuclei. (**A**) Immunoprecipitation of cytosolic and nuclear fractions of cell lysate from WT and *Jdp2*$^{-/-}$ MEFs with the treatment of 2 h TCDD by antibody target AhR **a.** Immunoprecipitation (IP): AhR, immunoblot (IB): Nrf2, **b.** IP: AhR, IB: Arnt **c.** IP: AhR, IB:AhR. (**B**) WT MEFs nuclear and cytosolic fractions of cell lysate after exposure to TCDD for 2, 6, or 24 h were immunoprecipitated with antibody against AhR **a.** IP: AhR, IB: Nrf2, **b.** IP: AhR, IB: Arnt, **c.** IP: AhR, IB: Jdp2, **d.** IP: AhR, IB: AhR. (**C**) Cell lysates of nuclear or cytosolic fractions from *Jdp2*$^{-/-}$ MEFs after exposure to TCDD for 2, 6, or 24 h were immunoprecipitated with antibody against AhR **a.** IP: AhR, IB: Nrf2, **b.** IP: AhR, IB: Arnt **c.** IP: AhR, IB: AhR. (**D**) Cytosolic and nuclear fractions of cell lysate from WT MEFs with exposure of TCDD for 2, 6, or 24 h were immunoprecipitated with Jdp2 speficic antibody, percipated proteins were detected with AhR, Jdp2, and Nrf2 speficic antibodies **a.** IP: AhR, IB: Nrf2, **b.** IP: AhR, IB: Arnt **c.** IP: AhR, IB: AhR. IgG was used as a negative control. The red arrows indicated the targeted proteins in each panel. Jdp2 is a spatiotemporal transcriptional activator of the AhR via the Nrf2 gene battery

In order to confrim the results by western blotting, AhR subcellular distributaion was examine the with time course treatment of TCDD in WT MEFs. Translocation of AhR was triggered after TCDD treatment for 30 min. After 2 h of TCDD treatment, the effect start to reduce, this reduction lasted for 24 h (Fig. 20A–C).

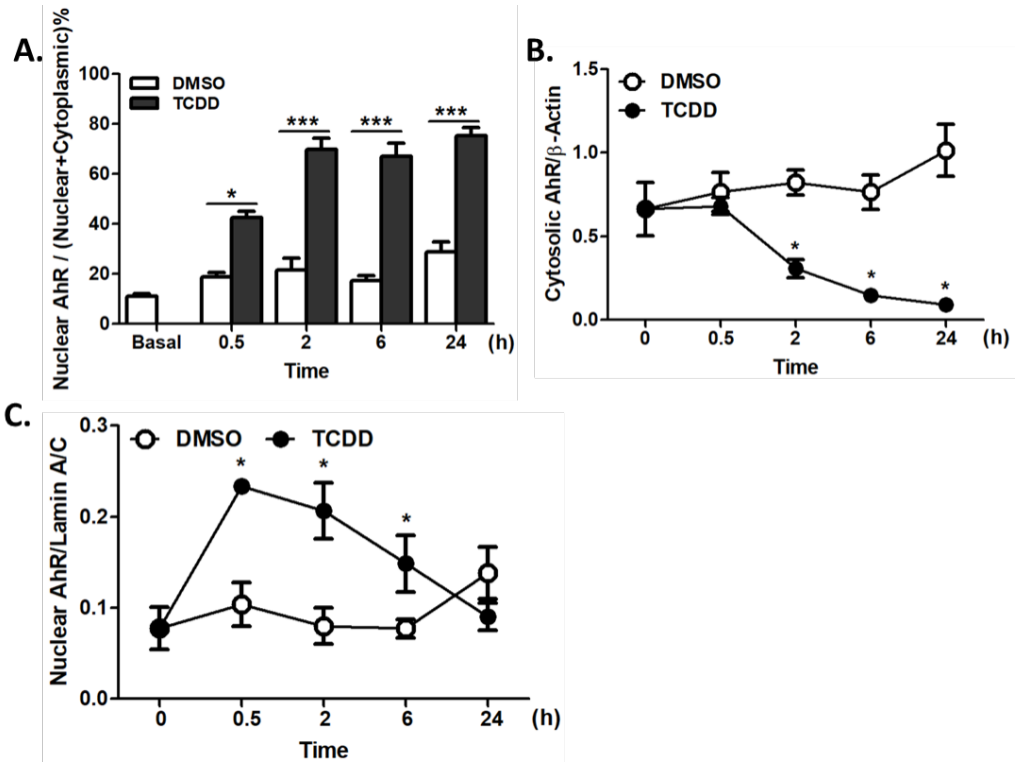

Fig. 20 Relative localization ratio protein of WT MEFs AhR exposed to TCDD or DMSO. (**A**) Relative localization ratio of AhR protein in the nucleus and cytoplasm in WT MEFs after exposure to DMSO and TCDD for 30 min, 2 h, 6 h, or 24 h (*$p < 0.05$; ***$p < 0.005$). The ratio was generated based on the β-actin expression **(B)** or lamin C expression **(C)** levels (*$p < 0.05$). All values are expressed as the mean ± SEM ($n = 5$). The results were calculated by two-way ANOVA followed with *post hoc* Bonferroni test for multiple comparisons. Jdp2 is a spatiotemporal transcriptional activator of the AhR via the Nrf2 gene battery

3.4 Jdp2 requried DRE3 and DRE2 sites for TCDD induced AhR promoter activation control

Next, we investigate the Jdp2 and Nrf2 ectopic expression on *AhR* promoter activity induced by TCDD treatment of DRE2 site mutants. In WT and *Jdp2*$^{-/-}$ MEFs, the activity of AhR promoter increased notably concomitant with the increase of Jdp2 concentration, and this result was abolished in DRE2 element mutant of WT and *Jdp2*$^{-/-}$ MEFs with the treatment of TCDD (Fig. 21A, B). These results indicated DRE2 site was required for the activation of *AhR* promoter by Nrf2 mediation. Nevertheless, Nrf2 can recognized sequences of DRE by direct interaction, or complex binding as examples: AhR–Arnt, Nrf2–MafK, with Jdp2 were remained unclear. The result of AhR protein interacting with ARE sequences showed the same issue.

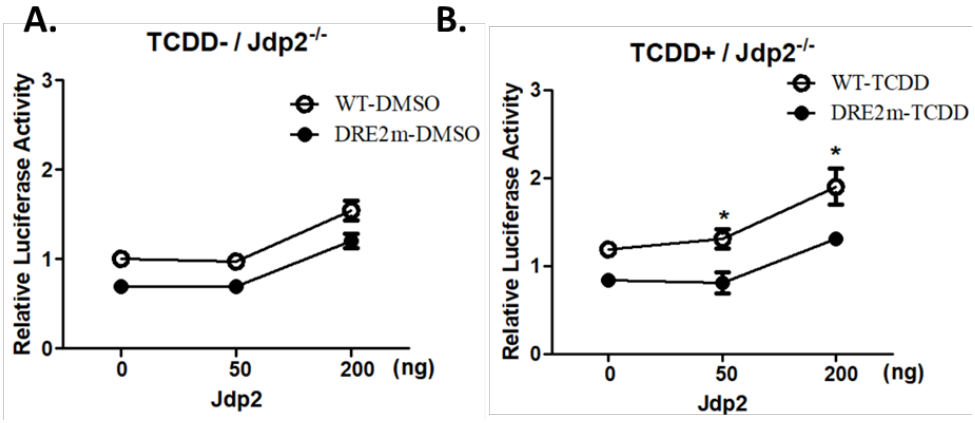

Fig. 21 The mutation of DRE2 in *AhR* promoter characterization and expression of Jdp2 downstream genes. DRE2 mutation effects on the *AhR* promoter without **(A)** or with **(B)** the treatment of TCDD in *Jdp2*$^{-/-}$ MEFs in the incubation of Jdp2 at 50 and 200 ng (*$p < 0.05$). The results were calculated by two-way ANOVA followed with *post hoc* Bonferroni test for multiple comparisons. Jdp2 is a spatiotemporal transcriptional activator of the AhR via the Nrf2 gene battery

To understand these process, electrophoresis migration shift assay (EMSA) was conducted *in vitro* to confirm ARE and DRE *cis*-elements interact with GST–AhR and GST–Nrf2 proteins (Fig. 22A, B). EMSA results revealed that single recombinant protein of GST–Nrf2 bound to DRE3 and DRE2 sites, and ARE1 site bound with GST–AhR basic helix–loop–helix (bHLH) recombinant protein. The binding affinity of

GST–AhR bHLH to DRE3 site was elevated in the presence of GST–Nrf2 (Fig. 22C). Moreover, DRE and ARE sites were detected bound with GST–Jdp2, possibly through the GC–rich sequences [79]. More detailed studies are required for examine the crucial residues that each *cis*-element binds to, with individual chromatin complex similar to Nrf2–Jdp2 or AhR–Jdp2 complexes [24].

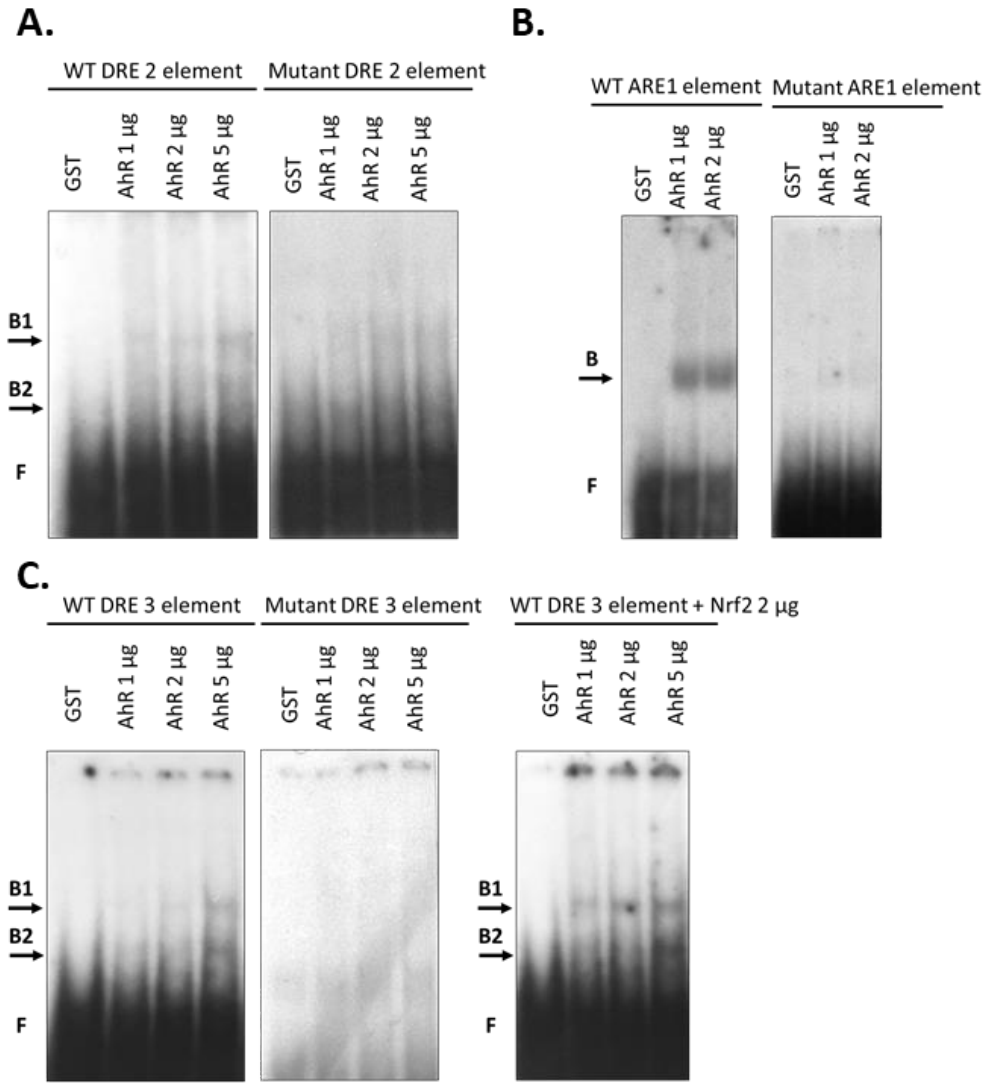

Fig. 22 GST–AhR–basic helix-loop-helix (bHLH) *in vitro* binding with ARE1, DRE2, and DRE3. (**A**) DNA binding of GST–AhR–bHLH protein (Hideaki Ito, Akita University, Japan) to DNA probe DRE2 and its mutant DRE2. (**B**) DNA binding of GST–AhR protein to the ARE1 and its mutant probe. (**C**) DNA binding of GST–AhR protein to the DRE3 and its mutant probe. The nucleotide sequences of these probes were listed in Table 7. EMSA reactions were performed for the respective DNA probes as described in the Methods section using [γ-^{32}P]-labeled double-stranded DRE2 or

DRE3 or ARE1 oligonucleotides. GST–AhR–bHLH were purified using GST affinity resins. “B” indicated the DNA-protein complexes and “F” indicated the respective DNA-free probes. Jdp2 is a spatiotemporal transcriptional activator of the AhR via the Nrf2 gene battery

3.5 TCDD-induced ROS accumulate by insufficient AhR expression in Jdp2 deficiency MEFs

TCDD were generally considered result in robust generation increased of ROS via AhR activation in keratinocytes [73,80]. To invistigate the ROS production induced by Jdp2 in of WT MEFs, flow cytometry with chloromethyl-2′,7′-dichlorofluorescein diacetate (H2DCFDA) were conducted as mentioned in previous literature [81]. The generation of ROS was lower in WT MEFs than that in *Jdp2*$^{-/-}$ MEFs at the resting state (Fig. 23A, B). TCDD-induced ROS production reached the maximum at 2 h treatment, sustaining through 6 h, and then reduced at 24 h in both *Jdp2*$^{-/-}$ MEFs and WT MEFs (Fig. 23C). TCDD-induced production of ROS elevated more in *Jdp2*$^{-/-}$ MEFs than that in WT MEFs, indicated *Jdp2*$^{-/-}$ MEFs express a greater oxidative stress. This finding agreed with the previous studies that Jdp2 plays a crucial role in to control the balance of antioxidation and oxidation [24].

Redox control and oxidative stress markers of different types were also investigated. One of the major products for DNA oxidization 7,8-dihydro-8-oxo-27-deoxyguanosine (8-oxodG) was observed elevated in both presence, and absence of TCDD exposure for 2 h in *Jdp2*$^{-/-}$ MEFs than that WT MEFs (Fig. 23D). The malondialdehyde (MDA) production, H_2O_2 lipid peroxidation was also observed to be elevated in *Jdp2*$^{-/-}$ MEFs than that in WT MEFs (Fig. 23E). These observations indicated the increased of oxidative stress in *Jdp2*$^{-/-}$ MEFs, and suggested lower activity of ARE in *Jdp2*$^{-/-}$ MEFs than that in WT MEFs with TCDD exposure for 2 h. 2–3 fold higher total glutathione (GSH) level was detected in WT that that in *Jdp2*$^{-/-}$ MEFs in both with or without the treatment of TCDD (Fig. 23F). In *Jdp2*$^{-/-}$ MEFs, the ratio of GSH/oxidized GSH reduced in both with or without the treatment of TCDD (Fig. 23G). NQO1 enzyme activity was 1.4-fold elevated without TCDD treatment and 1.5-fold increased with TCDD in *Jdp2*$^{-/-}$ MEFs than that in WT MEFs (Fig. 23H). Take these observations together, the data obtained in ROS production level shown consistent

results (Fig. 23A–C).

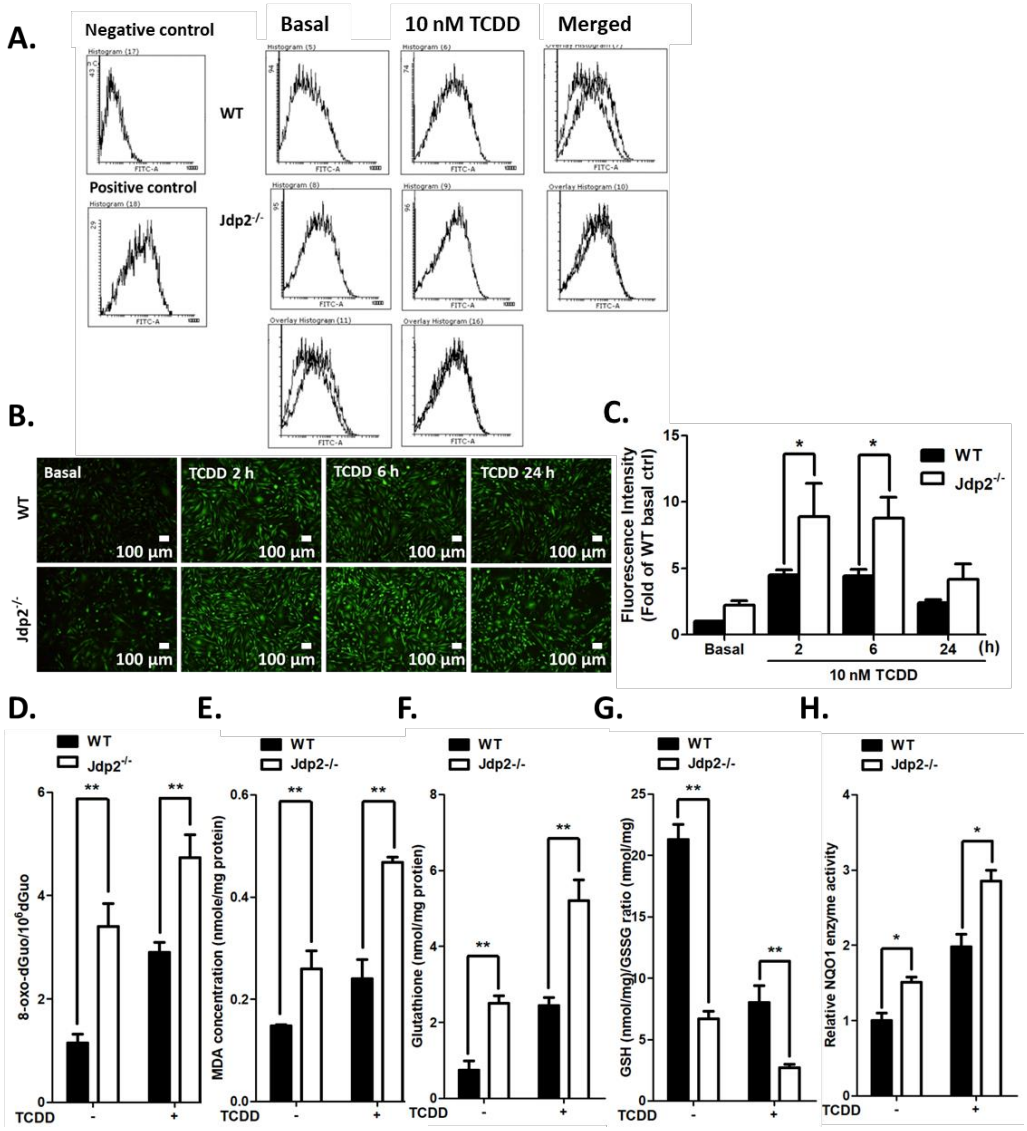

Fig. 23 WT and *Jdp2*$^{-/-}$ MEFs induces ROS production in response to TCDD treatment. (**A**) 10 nM of TCDD were used to incubate MEF for 2 h, CM-H_2-DCFDA 0.25 M were stained and quantify by flow cytometry assay. (**B**) WT and *Jdp2*$^{-/-}$ MEFs treated with 10 nM TCDD, the activity of ROS was measured in 0, 2, 6, or 24 h. CM-H_2DCFDA was used to detect ROS production. Representative ROS generation images of fluorescence. (**C**) The collected data from fluorescence images of CM-H_2DCFDA detected ROS levels with treatment of TCDD, results were calculated by ImageJ software. WT MEFs and *Jdp2*$^{-/-}$ MEFs fluorescence intensity with the treatment of TCDD was set at 1.0. Values are shown as mean ± SEM (n = 5). Two-way ANOVA with *post hoc* Bonferroni test were used to analyzwed the data (*p < 0.05). **(D-H)**

Antioxidation reaction and ROS production control by Jdp2 in MEFs. (**D**) Dection of 8-oxo-dGuo level, cells were collected at 24 h treatment of TCDD (10 nM) for 2 h in WT and *Jdp2*$^{-/-}$ MEFs. (**E**) Dection of malondialdehyde (MDA) level, cells collected 24 h after the exposure 2 h of TCDD (10 nM) in WT and *Jdp2*$^{-/-}$ MEFs. (**F, G**) Total glutathione (GSH) level (**F**) and ratio of GSH/oxidized glutathione (GSSG) (**G**) with or without the TCDD (10 nM) treatment for 2 h in WT and *Jdp2*$^{-/-}$ MEFs cells were collected 24 h after the exposure. (**H**) NQO1 enzyme relative activity of WT and *Jdp2*$^{-/-}$ MEFs, in the presence or the absence of 2 h treatment of TCDD (10 nM), cells collected 24 h after the exposure. Results shown as the mean ± SEM (n = 3), analyzed by using one-way ANOVA with *post hoc* Tukey test (*p < 0.05 and **p < 0.01). Jdp2 is a spatiotemporal transcriptional activator of the AhR via the Nrf2 gene battery

3.6 AhR target genes shown different expression between WT and Jdp2$^{-/-}$ MEFs

In order to confirm the effect of TCDD exposure, genes encoding *Cyp1b1*, aldehyde dehydrogenase 3 family member A1 (*Aldh3a1*), AhR repressor (*Ahrr*), and TCDD-inducible poly (ADP-ribose) polymerase (*Tiparp*) were detected by qPCR (Fig. 24A–C). The expression of mentioned genes shown similar level of mRNA in WT and *Jdp2*$^{-/-}$ MEFs with DMSO treatment. However, with 2 h incubation of TCDD 10 nM the increase of *Cyp1b1, Tiparp,* and *Aldh3a1* mRNA expressions were significant in WT MEFs. In comparison, the level of *Cyp1b1, Tiparp,* and *Aldh3a1* mRNA expression were lower in *Jdp2*$^{-/-}$ MEFs. These findings suggested AhR signaling and the downstream genes are modulated by Jdp2 in a ligand-dependent manner.

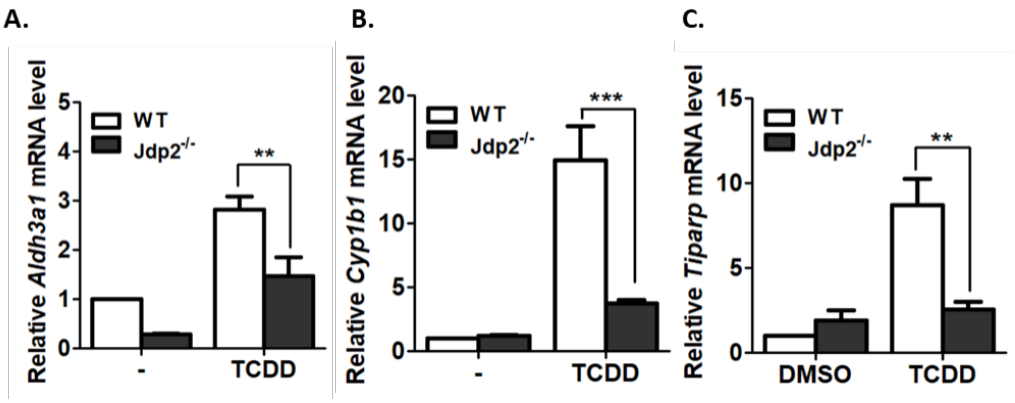

Fig. 24 Relative expression change in AhR target gene mRNAs. Expression level of *Aldh3a1* (**A**), *Cyp1b1* (**B**), and *Tiparp* (**C**) mRNA under the treatment of TCDD or DMSO for 2 h in WT and *Jdp2*$^{-/-}$ MEFs. Data were obtained using qPCR analysis, WT MEFs in response to DMSO was set at 1.0 (**$p < 0.01$, ***$p < 0.005$). All above data shown as the mean ± SEM ($n = 5$). Statistic analyzed as indicated by two-way ANOVA with *post hoc* Bonferroni test for multiple comparisons. Jdp2 is a spatiotemporal transcriptional activator of the AhR via the Nrf2 gene battery

3.7 Jdp2 deficiency limited cytoskeleton remodeling and spreading of cell structure

Emerging evidence showed that the modulation of mobility and plasticity of cells, which were correlated with remodeling of cytoskeleton, which may involved with AhR [82]. In order to determine the functional relevance of AhR in cytoskeleton remodeling by Jdp2, actin detection by phalloidin and cell spreading assay was conducted with the exposure of TCDD in WT and *Jdp2*$^{-/-}$ MEFs at the concentration of 0, 100, and 200 μM for 24 h. Formation of actin stress fiber was increased in WT MEFs under the treatment of TCDD when compared with DMSO. Increased of F-actin fibers formation in *Jdp2*$^{-/-}$ MEFs with TCDD treatment shown less than that in WT MEFs (Fig. 25A). In cell spreading analysis, cytoskeleton fluorescence intensity amd cell area both were slightly elevated in WT MEFs compared to *Jdp2*$^{-/-}$ MEFs with TCDD exposure (Fig. 25B, C).

One of the critical components for actin stress fiber remodeling is phosphorylated myosin light chain 2 (pMLC2). In order to determine the effect of TCDD on cytoskeleton remodeling, pMLC2 levels in WT and *Jdp2*$^{-/-}$ MEFs with TCDD treatment 10–200 nM for 6 h was measured by western blot analysis. Slightly decrease of MLC2 was shown during the steady condition of *Jdp2*$^{-/-}$ MEFs. MLC2 pattern showed increased on WT MEFs at TCDD treatment 100 nM, but at the treatment of TCDD 50 and 100 nM, significant reduction was observed in phosphorylation of WT MEFs. On the other hand, the phosphorylation and expression with TCDD treatment, MLC levels were always lower in *Jdp2*$^{-/-}$ MEFs concentrations (Fig. 25D, E).

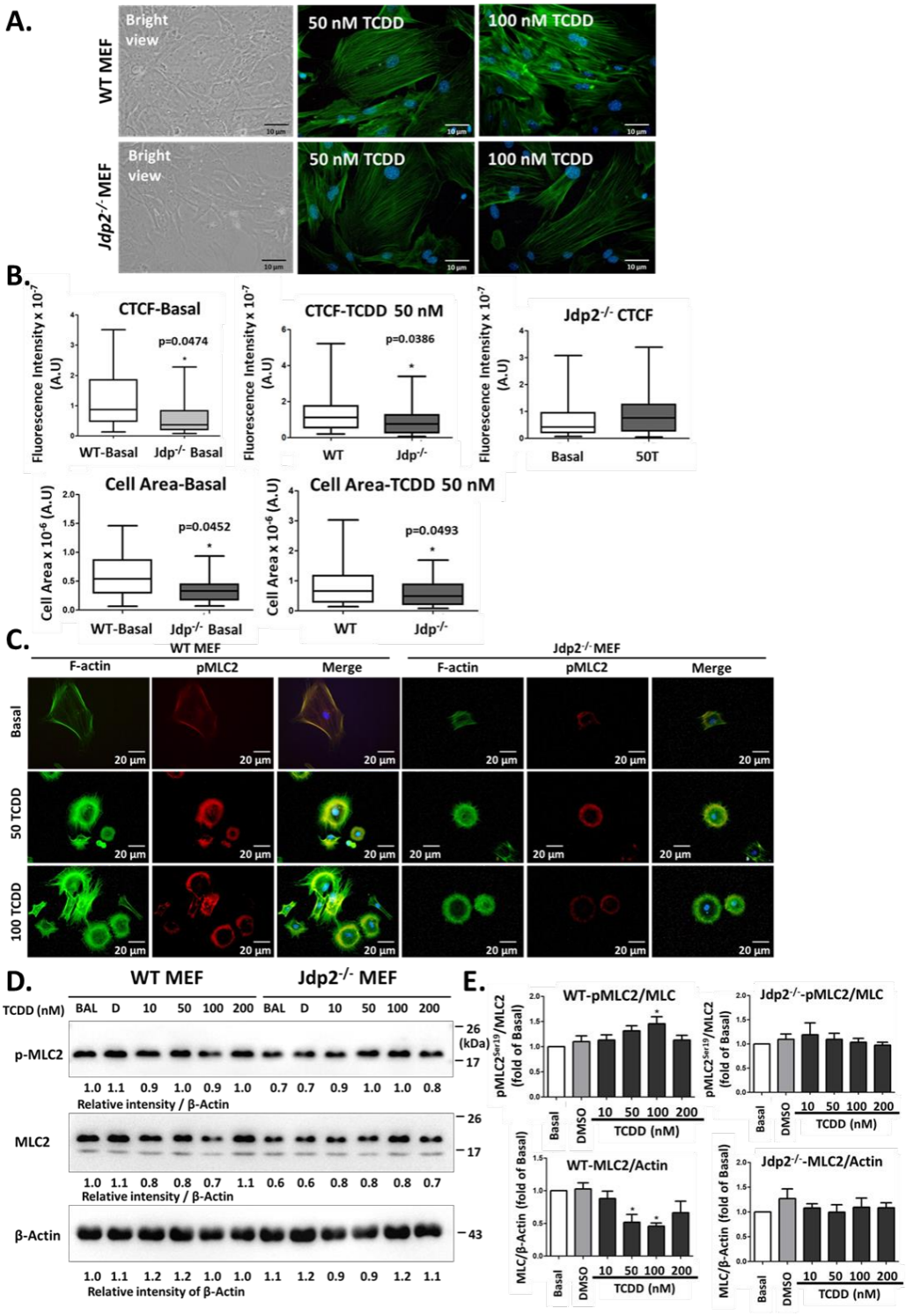
A.
Bright view
50 nM TCDD
100 nM TCDD
WT MEF
Jdp2-/- MEF
B.
CTCF-Basal
p=0.0474
WT-Basal
Jdp-/- Basal
CTCF-TCDD 50 nM
p=0.0386
WT
Jdp-/-
Jdp2-/- CTCF
Basal
50T
Fluorescence Intensity x 10-7 (A.U)
Cell Area-Basal
p=0.0452
Cell Area-TCDD 50 nM
p=0.0493
Cell Area x 10-6 (A.U)
C.
WT MEF
Jdp2-/- MEF
F-actin
pMLC2
Merge
Basal
50 TCDD
100 TCDD
20 µm
D.
WT MEF
Jdp2-/- MEF
TCDD (nM)
BAL D 10 50 100 200 BAL D 10 50 100 200
p-MLC2
MLC2
β-Actin
(kDa)
26
17
43
1.0 1.1 0.9 1.0 0.9 1.0 0.7 0.7 0.9 1.0 1.0 0.8
Relative intensity / β-Actin
1.0 1.1 0.8 0.8 0.7 1.1 0.6 0.6 0.8 0.8 0.8 0.7
Relative intensity / β-Actin
1.0 1.1 1.2 1.2 1.0 1.0 1.1 1.2 0.9 0.9 1.2 1.1
Relative intensity of β-Actin
E.
WT-pMLC2/MLC
Jdp2-/--pMLC2/MLC
pMLC2Ser19/MLC2 (fold of Basal)
Basal
DMSO
10 50 100 200
TCDD (nM)
WT-MLC2/Actin
Jdp2-/--MLC2/Actin
MLC/β-Actin (fold of Basal)

Fig. 25 TCDD-induced actin stress fibers spreading retardation by deficiency of Jdp2. (**A**) Cells were depleted with FBS before 24 h treatment of TCDD or DMSO. After the treatment, PBS were used to rinsed the cells, fixed with formaldehyde 4% and labeled F-actin with Alexa 488-conjugated phalloidin. DAPI were used for nuclei labeling, at least acquired five fields for each treatment. (**B**) WT and Jdp2$^{-/-}$ MEFs intensity of CCCTC binding factor CTCF, and cell area were measured with or without the treatment of TCDD 50 nM. (**C**) Cell spreading extensions of *Jdp2*$^{-/-}$ and WT MEFs with TCDD treatment,the expression of p-MLC2 and F-actin in *Jdp2*$^{-/-}$ and WT MEFs. Representative results of p-MLC2 and F-actin demonstrated. (**D, E**) Analysis of total MLC2 and p-MLC2 expression by western blot with the quantitative results (**D**). The intensity of bands was calculated, β-Actin normalized as relative ratio. (**E**). Cells were collected 6 h after 0–200 nM TCDD treatment, results are shown as mean ± SEM, p values were obtained from three independent experiments. Jdp2 is a spatiotemporal transcriptional activator of the AhR via the Nrf2 gene battery

3.8 Jdp2-dependent signaling is upstream of AhR at pancreatic cancer development and cell migration

The fact of Jdp2 decrease stress fiber spreading of actin is highly due to the cytoskeleton dysregulation. To further examine cell migration ability was affected by cell proliferation, wound healing assay was performed. Treatment with TCDD at 50 nM for 24 h was carried out and results were calculated by healed area mesured with imageJ software (Fig. 26A). The migration ability observed in *Jdp2*$^{-/-}$ MEFs was significantly lower than WT MEFs in both treatment of DMSO and TCDD. In order to clearfy the modulation of cell migration was involved with Jdp2, *pCDNA-AhR* was transfected into *Jdp2*$^{-/-}$ MEFs to determine if AhR overexpression can rescue the lowered migration. Interestingly, overexpression of AhR showed significant increase of wound area healed even with 50 nM TCDD incubation (Fig. 26B).

Take these findings together, the control of AhR-mediated ROS by Jdp2 functioned after the treatment of phase I ligand. In Jdp2 recruitment of transcriptional activation, Nrf2-MafK seemed to be included as spatiotemporal manner on *AhR* promoter; this also indicated Jdp2 is crucial for ROS regulation through transactivation of *AhR* promoter. Moreover, Jdp2 fucntionally control migration and cell sprearding in TCDD-induced mouse MEFs.

To clearfy the signaling, *kRAS–p53* double KO mice derived *kRAS–p53* knockout (KO) cancer cell line were used in our study [83]. The in order to study signaling of Jdp2-AhR on DRE2 effect through *AhR* promoter, Jdp2 dependent ROS activity and the recruitment of Jdp2 to DRE2/3 on *AhR* promoter were being examined. Pancreatic carcinoma 2545 cell line isolated from of *kRAS–p53* double KO mice were used to study the transactivation of Jdp2 on *AhR* promoter mediated by DRE element (Fig. 26A). Similar repression level was observed in DRE3 and DRE2 mutant with 2 h of TCDD treatment on *AhR* promoter in 2545 cells. By the treatment of TCDD, the activity of ROS was also invistigated in 2545 cells (Fig. 26B). ChIP assay with the treatment of TCDD for 2–24 h inducing ROS production was also performed on 2545 cells with or without shJdp2 treatment (Fig. 26C). After 2 h of TCDD treatment, Nrf2, Jdp2, AhR, Arnt, and MafK were recruited to DRE2/3 site (Fig. 26C). The colocalization of Jdp2, AhR, and Nrf2 protein waas observed by immunocytochemistry in 2545 cells (Fig. 26D). In constrast, no critical effect on TCDD-induced *AhR* promoter activation shown on DRE1 (Fig. 26A). These findings were similar to MEFs ones; moreover they also

suggested that DRE3 and DRE2 were crucial for *AhR* promoter activation induced by TCDD exposure.

Next, we performed xenograft transplantation assay of pancreatic cancer cells. The introduced shJdp2 resulted in enlargement of pancreatic tumor size1.5-fold. In the experiments, tumor supressor charaterstics were observed on Jdp2. By introducing AhR overexpression plasmid, tumor weight, size, and regions of necrosis showed to be decreased (Fig. 26E, F). No formation of blood vessels, sacroma, or EMT phenotypes were observed(Fig. 26G). These results indicated the role of DRE2 and 3 were critical for Jdp2–AhR pahtway in response to TCDD in 2545 cells; The similar result as observed in MEFs. Altogether, cascade of Jdp2–AhR is critical for the induction of TCDD on activation of AhR promoter, recruitment mediated by DRE2/3 to *AhR* promoter, and ROS generation. In MEFs and *kRAS–p53*-mutated pancreatic cancer 2545 cells, Jdp2 was shwon as the upstream of AhR in signaling cascade.

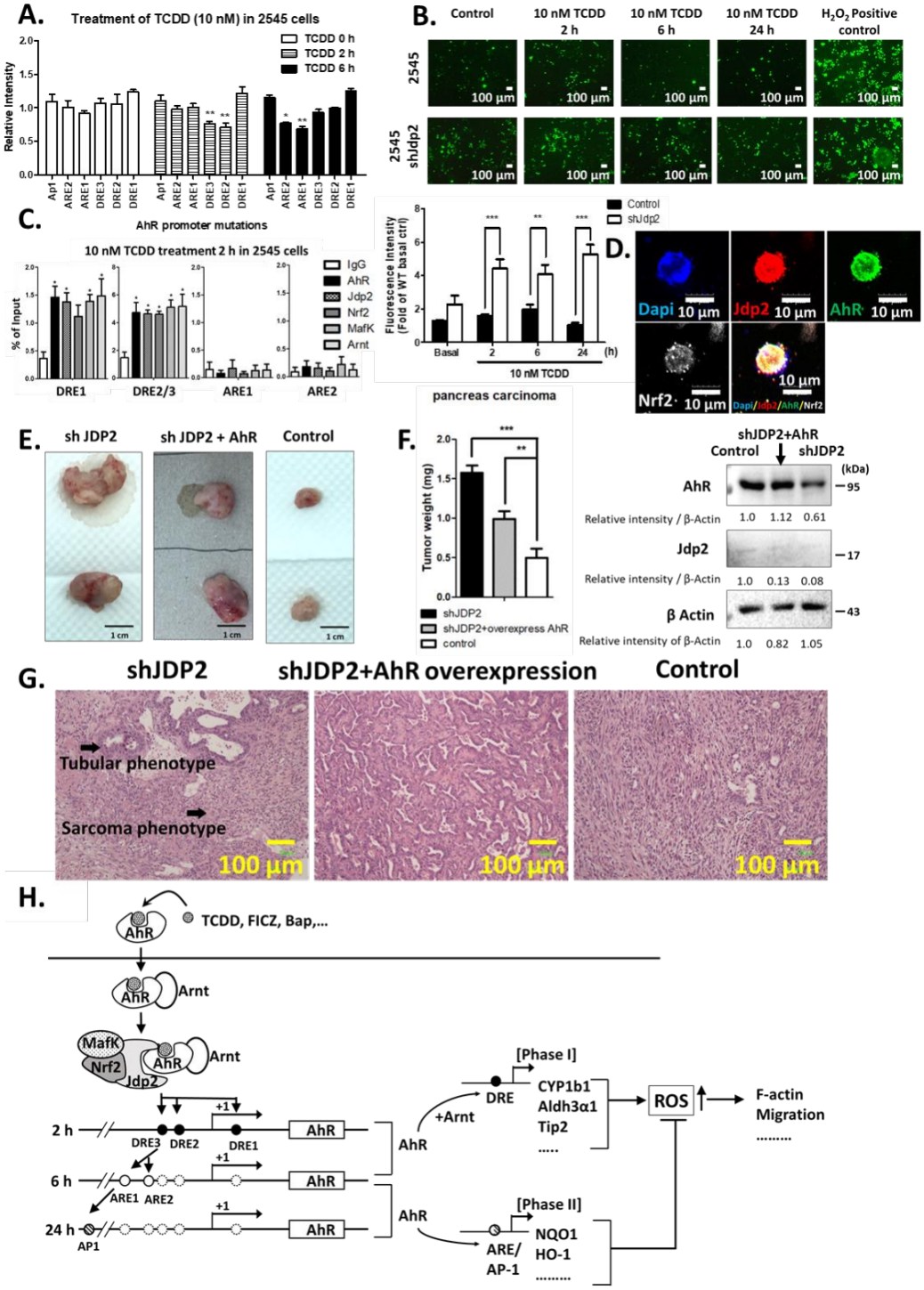

Fig. 26 Overexpression *AhR* in sh*Jdp2*-treated *kRas–p53*-mutated pancreatic carcinoma 2545 cells can diminish tumorigenesis benefits. (**A-C**) Response to TCDD treatment by luciferase AhR reporter through Jdp2–AhR axis in 2545 pancreatic cancer cells in ChIP assays, and ROS generation. (**A**) Each *cis*-elements, DRE1, DRE2, DRE3, ARE1, and ARE2, were mutated to observe effect on the *AhR* promoter. Activity

of reporter luciferase was obtained with the treatment of TCDD 10 nM at indicated periods of time in 2545 cells. Full-length (FL) *AhR* luciferase activity was set as arbitrarily unit 1.0 (*$p < 0.05$). (**B**) 2545 cells in TCDD 10 nM treatment of ROS production for indicted time periods, dection was done by using CM-H_2DCFDA. Fluorescence results of 2545 cells (top) and sh*Jdp2*-treated 2545 cells (bottom) ROS generation were shown. Results detected with CM-H_2DCFDA of ROS levels in the presence of TCDD were calculated by ImageJ. 2545 cells with TCDD free intensity was set as 1.0. Results were calculated by two-way ANOVA with *post hoc* Bonferroni test (**$p < 0.01$; ***$p < 0.001$). (**C**) AhR–Jdp2–Nrf2 axis detected with ChIP assay. Corresponding primers were used to amplify specific regions by PCR, and with primers that target DRE2 and DRE3 *cis*-elements region the as indicated. ChIP–qPCR were conducted by 2545 cell lysate extracts, with TCDD treatment for 2 h by using specific antibodies and a negative control normal IgG. Respective probes were used for ChIP-qPCR in cells with treated with 10 nM TCDD (*$p < 0.05$). (**D**) Protein complexes of AhR–Nrf2–Jdp2 coimmunostaining in 2545 tumor cells. Scale bars, 10 μm. **(E)** 2545 pancreatic cancers were xenografted on mouse with *AhR*-forced-expressed *Jdp2*-knockdown, *Jdp2*-knockdown, or original 2545 cells was performed. 2545 cells were transfected by *CSIV-CMV-AhR-IRES2-Venus* virus, 1×10^5 cells were inoculated into SCID mice. **(F)** Tumor weights with three replication. The intensity of each result were calculated to β-Actin and shown as ratio. **(G)** Tumor biopsies results of representative H&E stain. Different carcinoma phenotype were labeled as arrowhead indicates. The characteristics are shown as descriptions: sh*Jdp2* treatment result in necrosis of large area, sarcoma phenotype, and epithelial–mesenchymal transition phenotypes were increased; sh*Jdp2* + AhR overexpression observed reduced necrosis area and epithelial phenotype are the majority; control results shown similar with sh*Jdp2* treatment but with reduced necrosis. **(H)** Illustrative summary activation of *AhR* through DMSO-induced the complexes of Nrf2-Jdp2, AhR-Nrf2, and AhR-Jdp2 increase spreading of cell structure, apoptosis, and ROS production in WT MEFs. DRE2 and DRE3 elements of *Jdp2*$^{-/-}$ MEFs only recruit a limited amount of AhR–Arnt to the the *AhR* promoter. Above **(A, B, and F)** represented values shown as mean ± SEM ($n = 5$), results were calculated by one-way ANOVA with *post hoc* Tukey's test (*$p < 0.05$; **$p < 0.01$). Jdp2 is a spatiotemporal transcriptional activator of the AhR via the Nrf2 gene battery

3.9 Materials and Methods

3.9.1 Animals, cell culture, and reagents

Animal welfare approved guidelines were followed as shown in the previous **Chapter 2 Section 4.1**. MCF7, HepG2, and 293T cell lines were obtained from the RIKEN BRC Cell Bank (Tsukuba, Japan). 2545 mouse pancreatic cancer cell line was isolated and cultured [83]. TCDD was obtained from AccuStandard (New Haven, CT, USA). BaP, DMSO, tBHQ, FICZ, L-kynurenine, and sulforaphane were from Sigma-Aldrich (St. Louis, MO, USA).

3.9.2 Construction of plasmids, virus and antibodies

The repeated plasmids were shown in the previous **Chapter 2 Section 4.2**. *pcDNA-Jdp2A139C, and pcDNA-Jdp2* were obtained from RIKEN BRC, amplified by PCR, and cloned into a *pCMV_S-FLAG* vector with restriction sites [24]. Lentiviral vectors *CSII-CMV-MCS-IRES2-Bsd, pCMV-VSV-G-RSV-Rev,* and *pCAG-HIVgp* were purchased from the RIKEN BRC DNA Bank. All antibodies used in this study are listed in **Table 5.**

3.9.3 Immunocytochemistry

Cells of MEFs were fixed for 10 min with 4% formaldehyde, then washed twice with 4℃ phosphate-buffered saline (PBS). Fixed MEFs were blocked 15 min in blocking solution (10% FBS and 0.1% Triton X-100 in PBS) to reduce the nonspecific interactions, primary antibodies were incubated for overnight incubation with the fixed MEFs. After the incubation cells were washed twice with 4℃ PBS-T, then cells were treated with secondary antibodies for 90 min: Alexa-Fluor® 488 conjugated Rabbit anti-Goat IgG (Thermo Fisher Scientific; A-11078), Alexa Fluor® 594-labeled goat anti-rabbit IgG (Thermo Fisher Scientific, Waltham, MA, USA; A-11037), and Alexa Fluor® 647-labeled goat anti-rat IgG (H+L) (Cell Signal Technology; #4418), followed by nuclei staining through using 4′,6′-diamino-2-phenylindole (DAPI) (Merck, Darmstadt, Germany). Cells were mounted by ProLong Gold antifade mounting medium (Molecular Probes, P36034; Thermo Fisher Scientific) on slides, and immunofluorescence was observed by using Olympus FV1000 confocal laser scanning microscope (Olympus, Tokyo, Japan).

3.9.4 Western blotting, SDS-PAGE, and immunoprecipitation

The experiments of immunoprecipitation, SDS–PAGE, and western blot assays were conducted as mentioned in previous literature [24,58]. In general, 500 ×*g* for 5 min at 4℃ were used to separate cell lysates into nucleic and cytosolic fraction, using cytoplasmic and nuclear extraction reagents (NE-PER; 78833; Thermo Fisher Scientific). Fractionated cytoplasmic and nuclear lysates are loaded into 10% SDS–PAGE, transferred to Immobilon-P polyvinylidene difluoride (PVDF) membranes (0.45 μm IPVH00010; Merck) for 100 V (fixed) 1 h at 10°C using a Mini Trans-blot transfer system (Bio-Rad Laboratories, Hercules, CA, USA). Membranes of PVDF were then incubated with primary and secondary antibodies listed (**Material Table 5**). ChemiDoc XRS Plus detection system (Bio-Rad) were used to obtain the results. Protein A/G beads immunoprecipitation was conducted by coated with specific antibodies [24,58] for detection.

3.9.5 Chromatin immunoprecipitation (ChIP) assay

Detail procedures of ChIP assay was described in the previous **Chapter 2 Section 4.6.** The antibodies used in the study were listed as below: anti-Nrf2 (1:1000, sc-722), anti-Arnt (1:1000, NB100-124), anti-AhR (1:1000, sc-8088), anti-MafK (1:2000, ab229766), anti-Jdp2 (1:500, from Dr. Aronheim), and IgG (1:1000, C15400001015). The primers used to detect each fragment are listed in **Material Table 6**.

3.9.6 Luciferase reporter assay and transient transfection

Cells (4×10^4 cells/well) were seeded and cultured for 24 h into 24-well plates. Cotransfection was done with 500 ng of AhR plasmid or of the Cytochrome P450 Family 1 Subfamily B Member 1 (CYP1B1) (–2299/+25) luciferase with 10 ng of the control plasmid pRL-CMV encoding *Renilla* luciferase. Transfection was done by polyethylenimine (linear, molecular weight 25,000; Polysciences, Warrington, PA, USA; Cat# 23966) or Lipofectamine 2000 (Invitrogen). pGL3-CYP1B1 promoter DNA (-2,299~ +25) was given by Drs. K. Fujii-Kuriyama (Tsukuba University, Tsukuba, Ibaraki, Japan) and M. Nakajima (Kanazawa University, Kanazawa, Japan). Transfected DNA was maintaied at 1 μg/well by filling with a pBluescript II SK+ mock plasmid (Addgene, Watertown, MA, USA). TCDD or DMSO were treated for the mentioned times and harvested after 48 h transfection. Activity of luciferase was

recorded by dual-luciferase reporter assay system using a GloMax20/20 Luminometer (Promega). The relative luciferase activity was analyzed (firefly luciferase/*Renilla* luciferase) and demonstrated as fold induction with the mock vector in WT MEFs. All experients were conducted with duplicate, results are shown as mean ± standard error of the mean (SEM) from at least three independent experiments.

3.9.7 Gene knockdown mediated by siRNA and shRNA

ON-TARGETplus SMARTpool siRNA against mouse *ARNT*, *AhR*, *Ahrr*, *Nrf2,* and *MafK*, and a control scramble siRNA were purchased from GE Dharmacon (Austin, TX, USA). Mouse against *Nrf2*, *AhR*, *MafK*, *Jdp2*, *Arnt*, and *GFP* shRNA lentiviruses were purchased from RNAi Core Center at Academia Sinica (Taipei, Taiwan). Cells of MEFs were seeded into a 24-wells (for the luciferase reporter assay) or six-wells (for western blotting), transfect with indicated concentration of siRNA or negative control (20-40 nM) by Lipofectamine RNAiMAX in OPTI-MEM (both from Invitrogen). Multiplicity of infection of 10 was used to transfect shRNA into MEFs. Fresh culture medium with 10% FBS was added after 24 h, cells were then transfected with the luciferase plasmids. Knockdown efficiency of siRNA and shRNA were confrimed by harvested 48 and 72 h cells after siRNA transfection or shRNA infection, followed by immunoblotting.

3.9.8 qPCR and RNA isolation

PureLink™ RNA Mini Kit (Invitrogen) were used to purify total RNA. RNA was reverse transcribed to cDNA using SuperScript III Reverse Transcriptase (Invitrogen). StepOne or ABI7500 PCR instrument (Applied Biosystems, Foster City, CA, USA) were used to conduct real-time PCR with Applied Biosystems Fast SYBR® Green Master mix in 20 μL. Cycle *Ct* values threshold were averaged from technical duplicates. Gene transcripts were normalized to that of GAPDH. Relative gene expression level were analyzed by $2^{-\Delta\Delta Ct}$ method, normalized to the mRNA level in TCDD- or DMSO- treated WT MEFs as 1.0. Results were demnostrated as mean ± SEM with at least three replicate and indivisual experiments. The primers used are listed in **Material Table 6.**

3.9.9 Western blot and coimmunoprecipitation analysis

PRO-PREP™ protein extraction solution (iNTRON Biotechnology, Gyeonggi-dom, Korea) were used to prepare whole-cell lysates. NE-PER® Nuclear and Cytoplasmic Extraction kit (Thermo Fisher Scientific) were used to isolate subcellular fractionations. Bradford method were used to measure protein concentration with bovine serum albumin (Bio-Rad). For coimmunoprecipitation, 300 μg of lysate was cleared by using Protein A/G Agarose beads (Millipore, Burlington, MA, USA) for 1 h in rotation of 4°C, then blended with 1 μg of mentioned antibody or IgG with rotation in 4°C overnight. The targets were precipitated by using protein A/G beads, the proteins targets immunoprecipitated were added with 30 μL of 2× Laemmli buffer, boiled for 5 min, for western blot analysis.

p-MLC were detected by using serum starved overnight MEFs, incubated with TCDD or DMSO for 6 h, cells were treated with trichloroacetic acid 10%. Samples were precipitated and obtained throguh centrifugation, washed three times in absolute ethanol, solubilized in urea buffer (8 M urea, 20 mM Tris, 23 mM glycine, and 0.2 mM EDTA). Normalized protein samples were electrophoresed on a sodium dodecyl sulphate polyacrylamide gel electrophoresis apparatus and immunoblotted with (0.45 μm IPVH00010; Merck) for 100 V (fixed) 1 h at 10°C using a Mini Trans-blot transfer system (Bio-Rad Laboratories, Hercules, CA, USA). Membranes were then incubated with primary and secondary antibodies listed (**Material Table 5**). ChemiDoc XRS Plus detection system (Bio-Rad) were used to obtain the results.

3.9.10 Detection of ROS by flow cytometry and CM-H_2DCFDA fluorescence

Petri dishes of 3 cm with 0.1% gelatin-coated were used to culture MEFs. Cells were treated with 10 nM TCDD for the indicated time, warm Hank's balanced salts solution (HBSS: Gibco-Thermo Fisher Scientific) were used to wash the cells, then incubated with 5 μM chloromethyl-2′,7′-dichlorofluorescein diacetate (CM-H_2DCFDA; C-6827, Life Technologies) in the dark with growth medium for 30 min at 37℃. After the incubation, HBSS were used to wash the cells twice, then examined using a Nikon inverted fluorescence microscope. More than three fields were captured for imaging data with a 10× objective lens and quantified the results by ImageJ (National Institutes of Health, Bethesda, MD, USA). WT MEFs basal value set as 1.0 for normalization. In the case of flow cytometry, samples were incubated in HBSS with 10 μM CM-

H_2DCFDA suspended in for 20 min dark at 37°C, propidium iodide treated after incubation of 15 min. PMT F505 LP bandpass filter LSR II flow cytometry (Bio-Rad) was used to detect CM-H_2DCFDA events.

3.9.11 Measurement of glutathione, 8-oxo-dGuo, MDA, NQO1 levels, and ROS cellular accumulation

8-oxo-dGuo concentration was quantified by liquid chromatography- mass spectrometry as described elsewhere [84]. The concentrations of GSH and GSSG (mmol/mg protein) were calculated using GSH assay kit (Cayman Chemical Co., Ann Arbor, MI, USA; 703002) standard curve and normalized against the protein concentration. The activity of NQO1 was recorded by 2,6-dichlorophenolindophenol reduction assay [85]. Lipid peroxidation was observed by using MDA as indicator, its level was determined by thiobarbituric acid reactive substance assay kit (Abcam, Cambridge, UK; ab18970) protocol was followed as manufacturer's instructions [86]. Net intracellular accumulation of ROS was observed by ROS-Glo™ H_2O_2 assay (Promega). With 2 h treatment of antioxidants or H_2O_2, HBSS washed twice on cells and ROS-Glo™ Detection Solution were added for 20 min, fluorescence was observed by GloMax® fluorometer (Promega).

3.9.12 Injection of xenograft

1×10^6 cells were cultured in a 10 cm dish as recommended density, cells were transfected for 48 h with mentioned overexpression or shutdown vectors by lentivirus system. Inject cells was mixed with Matrigel Matrix (Corning, Glendale, AZ, USA). 1×10^5 cells were subcutaneously injected into severe deficient immunocompetency (SCID) mice. 3 weeks recoreded of xenografts, and tumor weights (mg) were shown. After mice were sacrificed, xenografts were fixed (4% formldehyde) and supplied to biopsy experiments.

3.9.13 Gene clustering, gene categorization, and RNA sequencing

Illumina GAIIX instrument (Illumina Inc., San Diego, CA, USA) was used for RNA sequencing, and followed to the 50 bp single-end protocol (Welgene Biotech, Taipei, Taiwan) [74,87]. Data of RNA sequencing were deposited in NCBI BioProject Database (http://www.ncbi.nlm.nih.gov/bioproject) with the accession numbers

SUB3541857, SUB3541902, SUB3541913, and SUB3541945.

3.9.14 Immunofluorescence staining of p-MLC2, actin stress fibers, measurement of cell area, and wound-healing assay

Cells were seeded in 8-well chamber slides, which were pre-coated with 0.1% gelatin and cultured in complete medium for 6 h at 37°C for attachment, then followed with the TCDD (50 or 100 nM) or DMSO (0.1%) treatment. 4% formaldehyde for 30 min were used for cell fixing, permeabilized with 0.2% Triton X-100 in PBS for 15 min at room temperature. Subsequently blocking with 5% goat serum in PBS, cells were incubated overnight with rabbit anti-p-MLC (1:50, Cell Signaling Technology, Danvers, MA, USA) at 4°C. PBS washed then incubated with Alexa Fluor 594 goat anti-rabbit secondary antibody (1:400, Invitrogen) for 60 min at room temperature. Alexa Fluor 488-labeled phalloidin (1:80, Invitrogen) were used for actin counterstained in green to detect actin stress fiber. DAPI were used for blue staining of cell nuclei. Images from five fields were obtained by Nikon epifluorescence microscope. Intensity of fluorescence and cell area were calculated by ImageJ software (National Institutes of Health, Bethesda, ML, USA). For another experiments, serum starved overnight MEFs were treated with TCDD or DMSO for 24 h. Cells were washed with PBS, fixed with 4% formaldehyde, and stained for nuclei and F-actin. At least five different fields were acquired for the quantification.

Fully confluent (1.2×10^6) MEFs cells was used to conduct wound-healing assay using a 0.1% gelatin precoated six-well dish. 10 μg/mL mitomycin C were incubated with cells for 4 h at 37°C. 1 mL micropipette tip were used to create wounds, and the scraped cells were rinsed off with warm PBS. DMSO as the negative control or TCDD (10 or 50 nM) in culture medium were treated to the cells, incubated for 24 h. Results were analyzed by ImageJ software.

3.9.15 Statistical analyses

All results were shown as the mean ± SEM. Statistics in respective samples were done by GraphPad Prism 5.0 (GraphPad Software, San Diego, CA, USA). One-way ANOVA followed by a Tukey *post hoc* test or a two-way ANOVA with a Bonferroni *post hoc* test were used for multiple comparisons. Unpaired, two-tailed Student *t* test was used for the control and treatment groups comparison. To determine the effect of each site-directed mutagenesis on the *AhR* promoter, paired, one-tailed Student *t* test

was used. For analyses of cell areas, Mann–Whitney nonparametric median statistical test was used. $p < 0.05$ was indicated statistically significant.

3.9.16 Material Tables

Table 5. Antibodies used in this study

Antibody name	Company	Cat. No.	RRIDs
Arnt	Cell Signaling Technology	CST#5537	AB_10694232
HIF-1beta	Gene Tex	GTX128795	AB_2861418
AhR	Santa Cruz Biotechnology	SC-8088	AB_2223957
AhR	Santa Cruz Biotechnology	SC-133088	AB_2273721
Nrf2	Santa Cruz Biotechnology	SC-722	AB_2108502
Nrf2	Gene Tex	GTX103322	AB_1950993
Nrf2	Cell Signaling Technology	CST#14596	AB_2798531
Mafk (NF-E2p18)	Santa Cruz Biotechnology	SC-477	AB_2137821
Jdp2	A gift from Dr. A. Aronheim		
Jdp2	Santa Cruz Biotechnology	SC-517133	AB_2861419
Ahrr	Sigma-Aldrich	HpA019614	AB_1855109
β-actin	Santa Cruz Biotechnology	SC-47778	AB_2714189
FLAG-M2	Merck Millipore	F1804	AB_262044
MLC2	Cell Signaling Technology	CST#3672	AB_10692513
pMLC2	Cell Signaling Technology	CST#3671	AB_330248
GAPDH	Millipore	MAB374	AB_2107445
Phalloidin (=F-actin) Alexa-Fluor488-Phalloidin	Thermo Fisher Scientific	A12379	N/A
Normal Rabbit IgG	Cell Signaling Technology	CST#2729	AB_1031062
Normal Mouse IgG	Merck Millipore	12-371	AB_145840
Anti-Rabbit IgG HRP	Cell Signaling Technology	CST#7074	AB_2099233
Anti-Mouse IgG	Cell Signaling	CST#7076	AB_330924

HRP	Technology		
Anti-Goat IgG HRP	Santa Cruz Biotechnology	SC-2020	AB_631728
Alexa-Fluor ® 488 conjugated Goat anti-Mouse IgG	Thermo Fisher Scientific	A-11029	AB_138404
Alexa-Fluor® 488 conjugated Goat anti-Rabbit IgG	Thermo Fisher Scientific	A-11034	AB_2576217
Alexa-Fluor® 488 conjugated Rabbit anti-Goat IgG	Thermo Fisher Scientific	A-11078	AB_2534122
Alexa-Fluor ® 594 conjugated Goat anti-Mouse IgG	Thermo Fisher Scientific	A-11032	AB_2534091
Alexa-Fluor ® 594 conjugated Goat anti-Rabbit IgG	Thermo Fisher Scientific	A-11037	AB_2534095
Alexa Fluor® 647-conjugated Goat anti-rat IgG (H+L)	Cell Signal Technology	#4418	AB_1904017
Annexin V	BD Bioscience	51-65874X	AB_2888981

Table 6. Oligonucleotides

Regions	**Primer sequences**	**Amplified size (bp)**
ARE1	Sense 5'-CCTGGTAAATCTTGATGTCTGGG-3' Antisense 5'-ATGACGCAGGACGTAGTGAC-3'	159
ARE2	Sense 5'- CAGAATTTCCACCTTTTCCCACA-3' Antisense 5'-AGGAAAGAACACAGGAGTGC-3'	223
DRE1	Sensei 5'- ACTGCGCGGGGTCG-3' Antisense 5'-GTCCACCAGTTCGTCCTCC-3'	139
DRE2/3	Sense 5'- GACGAACTGGTGGACGGA-3' Antisense 5'- GGAGAAACCCGCACGCTA-3'	145
Ahrr	Sense 5′-TAGGAAGAGAAGGAAGCCCATTCA-3′	

	Antisense 5′-GGTGCCGTTTGGAAGGATTTG-3′	
Aldh3a	Sense 5′-TGCTGGAGAGGACTGTGTAGA-3′ Antisense 5′-GGTCGAGTCTTGCCTGAGTT-3′	
Cyp1b1	Sense 5′-TTACGGACATCTTCGGAGCC-3′ Antisense 5′-CCCACAACCTGGTCCAACTC-3′	
Tiparp	Sense 5′-ACGAAGGCTGTCTACACCAC-3′ Antisense 5′-CCCGAGAGTTGGCTTCTT CA-3′	
EMSA WT AhR-DRE1	Sense 5′- ACCGGGCGCGGCTAGCGTGCGGGTTT -3′ Antisense 5′- GAGAAACCCGCACGCTAGCCGCGCCC -3′	
EMSA mutant AhR-DRE1	Sense 5′- ACCGGGCGCGGCGCTACATCGGGTTT -3′ Antisense 5′- GAGAAACCCGATGTAGCGCCGCGCCC -3′	
EMSA WT AhR-DRE2	Sense 5′- TCGGTGCCCCACGCGTGTCCCGGAGAG -3′ Antisense 5′- AGCCTCTCCGGGACACGCGTGGGGCAC -3′	
EMSA mutant AhR-DRE2	Sense 5′- TCGGTGCCCCACTTCCACGGCGGAGAG -3′ Antisense 5′- AGCCTCTCCGCCGTGGAAGTGGGGCAC -3′	
EMSA WT AhR-DRE3	Sense 5′- CGGGCGGCAGCGTGTGTGTGCGCTCCCTT -3′ Antisense 5′- TCAAAGGGAGCGCACACACACGCTGCCGC -3′	
EMSA mutant AhR-DRE3	Sense 5′- CGGGCGGCACGTACACTGCCACCTCCCTT -3′ Antisense 5′- TCAAAGGGAGGTGGCAGTGTACGTGCCGC -3′	
EMSA WT AhR-ARE1	Sense 5′- TTTCCCACAGTGACTTTCCCAAGAAAGATG -3′ Antisense 5′- TTCCATCTTTCTTGGGAAAGTCACTGTGGG -3′	
EMSA mutant AhR-ARE1	Sense 5′- TTTCCCACAACAGTCCCTTCAAGAAAGATG -3′ Antisense 5′- TTCCATCTTTCTTGAAGGGACTGTTGTGGG -3′	

Table 7. siRNAs used in this study

siRNA	Santa Cruz Co.	Other company
Control siRNA	SC-44234	N/A
Negative control	#01 siRNA	Ambion ®. Thermo Fisher Scientific
siAhR	SC-29658	N/A
siAhRR	SC-140918	N/A
siNrf2	SC-37049	N/A

Table 8. Experimental models: organism/ strains

Organism/ strain	Origin
C57/BL6J Jdp2$^{-/-}$	RIKEN BioResource Research Center
C57/BL6J	RIKEN BioResource Research Center

Table 9. Experimental models: cell line

Cell line	Catalog number
C57/BL6J WT mouse embryonic fibroblasts (MEFs)	N/A
C57/BL6J Jdp2$^{-/-}$ mouse embryonic fibroblasts (MEFs)	N/A
HepG2	HB8065™
MCF7	HTB-22™
HEK293T	CRL-3216; PRID-CVCL.0063
HeLa S3	CCL-2.2™
NIH3T3	CRL-1658

Table 10. Critical commercial assay

Commercial kit	Company	Catalog number
KAPA HiFi PCR kit	KAPABIOSYSTEMS	KR0368-v13.19
Quick-Change Lighting Site-Directed Mutagenesis kit	Agilent Technologies	210513
PRO-PREPTM protein extraction solution	iNtRON Biotechnology	17081
NE-PER®Nuclear and cytoplasmic extraction kit	Thermo scientific	78833
GSH assay kit	Cayman Chemical Co.,	703002
ROS-GloTM H2O2 assay	Promega Co.	G8820

Table 11. Chemicals, peptides, and recombinant proteins

Commercial product	Company	Catalog number
Dimethyl sulfoxide (DMSO)	Sigma-Aldrich	D8418
Benzo[α]pyrene	Sigma-Aldrich	B1760

Tert-benzo hydroquinone (tBHQ)	Sigma-Aldrich	DHR3512
L-sulforaphane (L-SNF)	Sigma-Aldrich	S6317
6-firmyllindole [3,2-b]carbazole (FICZ)	Sigma-Aldrich	SML1489
L-Kynurenine	Sigma-Aldrich	K8625
2,3,7,8-terrachlorodibenzo-*p*-dioxin (TCDD)	AccuStandard	D-404N
4'-,6-diamino-2-phenylindole (DAPI)	Sigma-Aldrich	D9542
ProLong®Gold antifade mountant	Thermo Fisher scientific	P10144
Polyvinylidene difluoride membrane (PVDF)	Thermo Fisher scientific	88518
Lipofectamine 2000	Invitrogen	11668-50
Polyethylenimine Linear MW 25,000	Polysciences Inc.	23966
Protein A/G agarose beads	Merck Millipore	16-266
Proteinase K	Promega	EO0491
CM-H2DCFDA	Life Technologies	C-6827
Matrigel Matrix	Corning	356234
Mitomycin C	FUJFILM	JAN 4548995058638

Table 12. Recombinant DNA

Recombinant DNA	**Origin**
pcDNA-Nrf2	Tanigawa et al. 2013
pcDNA-Mafk	Tanigawa et al. 2013
pcDNA-Jdp2	Tanigawa et al. 2013
pcDNA-Jdp2A139C	This paper
pCMV S-FLAG	Pan et al. 2010
pQCIN-CA-AhR-EGFP	This paper
pCYP1b-luciferase	This paper
pPyCAG-BstXI-IRES-Zeocin-pA	This paper
pPyZmJdp2	This paper
pCAG-HIVgp	Tanigawa et al. 2013
pCMV-VSV-G-RSV-Rev	Tanigawa et al. 2013
CSII-CMV-MCS-IRES2-Bsd	Tanigawa et al. 2013
pGL4.1	Promega
pRL-CMV-Renilla luciferase	Tanigawa et al. 2013
pRL-CMV-Firefly luciferase	Tanigawa et al. 2013

Table 13. Software and algorithms

Software and algorithms	Website
ALGGEN-PROMO	http://alggen.lsi.upc.es/
Image Lab software version 4.1	https://www.bio-rad.com/en-tw/product/image-lab-software
Image J	https://imagej.nih.gov/ij/

Chapter IV FOXM1-CD44 signaling is important for the acquisition of regorafenib resistance in human liver cancer cells

This chapter is a modified version of the original work reported in the International Journal of Molecular Sciences (2022), and the publisher MDPI licensed the respective authors in accordance with the Creative Commons Attribution (CC-BY) 4.0 license, which has allowed me to use this paper as a part of my doctoral dissertation.

CSCs were characterized by their ability for self-renewal, proliferation, and increasing tumor formation occurrence. Previous research indicated that CSCs could induce EMT and are responsible for cancer metastasis [88]. HCC has been identified and established by liver progenitor cell markers and stem cell markers [30,31]. These results suggest the possibility of liver CSCs gaining a specific undifferentiated property during cancer progression [89,90]. From previous research, CSCs had been known to show increased resistance to chemotherapy and radiotherapy. Our previous research demonstrated that HepG2 cell line derived CSC-like cells by C-MYC, OCT4, SOX2, and KLF4 (OSKM, Yamanaka factors [91]), exhibited drug resistance when shTP53 knockdown lentivirus was combined. In addition, EMT markers EpCAM, CD133, and CD44 upregulation was enhanced [92].

A cell population of sorafenib-resistance was reported to be elevated in tumorigenicity, cancer stem-like characteristics along with high expression levels of CD133, epithelial progenitor marker cytokeratin 19, EpCAM, and CD90 [93]. US Food and Drug Administration in 2017 had approved regorafenib for second-line treatment of previously received sorafenib HCC adult patients [94]. Although patients shown survival benefit from regorafenib treatment, but the overall clinical outcome remains limited. FOXM1 is a member of the FOX transcription factor family, which has been demonstrated to play an important role in cancer differentiation, CSC renewal, and drug resistance [95,96]. FOXM1 upregulation in patients with HCC was known to be associated with a poor prognosis, this is also observed in lung cancer, and colorectal cancer [37].

4.1 Establishments of regorafenib-resistant cell lines

HepG2_Rego_R cells were continuously cultured for 6 months at the concentrations of 2-6 μM regorafenib. In this culture condition, weak attachment of the cell to the substratum was observed, but cell-cell attachment remained intact, aggregating to form spheroid structure (Fig. 27A). Colony-forming ability was observed absent of regorafenib 3.75-fold increase in HepG2_Rego_R cells than that in the parental HepG2 cells. The colony size treated with 5μM regorafenib seemed to be staggered but still increased 1.45-fold than that in cells treated with DMSO as control. In HepG2 cells with regorafenib treatment, no colonies were observed (Fig. 27B). By using the regorafenib at the concentration of 5μM, Hep3B_Rego_R cells were also obtained. The size of colony, number, and characteristic of Hep3B_Rego_R were similar to HepG2_Rego_R cells. HepG2_Rego_R cells spheroids were observed 2 to 5-fold larger then HepG2 cells both with or without the treatment of regorafenib (Fig. 27C); similar observations were confirmed with Hep3B_Rego_R cells (data not shown).

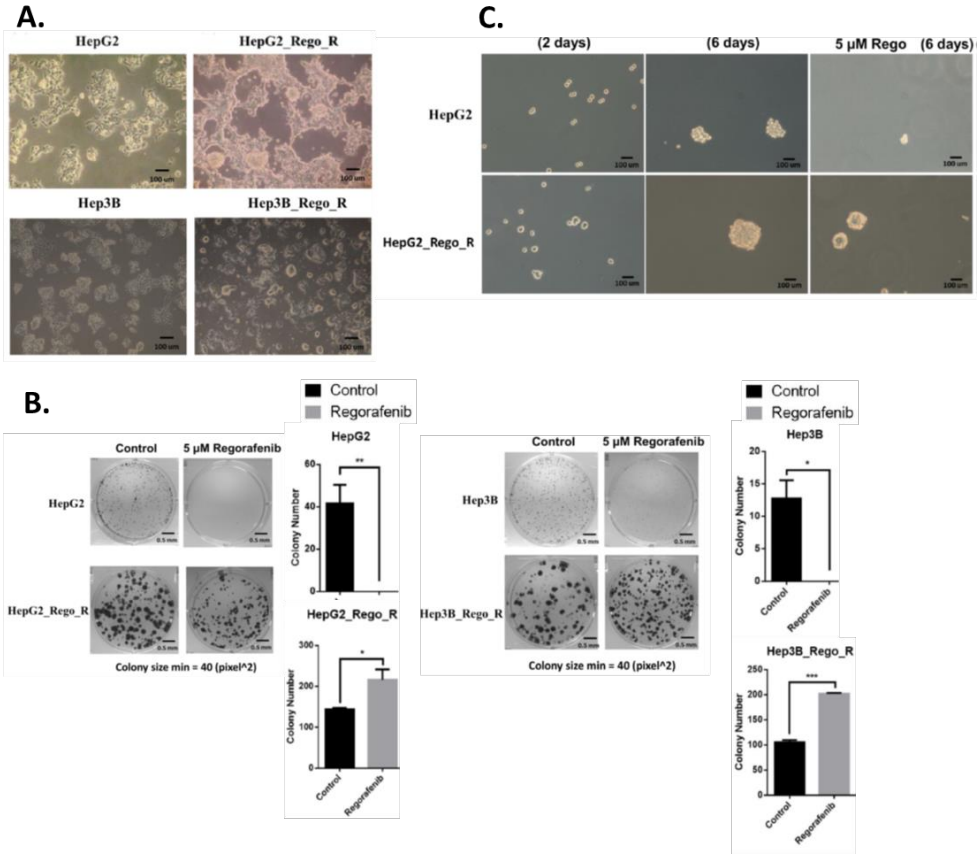

Fig. 27 Regorafenib insensitive HepG2 and Hep3B human hepatic cacinoma cells. **(A)** Morphologies of Hep3B cells, HepG2 cells, regorafenib-resistant cell lines

Hep3B_Rego_R cells, and HepG2_Rego_R cells. **(B)** HepG2, Hep3B, HepG2_Rego_R, and Hep3B_Rego_R cells colony-forming abilities. Results are shown as mean ± standard error of the mean (SEM; n = 3) and analyzed by one-way analysis of variance (ANOVA) with *post hoc* Tukey test (* $p < 0.05$ and ** $p < 0.01$). **(C)** Spheroids of HepG2 and HepG2_Rego_R cells morphology with the absent of regorafenib 2 and 6 days, and 5 μM regorafenib for 6 days. FOXM1-CD44 Signaling Is Critical for the Acquisition of Regorafenib Resistance in Human Liver Cancer Cells © 2023 by Wuputra K is licensed under CC BY 4.0.

4.1.1 Regorafenib-resistant cells shown CSC markers and *FOXM1* overexpression

By obtaining regorafenib-resistant cell lines, we next examined the expression of CD44, stage-specific embryonic antigen 4, GATA-binding factor 6, ATP binding cassette sub family G member 2 (ABCG2), and SOX2 as stem cell markers. These markers were upregulated in HepG2_Rego_R cells significantly (Fig. 28A) [97,98]. Previous studies indicated FoxM1 to be an oncogene in various kinds of cancers including lung [99], breast cancer [100], colorectal cancer [101], and HCC [102,103]. The expression level of FoxM1 was dramatically increased in HepG2_Rego_R cells; Aurora kinase A (AURKA) [103] and BIRC5/Survivin [104] the downstream targets of FoxM1 also significantly increased (Fig. 28B) in HepG2_Rego_R cells. The level of BIRC5/Survivin, AURKA, and FoxM1 protein expression was elevated compared with that in HepG2 cells (Fig. 28C). These findings indicated the regorafenib-resistant cancer cells exhibited characteristics of CSCs, with the expression of stem cell markers.

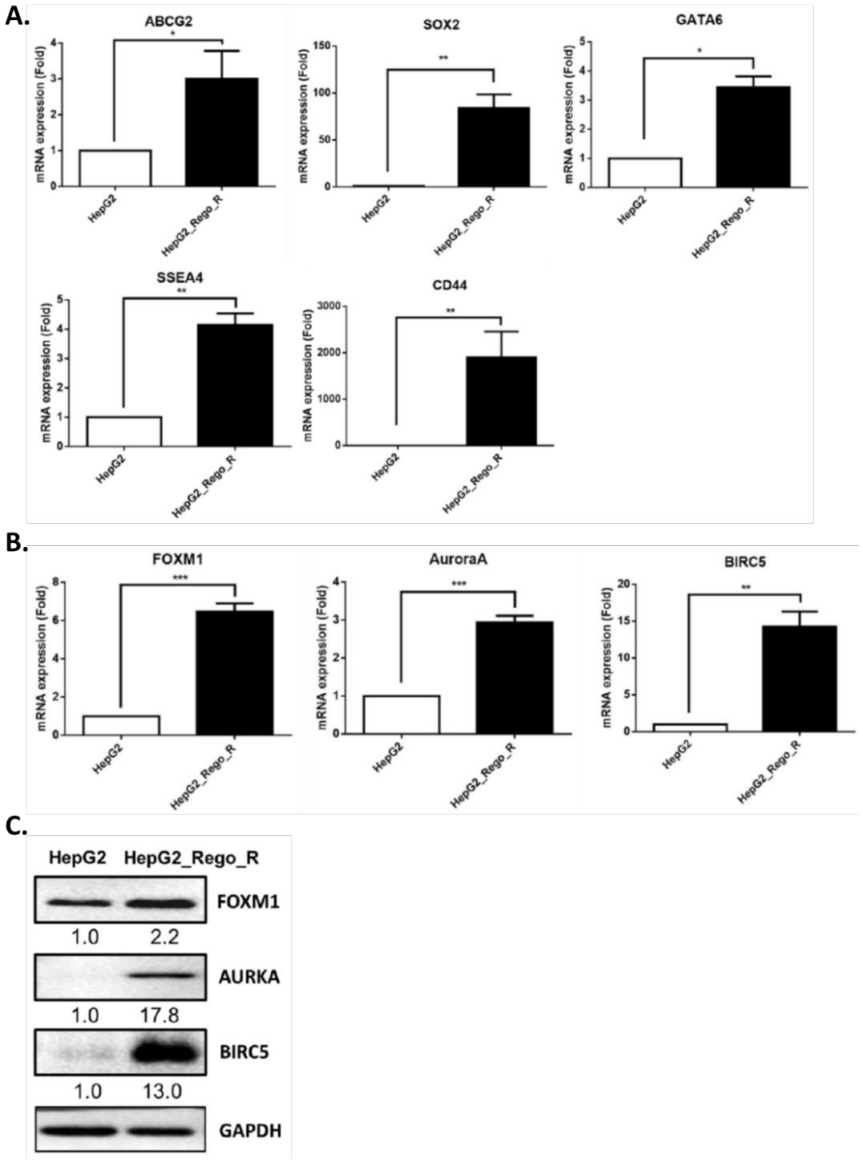

Fig. 28 HepG2 and HepG2_Rego_R cells CSC and Stem cell markers comparasion. **(A)** Different expression levels of SOX2, ABCG2, GATA-binding factor 6, CD44, and stage-specific embryonic antigen 4 RNA between HepG2 and HepG2_Rego_R cells. **(B)** Different expression levels of AURKA, BIRC5, and FOXM1 RNA compared of HepG2 and HepG2_Rego_R cells. **(C)** Protein levels of AURKA, BIRC5, and FOXM1 compared between HepG2 and HepG2_Rego_R cells. Relative levels of protein expression were analyzed by normalized to HepG2 cells. Results were shown as mean ± SEM (n = 5), analyzed by two-way ANOVA with *post hoc* Bonferroni test (* $p < 0.05$, ** $p < 0.01$, and *** $p < 0.005$). FOXM1-CD44 Signaling Is Critical for the Acquisition of Regorafenib Resistance in Human Liver Cancer Cells © 2023 by Wuputra K is licensed under CC BY 4.0.

4.2 Regorafenib-resistant cells shown EMT phenomenon

CSCs gaining the ability of self-renewal, invasion, and preventing apoptotic activity had been reported to be correlated with the EMT [105-107]. By using reverse transcription-quantitative polymerase chain reaction (RT-qPCR), EMT markers were measured in order to study changes in regorafenib-resistant cells (Fig. 28). Elevated expression level of zinc finger E-box binding homeobox 1 (ZEB1), twist family BHLH transcription factor 1 (TWIST1), and vimentin (VIMENTIN) were shown in HepG2_Rego_R cells. Results of EMT-related proteins, cadherin 1 (CDH1), CIMENTIN, TWIST1, ZEB1, cytokeratin 18 (CK18), and cytokeratin 7 (CK7) were also detected with western blotting. These mesenchymal cell markers have been reported to result in the elevation of cell motility, adhesion ability, and morphology change.[108-112]. Downregulation of epithelial markers CDH1, CK18, and CK7 indicated that cells were driven to express EMT phenotype [113-115]. Hep3B_Rego_R cells also display characteristics of EMT as observed in HepG2_Rego_R cells upregulate expression of ZEB1, VIMENTIN, and TWIST1/2 together with limited expression of epithelial markers CDH1, CK18, and CK7 (Fig. 29B). To further determine the HepG2_Rego_R cells migration properties, transwell migration assay was done. 2-fold or more of the migration ability of HepG2_Rego_R cells were increased than that in the parental HepG2 cells (Fig. 29C). These results suggested the liver cancer cells with regorafenib-resistant phenotype are more malignant than the parental cells.

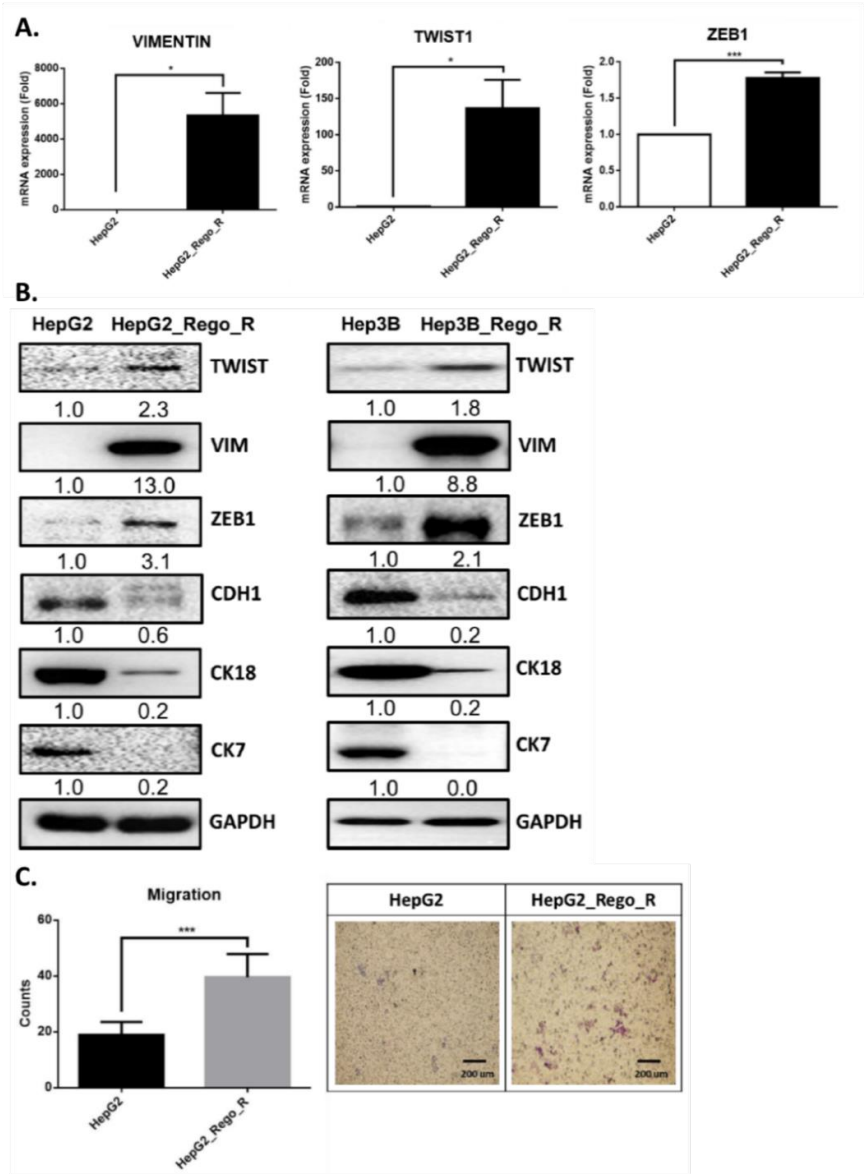

Fig. 29 EMT-related markers were compared between HepG2 and HepG2_Rego_R cells. (A) ZEB1, TWIST1, and VIMENTIN RNA expression were detected by RT-qPCR. Results shown as mean ± SEM (n = 5), analyzed by two-way ANOVA with *post hoc* Bonferroni test (*$p < 0.05$). **(B)** EMT-related proteins expression compared between Hep3B and Hep3B_Rego_R cells, or HepG2 and HepG2_Rego_R cells. Relative levels of protein expression are normalized as 1.0 in HepG2 and Hep3B cells. **(C)** Comparison of HepG2 and HepG2_Rego_R cells migration ability. Representative results were presented in the panel. All of the above results were shown as mean ± SEM (n = 3), and analyzed by Student's *t* test (*** $p < 0.005$). FOXM1-CD44 Signaling Is Critical for the Acquisition of Regorafenib Resistance in Human Liver Cancer Cells © 2023 by Wuputra K is licensed under CC BY 4.0.

4.3 FOXM1 inhibition promote regorafenib-resistant cancer cell death

In order to investigate the effect of FOXM1 in drug resistance and cancer progression, thiostrepton was used as FOXM1 inhibitor to clarify colony formation and cell death affect by FOXM1 [116]. 1μM thiostrepton were incubated with HepG2_Rego_R cells for 72 h, quantify the expression levels of CSCs and stem cell markers by western blotting. Remark decrease of RNA and protein expression were observed in BIRC5, FOXM1, CD44, as well as SOX2 levels of CSCs-related markers (Fig. 30A, B). Nevertheless, EMT markers expression revealed inconsistent results; while both of CDH1 and CK18 were upregulated, TWIST 1/2 shown downregulated pattern after the exposure to thiostrepton (Fig. 30A). These results suggested that the different expression pattern of EMT markers was due to heterogeneity, which possessed different sensitivity of TWIST 1/2 and other markers such as CK18 and CDH1 (Fig. 30A, B). Cell viability was tested in various dose of thiostrepton for 48 h (Fig. 30C), and 72 h (Fig. 30D). The inhibition of FOXM1 shown also significantly affected the volume of sphere and ability of sphere formation in Hep3B_Rego_R cells and HepG2_Rego_R (Fig. 31A, B). Furthermore, ability of forming colony in HepG2 and HepG2_Rego_R significantly reduced compared with DMSO-treated cells as control (Fig. 31C).

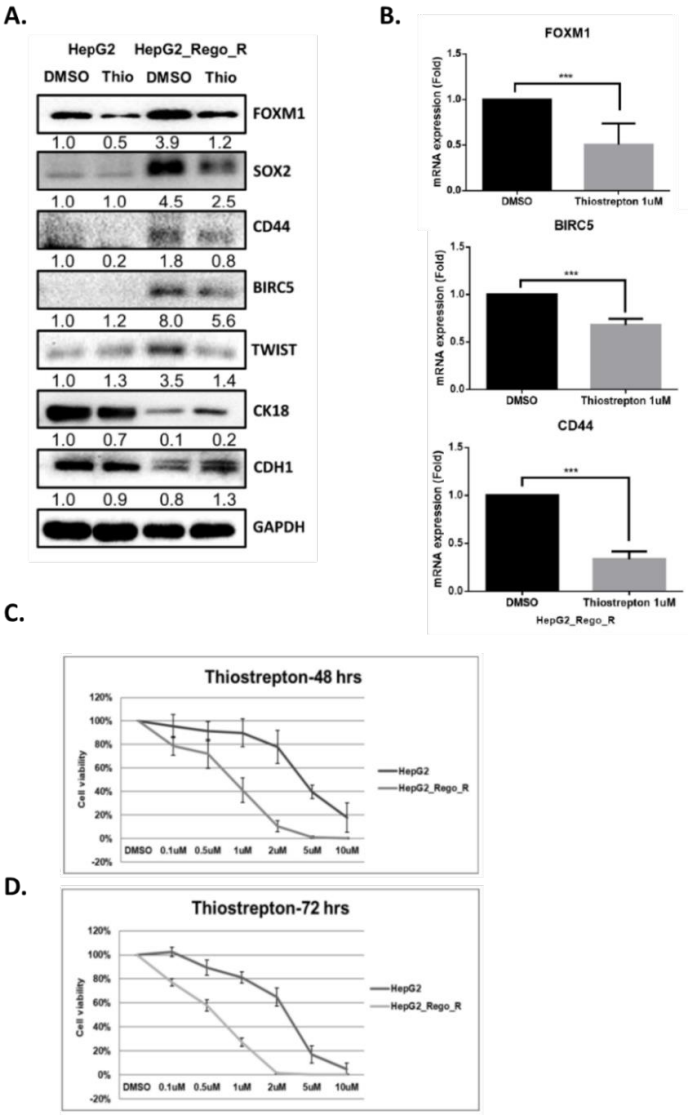

Fig. 30 Antibiotic thiostrepton treatment inhibits pathway-related proteins of FOXM1 signaling, sphere formation, and viability in HepG2_Rego_R cells. (A) Levels of related FOXM1 signaling proteins expression compared between HepG2 and HepG2_Rego_R cells in the presence of thiostrepton for 72 h by blotting. **(B)** BIRC5, CD44, and FOXM1 RNA expression level in HepG2 and HepG2_Rego_R cells in the presence of thiostrepton were analyzed by RT-qPCR. Results were shown as mean ± SEM (n = 5), analyzed by two-way ANOVA with *post hoc* Bonferroni test (*** $p <$ 0.005). **(C, D)** HepG2 and HepG2_Rego_R cells viabilities in the 48 h treatment of thiostrepton (panel C) and 72 h (panel D). Results were shown as mean ± SEM (n = 5) and calculated by Student's *t* test (*$p < 0.05$). FOXM1-CD44 Signaling Is Critical for the Acquisition of Regorafenib Resistance in Human Liver Cancer Cells © 2023 by Wuputra K is licensed under CC BY 4.0.

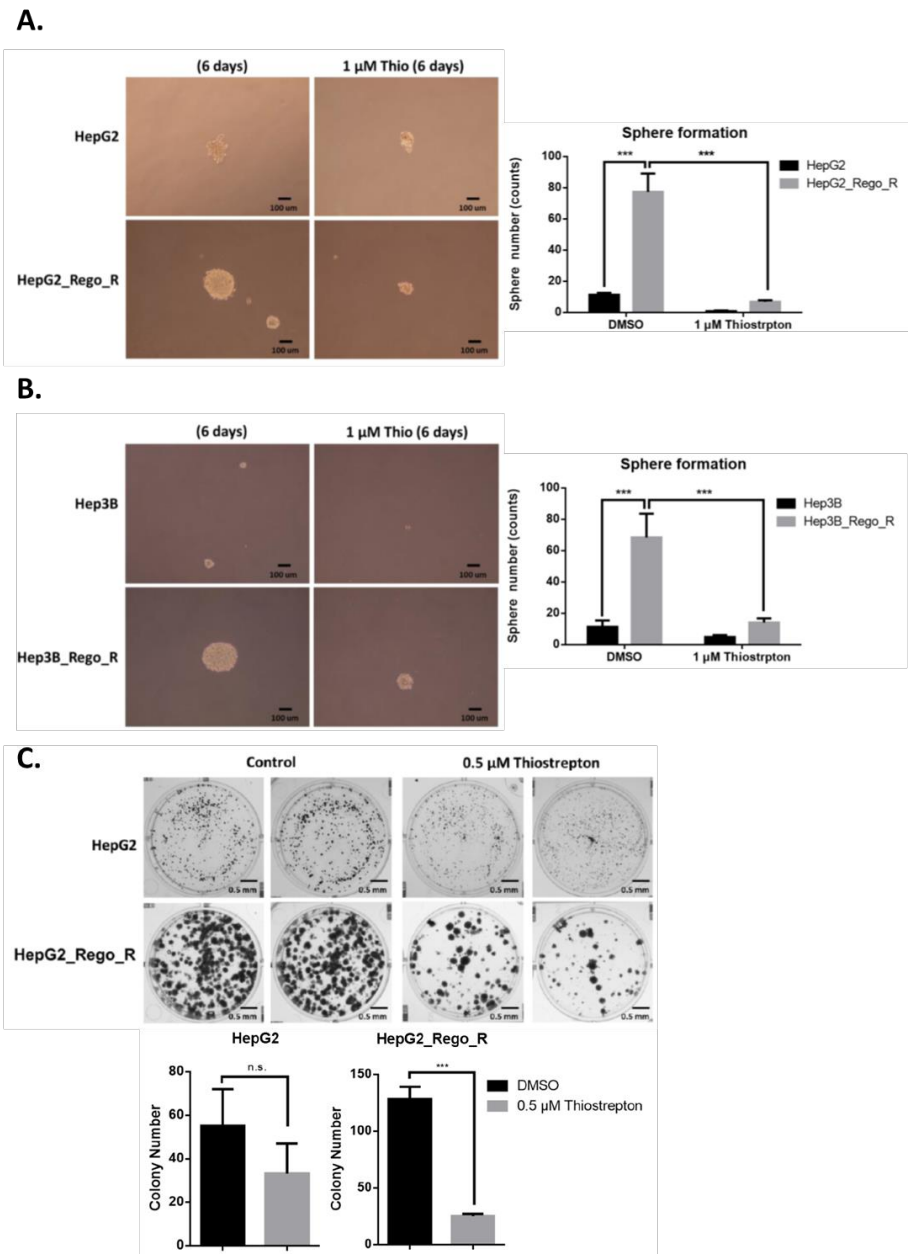

Fig. 31 Sphere forming comparation between regorafenib-resistant cell lines and their original cell lines. The HepG2 and HepG2_Rego_R cells **(A),** as well as Hep3B and Hep3B_Rego_R cells **(B)** were incubated with thiostrepton 1µM for 6 days. Statistical analysis was calculated by two-way ANOVA with *post hoc* Bonferroni tests (*** $p < 0.005$). **(C)** Comparative analysis of colony formation between HepG2 and HepG2_Rego_R cells. Colony number was calculated as represent mean ± SEM (n = 5). Data are analyzed using student t-test (***p<0.0005). FOXM1-CD44 Signaling Is Critical for the Acquisition of Regorafenib Resistance in Human Liver Cancer Cells © 2023 by Wuputra K is licensed under CC BY 4.0.

4.4 CSCs population and CD44 and SOX2 expression was inhibited by FOXM1 knockdown in regorafenib-resistant cells

By using siRNA (siFOXM1) and short hairpin RNA (shFOXM1), the knockdown experiments of FOXM1 were performed on Hep3B_Rego_R and HepG2_Rego_R cells. CSCs markers including CD44 and SOX2 expression in protein level were markedly reduced (Fig. 32A). AURKA protein level expression was also decreased 50% in knockdown cells (Fig. 32B) compared with controls in both Hep3B_Rego_R, and HepG2_Rego_R cells. This result may be controlled by availability of nutrient as previous studies described [117,118]. To further examine FOXM1 effect in CSCs, nutrient deprivation experiments were conducted. Hep3B_Rego_R and HepG2_Rego_R were transfected with or without shFOXM1, and their parental cells were cultured in Dulbecco's Modified Eagle's Medium (DMEM) containing 1% fetal bovine serum (Fig. 32E, F). Both Hep3B_Rego_R and HepG2_Rego_R showed moderate survival rate than their parental cells. The introduction of shFOXM1 also showed significant decrease of survival and sphere formation.

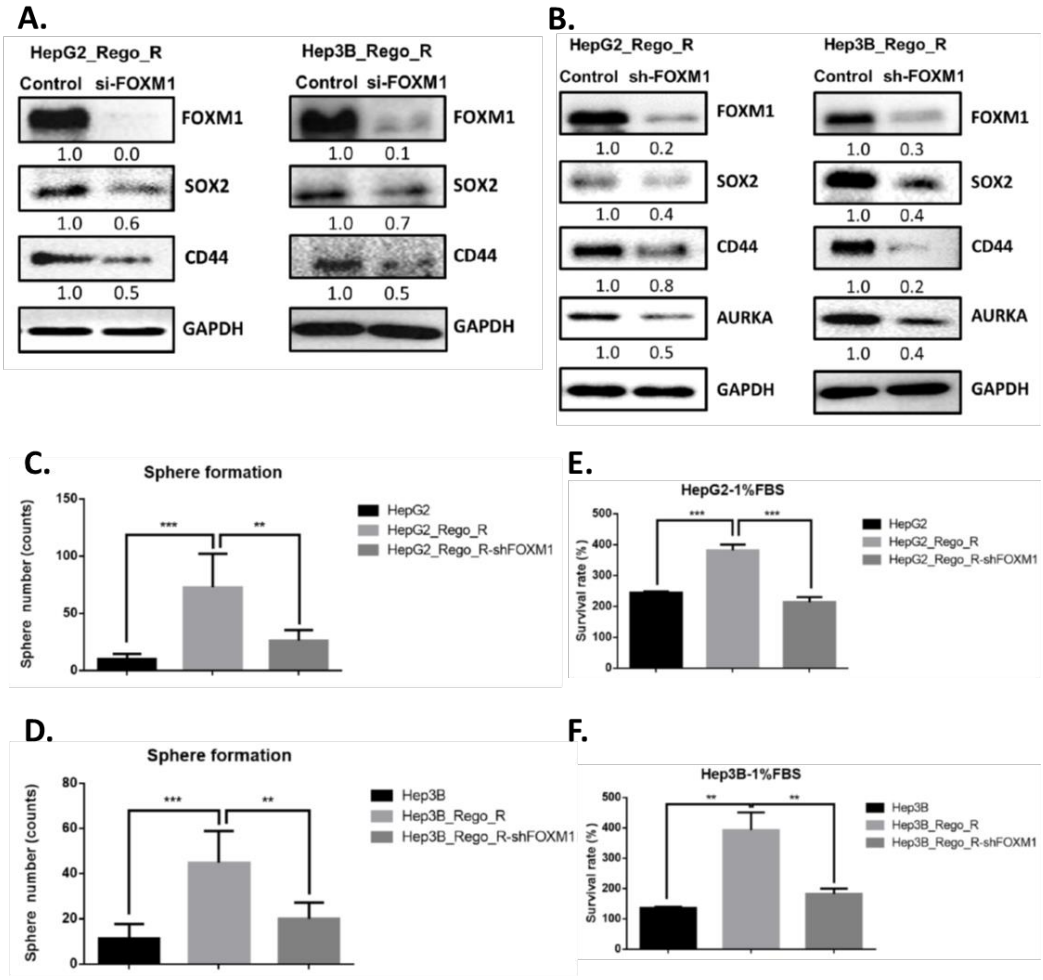

Fig. 32 FOXM1 knockdown results in downregulation of CD44 and SOX2 expression, CD44-promoter activities, and sphere formation in Hep3B_Rego_R and HepG2_Rego_R cells. (A, B) The expression of CSC-related proteins CD44, SOX2, and FOXM1 in Hep3B_Rego_R and HepG2_Rego_R cells were compared in the presence of siFOXM1 **(A)** and shFOXM1 **(B)**. Expression levels calculated as relative expression based on the in the cells treated with the scramble siRNA or mock shRNA. **(C)** Abilities of sphere-forming in Hep3B_Rego_R and HepG2_Rego_R cells in the presence of shFOXM1. Results were shown as mean ± SEM (n = 5) and calculated by one-way ANOVA and *post hoc* Tukey test (** $p < 0.01$ and *** $p < 0.001$). FOXM1-CD44 Signaling Is Critical for the Acquisition of Regorafenib Resistance in Human Liver Cancer Cells © 2023 by Wuputra K is licensed under CC BY 4.0.

The expression of CD44 was strongly correlated with protein level of FOXM1 [119]; FOXM1 can be an important factor of activating CD44 promoter. By conducting luciferase assay of CD44 promoter, HepG2_Rego_R_cells activity of CD44 promoter was significantly increased compared with parental HepG2 cells. FOXM1 knockdown resulted in limiting the luciferase activity of CD44 promoter (Fig. 33). These findings indicated CD44 and SOX2 expression can be reduced by knockdown of FOXM1, as well as sphere formation, cell death, and cell proliferation as CSCs property in regorafenib-resistant cells.

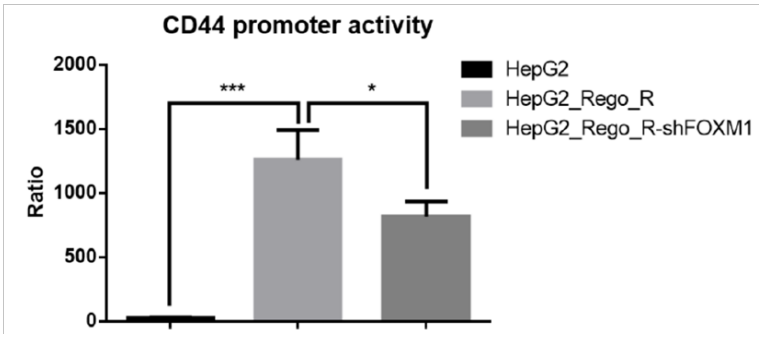

Fig. 33 HepG2 and HepG2_Rego_R cell activities of CD44-promoter compared. HepG2_Rego_R cells activity were significantly enhanced compared to HepG2. Treated with FOXM1 shRNA, the activity was reduced approximately by 65%. Results are shown as mean ± SEM (n = 4) and analyzed by one-way ANOVA with *post hoc* Tukey test (* $p < 0.05$ and *** $p < 0.001$). FOXM1-CD44 Signaling Is Critical for the Acquisition of Regorafenib Resistance in Human Liver Cancer Cells © 2023 by Wuputra K is licensed under CC BY 4.0.

4.5 Overexpression of *FOXM1* was associated with tumor growth and poor prognosis in HCC patients

In order to study possible downstream proteins of FOXM1 signaling pathway including BIRC5 and AURKA, whole HCC patient cohorts including hepatitis virus infection were separated into expression groups of low and high. By using Cancer Genome Atlas database, we discovered the high expression patient group of AURKA, BRIC5, and FOXM1 showed to have the worse overall survival rate compared to that in the low expression group regardless of the hepatitis virus infection (Fig. 34). In addition, CSCs and EMT markers expressed SOX2, CD44, VIMENTIN, and ABCG2 were highly correlated with HCC patient survival. Similar result was observed in FOXM1; total patient cohort with high level of SOX2, CD44, VIMENTIN, and ABCG2 expression exhibited poor prognosis than with low expression patient cohort (Fig. 34B, C). Nonetheless, HCC and hepatitis virus infection patients shown elevated level of VIMENTIN and ABCG2 expression with longer survival rate than low expression patients (Fig. 34B, C).

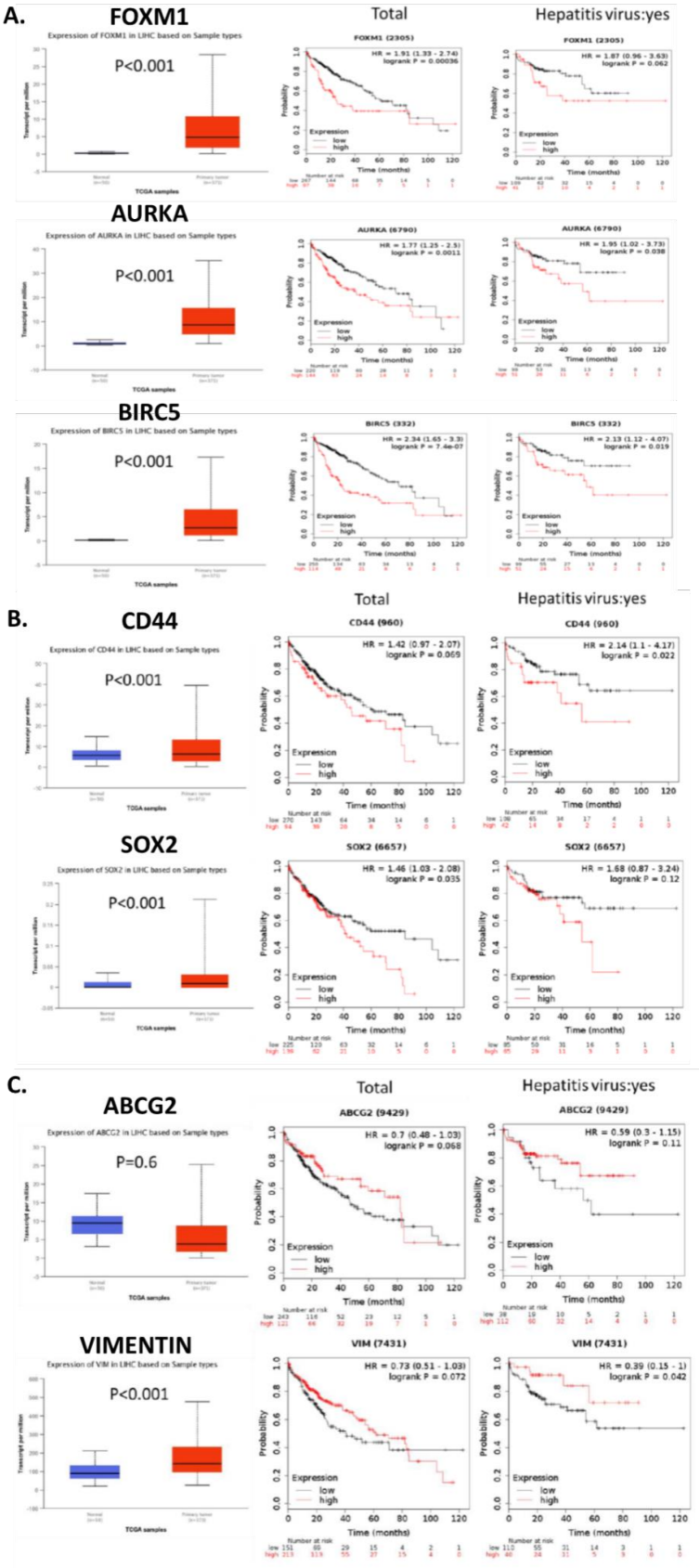
A.
FOXM1
Expression of FOXM1 in LIHC based on Sample types
P<0.001
Transcript per million
TCGA samples
Normal
Primary tumor
Total
FOXM1 (2305)
HR = 1.91 (1.33 - 2.74)
logrank P = 0.00036
Probability
Expression
low
high
Time (months)
Number at risk
Hepatitis virus:yes
FOXM1 (2305)
HR = 1.87 (0.96 - 3.63)
logrank P = 0.062
AURKA
Expression of AURKA in LIHC based on Sample types
P<0.001
AURKA (6790)
HR = 1.77 (1.25 - 2.5)
logrank P = 0.0011
HR = 1.95 (1.02 - 3.73)
logrank P = 0.038
BIRC5
Expression of BIRC5 in LIHC based on Sample types
P<0.001
BIRC5 (332)
HR = 2.34 (1.65 - 3.3)
logrank P = 7.4e-07
HR = 2.13 (1.12 - 4.07)
logrank P = 0.019
B.
CD44
Expression of CD44 in LIHC based on Sample types
P<0.001
CD44 (960)
HR = 1.42 (0.97 - 2.07)
logrank P = 0.069
HR = 2.14 (1.1 - 4.17)
logrank P = 0.022
SOX2
Expression of SOX2 in LIHC based on Sample types
P<0.001
SOX2 (6657)
HR = 1.46 (1.03 - 2.08)
logrank P = 0.035
HR = 1.68 (0.87 - 3.24)
logrank P = 0.12
C.
ABCG2
Expression of ABCG2 in LIHC based on Sample types
P=0.6
ABCG2 (9429)
HR = 0.7 (0.48 - 1.03)
logrank P = 0.068
HR = 0.59 (0.3 - 1.15)
logrank P = 0.11
VIMENTIN
Expression of VIM in LIHC based on Sample types
P<0.001
VIM (7431)
HR = 0.73 (0.51 - 1.03)
logrank P = 0.072
HR = 0.39 (0.15 - 1)
logrank P = 0.042

Fig. 34 Expression of FOXM1 positively correlated with HCC patient poor prognosis, and larger tumor growth of mice xenografts. (A-C) AURKA, FOXM1, BIRC5, SOX2, CD44, VIMENTIN, and ABCG2; Kaplan-Meier survival curve was calculated with the expression level of mentioned gene from The Cancer Genomic Atlas database from patients with hepatitis virus infection as well as HCC (n=150) and whole cohort of patient with HCC (n=364). FOXM1-CD44 Signaling Is Critical for the Acquisition of Regorafenib Resistance in Human Liver Cancer Cells © 2023 by Wuputra K is licensed under CC BY 4.0.

At last, to clarify FOXM1 in tumor progression, xenotransplantation experiment was conducted (Fig. 35A). HepG2_Rego_R and HepG2 cells were injected to severe combined immunodeficiency mice subcutaneously with or without treatment of thiostrepton. Tumor weight showed the HepG2_Rego_R tumors were around 10-fold increase than tumors of HepG2 group (Fig. 35B). Moreover, abnormal mitosis, necrosis, and numbers of giant cells all showed significant higher in HepG2_Rego_R cell group when compared with HepG2 control (Fig. 35C). These findings suggested FOXM1 played a crucial role in the HCC patients survival rate and HCC progression.

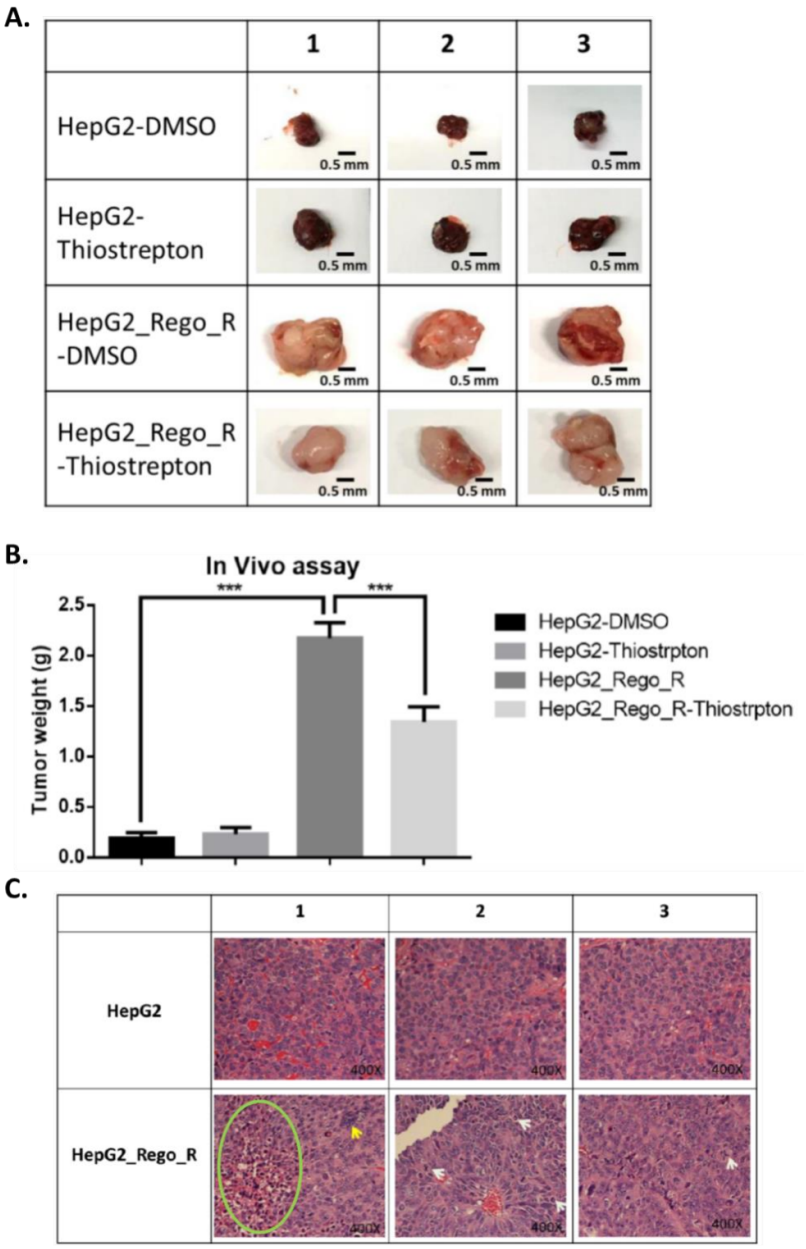

Fig. 35 Comparative growth of HepG2_Rego_R cells and HepG2 xenografts in the presence or absence of antibiotic thiostrepton treatment. (A) Morphologies of xenograft tumors, three representative trails were shown. **(B)** Tumor weight of each groups were measured with multiple repeats (n=3), analyzed by one-way ANOVA with *post hoc* Turkey test (***p <0.001). **(C)** Representative result of histochemical analysis using hematoxylin staining. Necrosis is indicated in green circle, label of giant cells in yellow arrow, white arrow stands for abnormal mitosis. FOXM1-CD44 Signaling Is Critical for the Acquisition of Regorafenib Resistance in Human Liver Cancer Cells © 2023 by Wuputra K is licensed under CC BY 4.0.

4.6 Materials and Methods

4.6.1 Cell preparation

Hep3B and HepG2 human HCC cell lines were produced as description [92]. Hep3B_Rego_R and HepG2_Rego_R regorafenib-resistant cell lines were established by incubating cells with regorafenib (concentration from 2 μM to 6 μM; for at least 6 weeks). The cells were kept to be exposure by 6 μM regorafenib for experiments hereafter.

4.6.2 Transfections of shRNA, plasmid DNA, and siRNA

Plasmid DNAs, shRNA, and siRNA for FOXM1 were transiently transfected into Cells (5×10^6) by using Lipofectamine 2000 (Thermo Fisher Scientific, Waltham, MA, USA). Cells were harvested for experiments after 48 h incubation. Efficient clones were selected after shRNA transfection for 48 h for further analysis, the reduction of FOXM1, were quantify by RT-qPCR and western blotting. The control nontarget siRNA and siRNA for FOXM1 were purchased from Horizon Discovery (Level Biotechnology, Inc., New Taipei, Taiwan; D-001810-10-05 and L-009762-00-0005). shRNAs were obtained from RNAi core, Academia Sinica, Taipei, Taiwan (TRCN0000273981 and ASN0000000003).

4.6.3 Cell viability assay

96-well plates were seeded with cells (5×10^3), incubated with mentioned concentrations of thiostrepton (T8902, Sigma-Aldrich, St. Louis, MO, USA) and regorafenib (Stivarga, Bayer Pharma AG, Berlin, Germany) for 72 h. Viability of cells was examined by using the 3-(4, 5-dimethylthiazolyl-2)-2, 5-diphenyltetrazolium bromide assay (0.5 mg/mL). The 50% inhibitory concentration of the drugs was determined from the assay.

4.6.4 Dual-luciferase assay

pRL-CMV plasmid encoding Renilla luciferase and CD44P pGL3 plasmid (19122; Addgene, Watertown, MA, USA) were transiently transfected into cells (5×10^6) by using Lipofectamine 2000 (Invitrogen, Waltham, MA, USA). The cells were incubated for 48 h, collected; Dual-Luciferase Reporter Assay System (Promega, Madison, WI, USA) were used to obtain luciferase activities. Protocols were followed according to the manufacturer's protocol.

4.6.5 3D-Sphere- and Colony- formation assays

Sphere- and colony-formation experiments were conducted as previous description [92]. In summary for sphere formation assay, cells were cultured in serum-free DMEM (HyClone, Cytiva, Tokyo, Japan) supplemented with B-27 (Invitrogen), 20 ng/mL basic fibroblast growth factor (ProSpec-Tany TechnoGene Ltd., Rehovot, Israel), and 20 ng/mL epidermal growth factor. Six well plates (ultra-low-attachment plates; Corning, Glendale, AZ, USA) were used for seeding cells, sphere formation was observed by microscope for 6 days incubation. In the case of colony-formation assay, gelatin-coated dish was seeded with 5×10^2 cells. After incubation for 14 days colonies were stained with Giemsa staining solution (Wako Chemicals, Tokyo, Japan), recorded. Colonies with diameter larger than 2 mm were included into analysis data.

4.6.6 Migration assay

Recommended cell concentrations were seeded on a transwell plate as manufacturer's instructions, cultured in serum free medium. The transwell was then placed on a well of 12-wells plate containing 10% fetal bovine serum in the culture medium for 48 h. Cells migrated to the lower surface of filter were fixed, labeled, and recorded under a microscope.

4.6.7 Western blot analysis

Western blot was conducted as described [92]. The following antibodies were used: anti-BIRC5 (GTX100441), anti-FOXM1 (GTX100276), anti-AURKA (GTX13824), anti-TWIST1/2 (GTX127310), anti-CD44 (GTX102111), anti-ZEB1 (GTX105278), anti-CK18 (GTX105624), anti-CDH1 (GTX02618), anti-VIMENTIN (GTX100619), and anti-CK7 (GTX109723), these antibodies were distributed from GeneTex, Hsinchu City, Taiwan; anti-SOX2 (AB5603), and anti-GAPDH (MAB374), were distributed from Merck Millipore (Burlington, MA, USA).

4.6.8 Animal and *in vivo* tumor xenograft model

Cells (1×10^6) were subcutaneously injected into severe combined immunodeficiency mice (male, 8 weeks; the National Laboratory Animal Center [NLAC], Taipei, Taiwan). Tumor size was evaluated by the formula, tumor volume = (length × width^2)/2. Mice were sacrificed after four weeks of incubation, tumors were cut-out, fixed in paraformaldehyde (4%), paraffin embedding, and sectioned. Then, they were stained by hematoxylin and

eosin. Animal welfare approved guidelines were followed in all of the experiments were proceeded. The care of animals in laboratory issued by the Kaohsiung Medical University, and National Laboratory Animal Center in Taiwan. All animal experiments were cunducted in accordance with these approved guidelines.

4.6.9 Statistical analyses

Results are shown as mean ± SEM from at least three experiments. One-way ANOVA ($p < 0.0001$) with *post hoc* two-tailed Student's t tests was used to evaluate statistical significance. Kaplan–Meier method were used to conduct survival analysis, and the curves were analyzed by log-rank test. Statistically significance was set at $p < 0.05$.

Chapter V Discussion

The balance of antioxidant and oxidant reactions is one of the most imoprtant factor of ROS homeostasis control. The collaboration of phase I detoxification and phase II detoxification enzyme systems is the most important propulsion of ROS signalling and modulation [120,121]. In the present study, AhR functions as phase I enzymes crucial regulator, and it is mediated by small Maf of phase II regulator enzymes and Nrf2 as spatiotemporal manner [24]. Several lines of evidence were provided in this research.

First, the phase I response activated by AhR agonists was involved in the activation of the Nrf2–Jdp2 axis in a spatiotemporal manner on the *AhR* promoter, which Jdp2 is crucial when *AhR* was activated (Figs. 4 and 12).

Second, Jdp2-mediated Nrf2 and AhR complexes ineract on *AhR* promoter DRE2 site, interaction followed with sequencial participation of ARE1 at the Ap-1 site activated by AhR agonists. Exposure to the phase I ligand TCDD for 2 h, DREs were shown to be critical for determine the selective gene expression in phase I response. Exposure to the ligand for 6 h, AREs were important for increasing the activity of the *AhR* promoter. For 24 h exposure, degradation of nuclear AhR protein was observed, and for maintaining *AhR* promoter activity the Ap-1 was shown to be responsible site (Fig. 17A). In order to deal with AhR agonists in cell, first Jdp2 acted as an coordinated component or upstream element in AhR gene battery, subsequently Nrf2 gene battery.

Third, ROS homeostasis was maintained through Jdp2 controlling AhR–Nrf2-mediated ROS production in order to response AhR agonists. In this study, 2 h of TCDD exposure shown to be elevated the ROS production, the response peaked at 6 h exposure, and shown to be reduced at 24 h of exposure. Judging from the information mentioned above, ROS production appears to depend on DRE commitment. Jdp2 was observed crucial for cell migration and spreading on TCDD triggered ROS response. Under the exposure of TCDD, Jdp2–Nrf2, Jdp2–AhR, AhR–Arnt, and Jdp2–MafK were identified as a massive complex (Figs. 18 and 19). This complex, was recruited to DRE2, further activated the AhR promoter, initiating RNA polymerase II and highly possible responding to the activity of Jdp2 as histone chaperone [26,122].

Fourth, the activated AhR agonists triggered Jdp2 activity. As an upstream factor Jdp2 serve as *AhR* transcription phase I enzyme, and a transcription factor Nrf2 in phase II enzyme, aided the sustain of ROS homeostasis. Various AhR agonists generate

different responses of the activation involving Nrf2 or Jdp2 complex. Compared with the resulting impact of 2 h TCDD incubation in Wild type (WT) MEFs, AhR and Nrf2 showed greater interaction than incubation with 2 h DMSO. Nevertheless, AhR and Arnt interaction was observed to be elevated for 2 h TCDD treatment than with DMSO. These results were not observed in *Jdp2*$^{-/-}$ MEFs (Fig. 19).

Fifth, CSCs insensitive to ROS and resistant to regorafenib can be rescued by deprivation of FOXM1 expression. It has been demonstrated that CSC-like cells created from the original HepG2 cells by introducing C-MYC, OCT4, SOX2, and KLF4 (OSKM, Yamanaka factors) by using knockdown lentivirus shTP53 have more resistance to chemotherapy and radiotherapy than previously observed. [92]. In this research, FOXM1 was identified as the key factor of resistance (Fig. 32). The FOXM1 inhibitor, thiostrepton, employed to restore cell death in regorafenib-resistant cells is much more efficient (Fig. 30).

The data acquired and described above were published in international scientific journals and subjected to peer review. The details of each finding will be discussed in the following sections.

5.1 The role of Jdp2 in AhR–Nrf2 ROS homeostasis signaling

In previous research, Jdp2 was reported to be an antioxidation ARE *cis*-element stimulator through interacting MafK and Nrf2 complex [24]. Our report demonstrated Jdp2 also functions as an AhR promoter stimulator, and can control ROS production in order to maintain the homeostasis of oxidative stress. The effect of Jdp2 exposed to phase I ligands interactct with phase I and phase II enzymes in cells was investigated. The reaction starts with the specific activation that govern AhR–ARNT recruitment to DREs, then followed by AhR degradation that switches from DRE to ARE to maintain oxidative homeostasis. The results shown the degradation of AhR is crucial for *ARE* gene activation, the role of Jdp2 acts as a positive modulator to drive the shifting of oxidation phase to antioxidation, maintaining the homeostasis of ROS.

5.2 Activation of AhR-dependent stimulation of homeostasis gene battery

In this study, DMSO at a concentration of 0.1% employed for cell exposure (v/v), and commonly used as a solvent for amphiphilic organic agents, can induce phase I enzymes by triggering the key transcription factor, AhR, and generate oxidative stress

through ROS. The treatment of DMSO can significantly increase *AhR* promoter at a concentration of 0.1% in MEFs. Nrf2, with Jdp2 and AhR–ARNT acting as the coupling factors of "AhR target gene batteries," triggers *AhR* promoter activation [24]. The AhR promoter activation, which was detected rapidly within DMSO treatment for 2 h, afterwards stimulate MEFs apoptosis and spreading (Fig. 10 and 11). We showed that the AhR transcription is regulated by Nrf2 and Jdp2 in response to DMSO. Jdp2 seems to be the linking factor for the phase I and II enzymes batteries, and their functions in ROS control (Fig. 10F).

One of the well known ligand of the AhR gene battery, TCDD activate AhR by binding to the AhR–Heat shock protein 90 complex ligand-binding pocket [3]. The encoded enzymes of *AhR* gene battery include both phase I, for examples CYP1B1, 1A1 and 1A2, phase II enzymes, UGT 1–6, GSTA2, and NQO1 [123]. TCDD as an AhR agonists, possess the ability to activate both types of enzymes. Yeager et al. [20] demonstrated Nrf2 was crucial for induction of AhR battery classical genes *Gst*, *Ugt,* and *Nqo1* in liver cells of mouse through TCDD, yet insufficient to promote drug-processing genes *in vivo* by themselves. Using chromosome immunoprecipitation (ChIP) assay in liver cells of mouse, AhR can bind to 5' flanking region of mouse *Nrf2* DRE-like sequences directly [14]. In addition, Wang et al. reported that TCDD stimulates interactions between Nrf2 and AhR, or Keap1 and AhR in the AhR–Arnt interactions [21]. Furthermore, AhR, ARNT, and Nrf2 complexes formed by TCDD stimulation bind to DRE- or ARE-containing enhancers.

The activation of AhR-dependent Nrf2 and DNA-binding kinetics shown consistent delayed of Nrf2 after the activation of AhR. These mediated expressions of genes are designated as a response to "AhR–Nrf2 gene battery" [64]. *Nrf2* promoter shown the implicates of AhR–ARNT involvement through the presence of DRE and ARE *cis*-elements and the Mrf2-mediated antioxidation response.[14]. Nevertheless, Nrf2 and AhR interactions on *cis*-elements, the product of AhR-elicited ROS, and the subsequent activation of Nrf2 are still unclear.

5.3 Modulation of Jdp2 in AhR–Nrf2 gene battery in cancers

In this study, in order to confirm the effect of Jdp2 in the Nrf2 gene battery a model pancreatic carcinoma of *kRAS-P53*-mutated cancer cell line was used. Endogenous and exogenous phase I ligands activate the production of ROS through AhR pathway, then

protect the cell against ROS via activation of the Nrf2 pathway. ROS production can alter cell functions, such as migration, apoptosis, inflammation, and EMT, by agitate the cellular generated ROS balance from AhR–Nrf2 gene battery, which is crucial for cancer initiation. AhR promoter response mediated by DRE2 *cis*-element required Jdp2 signaling in MEFs. Jdp2, Nrf2, and AhR was also involved in the production of ROS (Fig. 26). The growth of xenograft tumors can be significantly increased by inhibition of Jdp2 expression. But aberration through overexpressing AhR. This result suggests that Jdp2 is upstream of the AhR–Nrf2 gene battery and work as a tumor suppressor (Fig. 26E).

The obsearvation of cancer generated ROS revealed that Warburg effect was involved. Nrf2–MafK, AhR–ARNT, and Jdp2 components were detected by ChIP assay on ARE1 element for exposure to TCDD for 2 h in WT MEFs, but not detected in 2545 cells (Figs. 18B and 26B). However, AhR promoter activation after TCDD treatment for 2 h in either cell were not detected functional from ARE (Figs. 17A and 26A). One possibility for this observation is that the CM-H_2DCFDA basal signals in the experiment were significantly higher in 2545 cancer cells (Fig. 26B) than in WT MEFs (Fig. 23B), which masked the increased potential of TCDD-induced ROS. We observed relative sensitivity TCDD-induced production of ROS for expousre 2 h in WT MEFs, higher than that in 2545 cancer cells. These results demonstrated that TCDD treatment for 2 h the induced components were well prepared to be recruited to ARE1 in WT MEFs compared with those in 2545 cells. Notably, in both WT MEFs and 2545 cells complex recruitment to ARE1 was not functional for TCDD exposure 2 h in *AhR* promoter activation.

The phosphorylation of MLC2 was induced by TCDD exposure and the AhR expression in the presence of TCDD for rescuing cell migration in Jdp2$^{-/-}$ MEFs was also dependent upon Jdp2 regulated ROS control events (Fig. 25). The presence of AhR–Nrf2 affecting the ROS homeostasis axis was important for cancer progression, in which Jdp2 plays an important role (Fig. 26E–G). The mutant Jdp2 FL34R (114 and 121) of DNA-binding shown no association with AhR, MafK, and Nrf2 [24]. Jdp2 alanin mutations N91A and I47A of histone chaperone regions are not associate and functional with AhR [26]. Epigenetic control of Jdp2 regulating the AhR–Nrf2 axis may be an alternative strategy. Here, we believe ROS-dependent reactions were regarded as the effect of tumorigenesis (Fig. 26). To further address the effect of ROS in the cancer-

initiating cells that contribute to therapeutic resistance, regorafenib was used to create a ROS-insensitive cell line [124]. It has been demonstrated that regorafenib inhibiting migration and proliferation, inducing cytotoxicity and apoptosis in cells is ROS signaling dependent [35].

Regorafenib induced nuclear localization of FOXO3a, and this forkhead transcription factor functioned as an antagonist of FOXM1 [125]. While FOXO3a functioned as a tumor suppressor, FOXM1 itself was an oncogene [126]. FOXM1 has been reported to maintain stemness phenotype of various kinds of cancers including hepatocellular [127], pancreatic [128], and lung CSCs [129]. From this study, HepG2 and Hep3B cells with regorafenib resistance phenotype were detected with increased FOXM1 expression, enhanced CSC ability, and induced EMT (Figs. 27–29). Moreover, the reduction activity of FOXM1 through either siRNA or inhibitor can increase cell death, decrease cell proliferation, and reduce sphere-forming ability as well as the size of regorafenib-resistant Hep3B and HepG2 cells (Figs. 30 and 31) [99]. When siRNA was employed to knockdown FOXM1 in HepG2 and Hep3B regorafenib-resistant cell lines, downregulation of CD44 and CSC markers was observed (Fig. 32). FOXM1 has been reported to activate stem cell properties, upregulate CD44, and enhance RAS-driven HCC progression and survival [127]. Knockdown of FOXM1 reduce regorafenib-resistant Hep3B and HepG2 expression of CD44 in luciferase assay by using CD44 promoter (Fig. 33).

HCC paitents with higher expression of FOXM1, high expression levels of SOX2, CD44, VIMENTIN, and ABCG2 were detected combined with poor prognosis (Fig. 34). Studies have shown ARUKA and BIRC can mediate the expression of FOXM1 through regulation of spindle assembly [130] or G2/M checkpoint [131]. Our *in vivo* findings shown low survival rate and poor prognosis of HCC patients with high level of FOXM1, and downstream proteins BIRC5 and AURKA (Fig. 34A, B). These observations are consistent with previous research. To confirm this *in vivo* result, thiostrepton-treated regorafenib-resistant HepG2 cells was transplanted into mice with results of smaller tumors than those with untreated cells (Fig. 35A, B). Taken together, these results suggest that FOXM1 is crucial for regorafenib resistance controlled by CD44.

5.4 Conclusion

In this study, the evidence suggests that Jdp2 is crucial for linking both AhR-Nrf2 battery for AhR promoter activation and ROS homeostasis. These gene batteries are extremely sensitive and can be activated at a very low dose of 0.1% DMSO. This treatment can increase ROS concentration and cell apoptosis potentially if Jdp2 is knocked down. Furthermore, the detoxification response was shown to be retarded when Jdp2 knockdown. We observed significantly weaker response of AhR activation by detecting stress fiber formation in Jdp2 deficient MEFs. Moreover, the oxidative stress was significantly higher in Jdp2 deficient MEFs than that in WT MEFs. Our results also suggested the phase I and phase II detoxification response can be triggered through the same protein complex including AhR, Jdp2, and Nrf2. This complex is crucial for modulating the balance of ROS, and controls the shifting of phase I to phase II detoxification response. Activation of phase I detoxification enzymes by AhR-Jdp2-Nrf2 complex binding on DRE *cis*-elements will result in signification increase of ROS. When ROS accumulates to a point that triggers the AhR-Jdp2-Nrf2 complex, the complex will bind to ARE *cis*-elements in order to maintain the homeostasis of oxidative stress.

The induction of ROS through AhR and Nrf2 batteries can potentially offer a therapeutic strategy for cancer treatment. By combining the suppression of thiostrepton (a FOXM1 inhibitor) with regorafenib (a multi-kinase inhibitor) known to suppress cancer cells through severe ROS induction [124], this effect showed a significant reduction in the survival of regorafenib-resistant CSCs. Through activating the detoxification response induced by AhR–Jdp2–Nrf2 gene battery, this will result in sensitive response to ROS stress, and apoptosis. It is possible that our results can offer a new prospective for treating chemotherapy resistant tumors by sensitizing the oxidative response to ROS level in cancer treatment.

References

[1] The National Institute for Occupational Safety and Health (NIOSH). Availabe online: https://www.cdc.gov/niosh/docs/84-104/default.html (accessed on May 20).

[2] Gutierrez-Vazquez, C.; Quintana, F.J. Regulation of the Immune Response by the Aryl Hydrocarbon Receptor. Immunity. 48 (2018) 19-33, 10.1016/j.immuni.2017.12.012.

[3] Lo, R.; Matthews, J. High-resolution genome-wide mapping of AHR and ARNT binding sites by ChIP-Seq. Toxicol Sci. 130 (2012) 349-361, 10.1093/toxsci/kfs253.

[4] Denison, M.S.; Pandini, A.; Nagy, S.R.; Baldwin, E.P.; Bonati, L. Ligand binding and activation of the Ah receptor. Chem Biol Interact. 141 (2002) 3-24, 10.1016/s0009-2797(02)00063-7.

[5] Adachi, J.; Mori, Y.; Matsui, S.; Takigami, H.; Fujino, J.; Kitagawa, H.; Miller, C.A., 3rd; Kato, T.; Saeki, K.; Matsuda, T. Indirubin and indigo are potent aryl hydrocarbon receptor ligands present in human urine. J Biol Chem. 276 (2001) 31475-31478, 10.1074/jbc.C100238200.

[6] Meyer, B.K.; Pray-Grant, M.G.; Vanden Heuvel, J.P.; Perdew, G.H. Hepatitis B virus X-associated protein 2 is a subunit of the unliganded aryl hydrocarbon receptor core complex and exhibits transcriptional enhancer activity. Mol Cell Biol. 18 (1998) 978-988, 10.1128/MCB.18.2.978.

[7] Dere, E.; Lo, R.; Celius, T.; Matthews, J.; Zacharewski, T.R. Integration of Genome-Wide Computation DRE Search, AhR ChIP-chip and Gene Expression Analyses of TCDD-Elicited Responses in the Mouse Liver. BMC Genomics. 12 (2011) 365, 10.1186/1471-2164-12-365.

[8] Mimura, J.; Fujii-Kuriyama, Y. Functional role of AhR in the expression of toxic effects by TCDD. Biochim Biophys Acta. 1619 (2003) 263-268, 10.1016/s0304-4165(02)00485-3.

[9] Barroso, A.; Gualdron-Lopez, M.; Esper, L.; Brant, F.; Araujo, R.R.; Carneiro, M.B.; Avila, T.V.; Souza, D.G.; Vieira, L.Q.; Rachid, M.A., et al. The Aryl Hydrocarbon Receptor Modulates Production of Cytokines and Reactive Oxygen Species and Development of Myocarditis during Trypanosoma cruzi Infection. Infect Immun. 84 (2016) 3071-3082, 10.1128/IAI.00575-16.

[10] Shinde, R.; Hezaveh, K.; Halaby, M.J.; Kloetgen, A.; Chakravarthy, A.; da Silva Medina, T.; Deol, R.; Manion, K.P.; Baglaenko, Y.; Eldh, M., et al. Apoptotic cell–induced AhR activity is required for immunological tolerance and suppression of systemic lupus erythematosus in mice and humans. Nature Immunology. 19 (2018) 571-582, 10.1038/s41590-018-0107-1.

[11] Swanson, H.I.; Chan, W.K.; Bradfield, C.A. DNA binding specificities and pairing rules of the Ah receptor, ARNT, and SIM proteins. J Biol Chem. 270 (1995) 26292-26302, 10.1074/jbc.270.44.26292.

[12] Zhang, L.; Savas, U.; Alexander, D.L.; Jefcoate, C.R. Characterization of the mouse Cyp1B1 gene. Identification of an enhancer region that directs aryl hydrocarbon receptor-mediated constitutive and induced expression. J Biol Chem. 273 (1998) 5174-5183, 10.1074/jbc.273.9.5174.

[13] Whitlock, J.P., Jr. Induction of cytochrome P4501A1. Annu Rev Pharmacol Toxicol. 39 (1999) 103-125, 10.1146/annurev.pharmtox.39.1.103.

[14] Miao, W.; Hu, L.; Scrivens, P.J.; Batist, G. Transcriptional regulation of NF-E2 p45-related factor (NRF2) expression by the aryl hydrocarbon receptor-xenobiotic response element signaling pathway: direct cross-talk between phase I and II drug-metabolizing enzymes. J Biol Chem. 280 (2005) 20340-20348, 10.1074/jbc.M412081200.

[15] Nakata, K.; Tanaka, Y.; Nakano, T.; Adachi, T.; Tanaka, H.; Kaminuma, T.; Ishikawa, T. Nuclear receptor-mediated transcriptional regulation in Phase I, II, and III xenobiotic metabolizing systems. Drug Metab Pharmacokinet. 21 (2006) 437-457, 10.2133/dmpk.21.437.

[16] Primiano, T.; Sutter, T.R.; Kensler, T.W. Antioxidant-inducible genes. Adv Pharmacol. 38 (1997) 293-328, 10.1016/s1054-3589(08)60989-8.

[17] Kwak, M.K.; Wakabayashi, N.; Kensler, T.W. Chemoprevention through the Keap1-Nrf2 signaling pathway by phase 2 enzyme inducers. Mutat Res. 555 (2004) 133-148, 10.1016/j.mrfmmm.2004.06.041.

[18] Katsuoka, F.; Motohashi, H.; Ishii, T.; Aburatani, H.; Engel, J.D.; Yamamoto, M. Genetic evidence that small maf proteins are essential for the activation of antioxidant response element-dependent genes. Mol Cell Biol. 25 (2005) 8044-8051, 10.1128/MCB.25.18.8044-8051.2005.

[19] Shin, S.; Wakabayashi, N.; Misra, V.; Biswal, S.; Lee, G.H.; Agoston, E.S.; Yamamoto, M.; Kensler, T.W. NRF2 modulates aryl hydrocarbon receptor signaling: influence on adipogenesis. Mol Cell Biol. 27 (2007) 7188-7197, 10.1128/MCB.00915-07.

[20] Yeager, R.L.; Reisman, S.A.; Aleksunes, L.M.; Klaassen, C.D. Introducing the "TCDD-inducible AhR-Nrf2 gene battery". Toxicol Sci. 111 (2009) 238-246, 10.1093/toxsci/kfp115.

[21] Wang, L.; He, X.; Szklarz, G.D.; Bi, Y.; Rojanasakul, Y.; Ma, Q. The aryl hydrocarbon receptor interacts with nuclear factor erythroid 2-related factor 2 to mediate induction of NAD(P)H:quinoneoxidoreductase 1 by 2,3,7,8-tetrachlorodibenzo-p-dioxin. Arch Biochem Biophys. 537 (2013) 31-38,

10.1016/j.abb.2013.06.001.

[22] Fuyuno, Y.; Uchi, H.; Yasumatsu, M.; Morino-Koga, S.; Tanaka, Y.; Mitoma, C.; Furue, M. Perillaldehyde Inhibits AHR Signaling and Activates NRF2 Antioxidant Pathway in Human Keratinocytes. Oxid Med Cell Longev. 2018 (2018) 9524657, 10.1155/2018/9524657.

[23] Chiou, S.S.; Wang, S.S.; Wu, D.C.; Lin, Y.C.; Kao, L.P.; Kuo, K.K.; Wu, C.C.; Chai, C.Y.; Lin, C.L.; Lee, C.Y., et al. Control of Oxidative Stress and Generation of Induced Pluripotent Stem Cell-like Cells by Jun Dimerization Protein 2. Cancers (Basel). 5 (2013) 959-984, 10.3390/cancers5030959.

[24] Tanigawa, S.; Lee, C.H.; Lin, C.S.; Ku, C.C.; Hasegawa, H.; Qin, S.; Kawahara, A.; Korenori, Y.; Miyamori, K.; Noguchi, M., et al. Jun dimerization protein 2 is a critical component of the Nrf2/MafK complex regulating the response to ROS homeostasis. Cell Death Dis. 4 (2013) e921, 10.1038/cddis.2013.448.

[25] Aronheim, A.; Zandi, E.; Hennemann, H.; Elledge, S.J.; Karin, M. Isolation of an AP-1 repressor by a novel method for detecting protein-protein interactions. Mol Cell Biol. 17 (1997) 3094-3102, 10.1128/MCB.17.6.3094.

[26] Jin, C.; Li, H.; Murata, T.; Sun, K.; Horikoshi, M.; Chiu, R.; Yokoyama, K.K. JDP2, a repressor of AP-1, recruits a histone deacetylase 3 complex to inhibit the retinoic acid-induced differentiation of F9 cells. Mol Cell Biol. 22 (2002) 4815-4826, 10.1128/MCB.22.13.4815-4826.2002.

[27] Wuputra, K.; Tsai, M.H.; Kato, K.; Yang, Y.H.; Pan, J.B.; Ku, C.C.; Noguchi, M.; Kishikawa, S.; Nakade, K.; Chen, H.L., et al. Dimethyl sulfoxide stimulates the AhR-Jdp2 axis to control ROS accumulation in mouse embryonic fibroblasts. Cell Biol Toxicol. 38 (2022) 203-222, 10.1007/s10565-021-09592-2.

[28] Barbarov, Y.; Timaner, M.; Alishekevitz, D.; Hai, T.; Yokoyama, K.K.; Shaked, Y.; Aronheim, A. Host JDP2 expression in the bone marrow contributes to metastatic spread. Oncotarget. 6 (2015) 37737-37749, 10.18632/oncotarget.5648.

[29] Beck, B.; Blanpain, C. Unravelling cancer stem cell potential. Nat Rev Cancer. 13 (2013) 727-738, 10.1038/nrc3597.

[30] Sun, J.H.; Luo, Q.; Liu, L.L.; Song, G.B. Liver cancer stem cell markers: Progression and therapeutic implications. World J Gastroenterol. 22 (2016) 3547-3557, 10.3748/wjg.v22.i13.3547.

[31] Xiao, Y.; Lin, M.; Jiang, X.; Ye, J.; Guo, T.; Shi, Y.; Bian, X. The Recent Advances on Liver Cancer Stem Cells: Biomarkers, Separation, and Therapy. Anal Cell Pathol (Amst). 2017 (2017) 5108653, 10.1155/2017/5108653.

[32] Aggarwal, V.; Tuli, H.S.; Varol, A.; Thakral, F.; Yerer, M.B.; Sak, K.; Varol, M.; Jain, A.; Khan, M.A.; Sethi, G. Role of Reactive Oxygen Species in Cancer

Progression: Molecular Mechanisms and Recent Advancements. Biomolecules. 9 (2019) 10.3390/biom9110735.

[33] Chan, J.S.; Tan, M.J.; Sng, M.K.; Teo, Z.; Phua, T.; Choo, C.C.; Li, L.; Zhu, P.; Tan, N.S. Cancer-associated fibroblasts enact field cancerization by promoting extratumoral oxidative stress. Cell Death Dis. 8 (2017) e2562, 10.1038/cddis.2016.492.

[34] Fondevila, F.; Mendez-Blanco, C.; Fernandez-Palanca, P.; Gonzalez-Gallego, J.; Mauriz, J.L. Anti-tumoral activity of single and combined regorafenib treatments in preclinical models of liver and gastrointestinal cancers. Exp Mol Med. 51 (2019) 1-15, 10.1038/s12276-019-0308-1.

[35] Sun, B.; Chen, H.; Wang, X.; Chen, T. Regorafenib induces Bim-mediated intrinsic apoptosis by blocking AKT-mediated FOXO3a nuclear export. Cell Death Discov. 9 (2023) 37, 10.1038/s41420-023-01338-9.

[36] Aljubran, A.; Elshenawy, M.A.; Kandil, M.; Zahir, M.N.; Shaheen, A.; Gad, A.; Alshaer, O.; Alzahrani, A.; Eldali, A.; Bazarbashi, S. Efficacy of Regorafenib in Metastatic Colorectal Cancer: A Multi-institutional Retrospective Study. Clin Med Insights Oncol. 13 (2019) 1179554918825447, 10.1177/1179554918825447.

[37] Li, L.; Wu, D.; Yu, Q.; Li, L.; Wu, P. Prognostic value of FOXM1 in solid tumors: a systematic review and meta-analysis. Oncotarget. 8 (2017) 32298-32308, 10.18632/oncotarget.15764.

[38] Tsai, J.J.; Pan, P.J.; Hsu, F.T. Regorafenib induces extrinsic and intrinsic apoptosis through inhibition of ERK/NF-kappaB activation in hepatocellular carcinoma cells. Oncol Rep. 37 (2017) 1036-1044, 10.3892/or.2016.5328.

[39] Capriotti, K.; Capriotti, J.A. Dimethyl sulfoxide: history, chemistry, and clinical utility in dermatology. J Clin Aesthet Dermatol. 5 (2012) 24-26,

[40] Notman, R.; den Otter, W.K.; Noro, M.G.; Briels, W.J.; Anwar, J. The permeability enhancing mechanism of DMSO in ceramide bilayers simulated by molecular dynamics. Biophys J. 93 (2007) 2056-2068, 10.1529/biophysj.107.104703.

[41] Rivers-Auty, J.; Ashton, J.C. Vehicles for lipophilic drugs: implications for experimental design, neuroprotection, and drug discovery. Curr Neurovasc Res. 10 (2013) 356-360, 10.2174/15672026113109990021.

[42] da Silva Duarte, I.; Gragnani, A.; Ferreira, L.M. Dimethyl sulfoxide and oxidative stress on cultures of human keratinocytes. Can J Plast Surg. 12 (2004) 13-16,

[43] Laskar, A.; Yuan, X.M.; Li, W. Dimethyl sulfoxide prevents 7beta-hydroxycholesterol-induced apoptosis by preserving lysosomes and

mitochondria. J Cardiovasc Pharmacol. 56 (2010) 263-267, 10.1097/FJC.0b013e3181eb3063.

[44] Sadowska-Bartosz, I.; Paczka, A.; Molon, M.; Bartosz, G. Dimethyl sulfoxide induces oxidative stress in the yeast Saccharomyces cerevisiae. FEMS Yeast Res. 13 (2013) 820-830, 10.1111/1567-1364.12091.

[45] Rawls, W.F.; Cox, L.; Rovner, E.S. Dimethyl sulfoxide (DMSO) as intravesical therapy for interstitial cystitis/bladder pain syndrome: A review. Neurourol Urodyn. 36 (2017) 1677-1684, 10.1002/nau.23204.

[46] Lin, S.; Talbot, P. Methods for culturing mouse and human embryonic stem cells. Methods Mol Biol. 690 (2011) 31-56, 10.1007/978-1-60761-962-8_2.

[47] Mitra, S.K.; Hanson, D.A.; Schlaepfer, D.D. Focal adhesion kinase: in command and control of cell motility. Nat Rev Mol Cell Biol. 6 (2005) 56-68, 10.1038/nrm1549.

[48] Li, S.; Guan, J.L.; Chien, S. Biochemistry and biomechanics of cell motility. Annu Rev Biomed Eng. 7 (2005) 105-150, 10.1146/annurev.bioeng.7.060804.100340.

[49] Ikuta, T.; Okabe-Kado, J. Aryl Hydrocarbon Receptor Controls Adhesion and Migration of Colon Cancer Cells. British Journal of Cancer Research. 1 (2018) 10X-11xx, 10.31488/bjcr.113.

[50] Novikov, O.; Wang, Z.; Stanford, E.A.; Parks, A.J.; Ramirez-Cardenas, A.; Landesman, E.; Laklouk, I.; Sarita-Reyes, C.; Gusenleitner, D.; Li, A., et al. An Aryl Hydrocarbon Receptor-Mediated Amplification Loop That Enforces Cell Migration in ER-/PR-/Her2- Human Breast Cancer Cells. Mol Pharmacol. 90 (2016) 674-688, 10.1124/mol.116.105361.

[51] Barouki, R.; Coumoul, X.; Fernandez-Salguero, P.M. The aryl hydrocarbon receptor, more than a xenobiotic-interacting protein. FEBS Lett. 581 (2007) 3608-3615, 10.1016/j.febslet.2007.03.046.

[52] Beg, A.A.; Sha, W.C.; Bronson, R.T.; Ghosh, S.; Baltimore, D. Embryonic lethality and liver degeneration in mice lacking the RelA component of NF-kappa B. Nature. 376 (1995) 167-170, 10.1038/376167a0.

[53] Carvajal-Gonzalez, J.M.; Mulero-Navarro, S.; Roman, A.C.; Sauzeau, V.; Merino, J.M.; Bustelo, X.R.; Fernandez-Salguero, P.M. The dioxin receptor regulates the constitutive expression of the vav3 proto-oncogene and modulates cell shape and adhesion. Mol Biol Cell. 20 (2009) 1715-1727, 10.1091/mbc.E08-05-0451.

[54] Bisaria, A.; Hayer, A.; Garbett, D.; Cohen, D.; Meyer, T. Membrane-proximal F-actin restricts local membrane protrusions and directs cell migration. Science. 368 (2020) 1205-1210, 10.1126/science.aay7794.

[55] Shang, H.S.; Shih, Y.L.; Lee, C.H.; Hsueh, S.C.; Liu, J.Y.; Liao, N.C.; Chen, Y.L.; Huang, Y.P.; Lu, H.F.; Chung, J.G. Sulforaphane-induced apoptosis in human leukemia HL-60 cells through extrinsic and intrinsic signal pathways and altering associated genes expression assayed by cDNA microarray. Environ Toxicol. 32 (2017) 311-328, 10.1002/tox.22237.

[56] Moldogazieva, N.T.; Mokhosoev, I.M.; Feldman, N.B.; Lutsenko, S.V. ROS and RNS signalling: adaptive redox switches through oxidative/nitrosative protein modifications. Free Radic Res. 52 (2018) 507-543, 10.1080/10715762.2018.1457217.

[57] Wolfle, U.; Seelinger, G.; Bauer, G.; Meinke, M.C.; Lademann, J.; Schempp, C.M. Reactive molecule species and antioxidative mechanisms in normal skin and skin aging. Skin Pharmacol Physiol. 27 (2014) 316-332, 10.1159/000360092.

[58] Pan, J.; Nakade, K.; Huang, Y.C.; Zhu, Z.W.; Masuzaki, S.; Hasegawa, H.; Murata, T.; Yoshiki, A.; Yamaguchi, N.; Lee, C.H., et al. Suppression of cell-cycle progression by Jun dimerization protein-2 (JDP2) involves downregulation of cyclin-A2. Oncogene. 29 (2010) 6245-6256, 10.1038/onc.2010.355.

[59] Jin, C.; Kato, K.; Chimura, T.; Yamasaki, T.; Nakade, K.; Murata, T.; Li, H.; Pan, J.; Zhao, M.; Sun, K., et al. Regulation of histone acetylation and nucleosome assembly by transcription factor JDP2. Nat Struct Mol Biol. 13 (2006) 331-338, 10.1038/nsmb1063.

[60] Nakade, K.; Pan, J.; Yoshiki, A.; Ugai, H.; Kimura, M.; Liu, B.; Li, H.; Obata, Y.; Iwama, M.; Itohara, S., et al. JDP2 suppresses adipocyte differentiation by regulating histone acetylation. Cell Death Differ. 14 (2007) 1398-1405, 10.1038/sj.cdd.4402129.

[61] Cheng, Y.H.; Ou, B.R.; Cheng, L.C.; Lu, J.H.; Yeh, J.Y. Glutathione regulation in arsenic-induced porcine aortic endothelial cells. Toxicol In Vitro. 22 (2008) 1832-1839, 10.1016/j.tiv.2008.08.006.

[62] Blank, V. Small Maf proteins in mammalian gene control: mere dimerization partners or dynamic transcriptional regulators? J Mol Biol. 376 (2008) 913-925, 10.1016/j.jmb.2007.11.074.

[63] Yamamoto, M.; Kensler, T.W.; Motohashi, H. The KEAP1-NRF2 System: a Thiol-Based Sensor-Effector Apparatus for Maintaining Redox Homeostasis. Physiol Rev. 98 (2018) 1169-1203, 10.1152/physrev.00023.2017.

[64] Haarmann-Stemmann, T.; Abel, J.; Fritsche, E.; Krutmann, J. The AhR-Nrf2 pathway in keratinocytes: on the road to chemoprevention? J Invest Dermatol. 132 (2012) 7-9, 10.1038/jid.2011.359.

[65] Tsuji, G.; Takahara, M.; Uchi, H.; Matsuda, T.; Chiba, T.; Takeuchi, S.; Yasukawa, F.; Moroi, Y.; Furue, M. Identification of ketoconazole as an AhR-Nrf2 activator in cultured human keratinocytes: the basis of its anti-inflammatory effect. J Invest Dermatol. 132 (2012) 59-68, 10.1038/jid.2011.194.

[66] Wells, P.G.; Lee, C.J.; McCallum, G.P.; Perstin, J.; Harper, P.A. Receptor- and reactive intermediate-mediated mechanisms of teratogenesis. Handb Exp Pharmacol. 10.1007/978-3-642-00663-0_6 (2010) 131-162, 10.1007/978-3-642-00663-0_6.

[67] Hayes, J.D.; Dinkova-Kostova, A.T.; McMahon, M. Cross-talk between transcription factors AhR and Nrf2: lessons for cancer chemoprevention from dioxin. Toxicol Sci. 111 (2009) 199-201, 10.1093/toxsci/kfp168.

[68] Filbrandt, C.R.; Wu, Z.; Zlokovic, B.; Opanashuk, L.; Gasiewicz, T.A. Presence and functional activity of the aryl hydrocarbon receptor in isolated murine cerebral vascular endothelial cells and astrocytes. Neurotoxicology. 25 (2004) 605-616, 10.1016/j.neuro.2003.08.007.

[69] Dauchy, S.; Miller, F.; Couraud, P.O.; Weaver, R.J.; Weksler, B.; Romero, I.A.; Scherrmann, J.M.; De Waziers, I.; Decleves, X. Expression and transcriptional regulation of ABC transporters and cytochromes P450 in hCMEC/D3 human cerebral microvascular endothelial cells. Biochem Pharmacol. 77 (2009) 897-909, 10.1016/j.bcp.2008.11.001.

[70] Dhakshinamoorthy, S.; Jaiswal, A.K. Small maf (MafG and MafK) proteins negatively regulate antioxidant response element-mediated expression and antioxidant induction of the NAD(P)H:Quinone oxidoreductase1 gene. J Biol Chem. 275 (2000) 40134-40141, 10.1074/jbc.M003531200.

[71] Nguyen, T.; Sherratt, P.J.; Huang, H.C.; Yang, C.S.; Pickett, C.B. Increased protein stability as a mechanism that enhances Nrf2-mediated transcriptional activation of the antioxidant response element. Degradation of Nrf2 by the 26 S proteasome. J Biol Chem. 278 (2003) 4536-4541, 10.1074/jbc.M207293200.

[72] Xu, C.; Li, C.Y.; Kong, A.N. Induction of phase I, II and III drug metabolism/transport by xenobiotics. Arch Pharm Res. 28 (2005) 249-268, 10.1007/BF02977789.

[73] Pan, J.S.; Hong, M.Z.; Ren, J.L. Reactive oxygen species: a double-edged sword in oncogenesis. World J Gastroenterol. 15 (2009) 1702-1707, 10.3748/wjg.15.1702.

[74] Wu, D.C.; Wang, S.S.W.; Liu, C.J.; Wuputra, K.; Kato, K.; Lee, Y.L.; Lin, Y.C.; Tsai, M.H.; Ku, C.C.; Lin, W.H., et al. Reprogramming Antagonizes the Oncogenicity of HOXA13-Long Noncoding RNA HOTTIP Axis in Gastric Cancer Cells. Stem Cells. 35 (2017) 2115-2128, 10.1002/stem.2674.

[75] Ma, Q. Role of nrf2 in oxidative stress and toxicity. Annu Rev Pharmacol Toxicol. 53 (2013) 401-426, 10.1146/annurev-pharmtox-011112-140320.

[76] Uchi, H.; Yasumatsu, M.; Morino-Koga, S.; Mitoma, C.; Furue, M. Inhibition of aryl hydrocarbon receptor signaling and induction of NRF2-mediated antioxidant activity by cinnamaldehyde in human keratinocytes. J Dermatol Sci. 85 (2017) 36-43, 10.1016/j.jdermsci.2016.10.003.

[77] Sekhar, K.R.; Freeman, M.L. Nrf2 promotes survival following exposure to ionizing radiation. Free Radic Biol Med. 88 (2015) 268-274, 10.1016/j.freeradbiomed.2015.04.035.

[78] Ma, Q.; Baldwin, K.T. 2,3,7,8-tetrachlorodibenzo-p-dioxin-induced degradation of aryl hydrocarbon receptor (AhR) by the ubiquitin-proteasome pathway. Role of the transcription activaton and DNA binding of AhR. J Biol Chem. 275 (2000) 8432-8438, 10.1074/jbc.275.12.8432.

[79] Vierstra, J.; Lazar, J.; Sandstrom, R.; Halow, J.; Lee, K.; Bates, D.; Diegel, M.; Dunn, D.; Neri, F.; Haugen, E., et al. Global reference mapping of human transcription factor footprints. Nature. 583 (2020) 729-736, 10.1038/s41586-020-2528-x.

[80] Jaramillo, M.C.; Zhang, D.D. The emerging role of the Nrf2-Keap1 signaling pathway in cancer. Genes Dev. 27 (2013) 2179-2191, 10.1101/gad.225680.113.

[81] DeNicola, G.M.; Karreth, F.A.; Humpton, T.J.; Gopinathan, A.; Wei, C.; Frese, K.; Mangal, D.; Yu, K.H.; Yeo, C.J.; Calhoun, E.S., et al. Oncogene-induced Nrf2 transcription promotes ROS detoxification and tumorigenesis. Nature. 475 (2011) 106-109, 10.1038/nature10189.

[82] Sies, H.; Jones, D.P. Reactive oxygen species (ROS) as pleiotropic physiological signalling agents. Nat Rev Mol Cell Biol. 21 (2020) 363-383, 10.1038/s41580-020-0230-3.

[83] Weng, C.C.; Ding, P.Y.; Liu, Y.H.; Hawse, J.R.; Subramaniam, M.; Wu, C.C.; Lin, Y.C.; Chen, C.Y.; Hung, W.C.; Cheng, K.H. Mutant Kras-induced upregulation of CD24 enhances prostate cancer stemness and bone metastasis. Oncogene. 38 (2019) 2005-2019, 10.1038/s41388-018-0575-7.

[84] Park, J.H.; Gelhaus, S.; Vedantam, S.; Oliva, A.L.; Batra, A.; Blair, I.A.; Troxel, A.B.; Field, J.; Penning, T.M. The pattern of p53 mutations caused by PAH o-quinones is driven by 8-oxo-dGuo formation while the spectrum of mutations is determined by biological selection for dominance. Chem Res Toxicol. 21 (2008) 1039-1049, 10.1021/tx700404a.

[85] Wang, X.J.; Hayes, J.D.; Wolf, C.R. Generation of a stable antioxidant response element-driven reporter gene cell line and its use to show redox-dependent activation of nrf2 by cancer chemotherapeutic agents. Cancer Res. 66 (2006)

10983-10994, 10.1158/0008-5472.Can-06-2298.

[86] Mihara, M.; Uchiyama, M. Determination of malonaldehyde precursor in tissues by thiobarbituric acid test. Anal Biochem. 86 (1978) 271-278, 10.1016/0003-2697(78)90342-1.

[87] Kuo, K.K.; Lee, K.T.; Chen, K.K.; Yang, Y.H.; Lin, Y.C.; Tsai, M.H.; Wuputra, K.; Lee, Y.L.; Ku, C.C.; Miyoshi, H., et al. Positive Feedback Loop of OCT4 and c-JUN Expedites Cancer Stemness in Liver Cancer. Stem Cells. 34 (2016) 2613-2624, 10.1002/stem.2447.

[88] Hashimoto, N.; Tsunedomi, R.; Yoshimura, K.; Watanabe, Y.; Hazama, S.; Oka, M. Cancer stem-like sphere cells induced from de-differentiated hepatocellular carcinoma-derived cell lines possess the resistance to anti-cancer drugs. BMC Cancer. 14 (2014) 722, 10.1186/1471-2407-14-722.

[89] Flores-Tellez, T.N.; Villa-Trevino, S.; Pina-Vazquez, C. Road to stemness in hepatocellular carcinoma. World J Gastroenterol. 23 (2017) 6750-6776, 10.3748/wjg.v23.i37.6750.

[90] Lee, T.K.; Guan, X.Y.; Ma, S. Cancer stem cells in hepatocellular carcinoma - from origin to clinical implications. Nat Rev Gastroenterol Hepatol. 19 (2022) 26-44, 10.1038/s41575-021-00508-3.

[91] Takahashi, K.; Yamanaka, S. A decade of transcription factor-mediated reprogramming to pluripotency. Nat Rev Mol Cell Biol. 17 (2016) 183-193, 10.1038/nrm.2016.8.

[92] Kuo, K.K.; Hsiao, P.J.; Chang, W.T.; Chuang, S.C.; Yang, Y.H.; Wuputra, K.; Ku, C.C.; Pan, J.B.; Li, C.P.; Kato, K., et al. Therapeutic Strategies Targeting Tumor Suppressor Genes in Pancreatic Cancer. Cancers (Basel). 13 (2021) 10.3390/cancers13153920.

[93] Tovar, V.; Cornella, H.; Moeini, A.; Vidal, S.; Hoshida, Y.; Sia, D.; Peix, J.; Cabellos, L.; Alsinet, C.; Torrecilla, S., et al. Tumour initiating cells and IGF/FGF signalling contribute to sorafenib resistance in hepatocellular carcinoma. Gut. 66 (2017) 530-540, 10.1136/gutjnl-2015-309501.

[94] Heo, Y.A.; Syed, Y.Y. Regorafenib: A Review in Hepatocellular Carcinoma. Drugs. 78 (2018) 951-958, 10.1007/s40265-018-0932-4.

[95] Raychaudhuri, P.; Park, H.J. FoxM1: a master regulator of tumor metastasis. Cancer Res. 71 (2011) 4329-4333, 10.1158/0008-5472.CAN-11-0640.

[96] Liao, G.B.; Li, X.Z.; Zeng, S.; Liu, C.; Yang, S.M.; Yang, L.; Hu, C.J.; Bai, J.Y. Regulation of the master regulator FOXM1 in cancer. Cell Commun Signal. 16 (2018) 57, 10.1186/s12964-018-0266-6.

[97] Hadjimichael, C.; Chanoumidou, K.; Papadopoulou, N.; Arampatzi, P.; Papamatheakis, J.; Kretsovali, A. Common stemness regulators of embryonic

and cancer stem cells. World J Stem Cells. 7 (2015) 1150-1184, 10.4252/wjsc.v7.i9.1150.

[98] Allison, T.F.; Smith, A.J.H.; Anastassiadis, K.; Sloane-Stanley, J.; Biga, V.; Stavish, D.; Hackland, J.; Sabri, S.; Langerman, J.; Jones, M., et al. Identification and Single-Cell Functional Characterization of an Endodermally Biased Pluripotent Substate in Human Embryonic Stem Cells. Stem Cell Reports. 10 (2018) 1895-1907, 10.1016/j.stemcr.2018.04.015.

[99] Li, M.; Yang, J.; Zhou, W.; Ren, Y.; Wang, X.; Chen, H.; Zhang, J.; Chen, J.; Sun, Y.; Cui, L., et al. Activation of an AKT/FOXM1/STMN1 pathway drives resistance to tyrosine kinase inhibitors in lung cancer. Br J Cancer. 117 (2017) 974-983, 10.1038/bjc.2017.292.

[100] Abdeljaoued, S.; Bettaieb, L.; Nasri, M.; Adouni, O.; Goucha, A.; Bouzaiene, H.; Boussen, H.; Rahal, K.; Gamoudi, A. Forkhead box M1 (FOXM1) expression predicts disease free survival and may mediate resistance to chemotherapy and hormonotherapy in male breast cancer. Breast Dis. 37 (2018) 109-114, 10.3233/BD-170315.

[101] Laissue, P. The forkhead-box family of transcription factors: key molecular players in colorectal cancer pathogenesis. Mol Cancer. 18 (2019) 5, 10.1186/s12943-019-0938-x.

[102] Su, W.L.; Chuang, S.C.; Wang, Y.C.; Chen, L.A.; Huang, J.W.; Chang, W.T.; Wang, S.N.; Lee, K.T.; Lin, C.S.; Kuo, K.K. Expression of FOXM1 and Aurora-A predicts prognosis and sorafenib efficacy in patients with hepatocellular carcinoma. Cancer Biomark. 28 (2020) 341-350, 10.3233/CBM-190507.

[103] Yang, N.; Wang, C.; Wang, Z.; Zona, S.; Lin, S.X.; Wang, X.; Yan, M.; Zheng, F.M.; Li, S.S.; Xu, B., et al. FOXM1 recruits nuclear Aurora kinase A to participate in a positive feedback loop essential for the self-renewal of breast cancer stem cells. Oncogene. 36 (2017) 3428-3440, 10.1038/onc.2016.490.

[104] Duffy, M.J.; O'Donovan, N.; Brennan, D.J.; Gallagher, W.M.; Ryan, B.M. Survivin: a promising tumor biomarker. Cancer Lett. 249 (2007) 49-60, 10.1016/j.canlet.2006.12.020.

[105] Chen, T.; You, Y.; Jiang, H.; Wang, Z.Z. Epithelial-mesenchymal transition (EMT): A biological process in the development, stem cell differentiation, and tumorigenesis. J Cell Physiol. 232 (2017) 3261-3272, 10.1002/jcp.25797.

[106] Li, C.H.; Hsu, T.I.; Chang, Y.C.; Chan, M.H.; Lu, P.J.; Hsiao, M. Stationed or Relocating: The Seesawing EMT/MET Determinants from Embryonic Development to Cancer Metastasis. Biomedicines. 9 (2021) 10.3390/biomedicines9091265.

[107] Wang, H.; Unternaehrer, J.J. Epithelial-mesenchymal Transition and Cancer

Stem Cells: At the Crossroads of Differentiation and Dedifferentiation. Dev Dyn. 248 (2019) 10-20, 10.1002/dvdy.24678.

[108] Francart, M.E.; Vanwynsberghe, A.M.; Lambert, J.; Bourcy, M.; Genna, A.; Ancel, J.; Perez-Boza, J.; Noel, A.; Birembaut, P.; Struman, I., et al. Vimentin prevents a miR-dependent negative regulation of tissue factor mRNA during epithelial-mesenchymal transitions and facilitates early metastasis. Oncogene. 39 (2020) 3680-3692, 10.1038/s41388-020-1244-1.

[109] Mendez, M.G.; Kojima, S.; Goldman, R.D. Vimentin induces changes in cell shape, motility, and adhesion during the epithelial to mesenchymal transition. FASEB J. 24 (2010) 1838-1851, 10.1096/fj.09-151639.

[110] Wang, Y.; Liao, R.; Chen, X.; Ying, X.; Chen, G.; Li, M.; Dong, C. Twist-mediated PAR1 induction is required for breast cancer progression and metastasis by inhibiting Hippo pathway. Cell Death Dis. 11 (2020) 520, 10.1038/s41419-020-2725-4.

[111] Wang, Y.; Liu, J.; Ying, X.; Lin, P.C.; Zhou, B.P. Twist-mediated Epithelial-mesenchymal Transition Promotes Breast Tumor Cell Invasion via Inhibition of Hippo Pathway. Sci Rep. 6 (2016) 24606, 10.1038/srep24606.

[112] Zhang, P.; Sun, Y.; Ma, L. ZEB1: at the crossroads of epithelial-mesenchymal transition, metastasis and therapy resistance. Cell Cycle. 14 (2015) 481-487, 10.1080/15384101.2015.1006048.

[113] Aban, C.E.; Lombardi, A.; Neiman, G.; Biani, M.C.; La Greca, A.; Waisman, A.; Moro, L.N.; Sevlever, G.; Miriuka, S.; Luzzani, C. Downregulation of E-cadherin in pluripotent stem cells triggers partial EMT. Sci Rep. 11 (2021) 2048, 10.1038/s41598-021-81735-1.

[114] Matthew, E.M.; Zhou, L.; Yang, Z.; Dicker, D.T.; Holder, S.L.; Lim, B.; Harouaka, R.; Zheng, S.Y.; Drabick, J.J.; Lamparella, N.E., et al. A multiplexed marker-based algorithm for diagnosis of carcinoma of unknown primary using circulating tumor cells. Oncotarget. 7 (2016) 3662-3676, 10.18632/oncotarget.6657.

[115] Shi, R.; Liu, L.; Wang, F.; He, Y.; Niu, Y.; Wang, C.; Zhang, X.; Zhang, X.; Zhang, H.; Chen, M., et al. Downregulation of cytokeratin 18 induces cellular partial EMT and stemness through increasing EpCAM expression in breast cancer. Cell Signal. 76 (2020) 109810, 10.1016/j.cellsig.2020.109810.

[116] Hegde, N.S.; Sanders, D.A.; Rodriguez, R.; Balasubramanian, S. The transcription factor FOXM1 is a cellular target of the natural product thiostrepton. Nat Chem. 3 (2011) 725-731, 10.1038/nchem.1114.

[117] Peiris-Pages, M.; Martinez-Outschoorn, U.E.; Pestell, R.G.; Sotgia, F.; Lisanti, M.P. Cancer stem cell metabolism. Breast Cancer Res. 18 (2016) 55,

10.1186/s13058-016-0712-6.

[118] Sun, H.; Zhang, M.; Cheng, K.; Li, P.; Han, S.; Li, R.; Su, M.; Zeng, W.; Liu, J.; Guo, J., et al. Resistance of glioma cells to nutrient-deprived microenvironment can be enhanced by CD133-mediated autophagy. Oncotarget. 7 (2016) 76238-76249, 10.18632/oncotarget.12803.

[119] Yao, Z.; Mishra, L. Cancer stem cells and hepatocellular carcinoma. Cancer Biol Ther. 8 (2009) 1691-1698, 10.4161/cbt.8.18.9843.

[120] Nebert, D.W. Extreme discordant phenotype methodology: an intuitive approach to clinical pharmacogenetics. Eur J Pharmacol. 410 (2000) 107-120, 10.1016/s0014-2999(00)00809-8.

[121] Itoh, K.; Chiba, T.; Takahashi, S.; Ishii, T.; Igarashi, K.; Katoh, Y.; Oyake, T.; Hayashi, N.; Satoh, K.; Hatayama, I., et al. An Nrf2/small Maf heterodimer mediates the induction of phase II detoxifying enzyme genes through antioxidant response elements. Biochem Biophys Res Commun. 236 (1997) 313-322, 10.1006/bbrc.1997.6943.

[122] Tsai, M.H.; Wuputra, K.; Lin, Y.C.; Lin, C.S.; Yokoyama, K.K. Multiple functions of the histone chaperone Jun dimerization protein 2. Gene. 590 (2016) 193-200, 10.1016/j.gene.2016.03.048.

[123] Wang, X.J.; Sun, Z.; Villeneuve, N.F.; Zhang, S.; Zhao, F.; Li, Y.; Chen, W.; Yi, X.; Zheng, W.; Wondrak, G.T., et al. Nrf2 enhances resistance of cancer cells to chemotherapeutic drugs, the dark side of Nrf2. Carcinogenesis. 29 (2008) 1235-1243, 10.1093/carcin/bgn095.

[124] Sui, H.; Xiao, S.; Jiang, S.; Wu, S.; Lin, H.; Cheng, L.; Ye, L.; Zhao, Q.; Yu, Y.; Tao, L., et al. Regorafenib induces NOX5-mediated endoplasmic reticulum stress and potentiates the anti-tumor activity of cisplatin in non-small cell lung cancer cells. Neoplasia. 39 (2023) 100897, 10.1016/j.neo.2023.100897.

[125] Wang, I.C.; Ustiyan, V.; Zhang, Y.; Cai, Y.; Kalin, T.V.; Kalinichenko, V.V. Foxm1 transcription factor is required for the initiation of lung tumorigenesis by oncogenic Kras(G12D.). Oncogene. 33 (2014) 5391-5396, 10.1038/onc.2013.475.

[126] Yao, S.; Fan, L.Y.; Lam, E.W. The FOXO3-FOXM1 axis: A key cancer drug target and a modulator of cancer drug resistance. Semin Cancer Biol. 50 (2018) 77-89, 10.1016/j.semcancer.2017.11.018.

[127] Kopanja, D.; Pandey, A.; Kiefer, M.; Wang, Z.; Chandan, N.; Carr, J.R.; Franks, R.; Yu, D.Y.; Guzman, G.; Maker, A., et al. Essential roles of FoxM1 in Ras-induced liver cancer progression and in cancer cells with stem cell features. J Hepatol. 63 (2015) 429-436, 10.1016/j.jhep.2015.03.023.

[128] Quan, M.; Wang, P.; Cui, J.; Gao, Y.; Xie, K. The roles of FOXM1 in pancreatic

stem cells and carcinogenesis. Mol Cancer. 12 (2013) 159, 10.1186/1476-4598-12-159.

[129] Su, J.; Wu, S.; Wu, H.; Li, L.; Guo, T. CD44 is functionally crucial for driving lung cancer stem cells metastasis through Wnt/beta-catenin-FoxM1-Twist signaling. Mol Carcinog. 55 (2016) 1962-1973, 10.1002/mc.22443.

[130] Huang, L.; Jiang, S.; Shi, Y. Tyrosine kinase inhibitors for solid tumors in the past 20 years (2001-2020). J Hematol Oncol. 13 (2020) 143, 10.1186/s13045-020-00977-0.

[131] Zhang, J.; Yang, P.L.; Gray, N.S. Targeting cancer with small molecule kinase inhibitors. Nat Rev Cancer. 9 (2009) 28-39, 10.1038/nrc2559.

Acknowledgements

I would like to express my deepest gratitude to Professor K. Yokoyama for continuous supports during my research training period in Kaohsiung Medical University. I have learned a lot from him in the attitude and enthusiasm to the science. I would follow to his footsteps and try to brush up my research carrier to advance attitude and enthusiasm of the research life.

Furthermore, I would like to express my deepest gratitude to Professor E. Ito in Waseda University in Japan. I couldn't have applied the doctoral degree of Waseda University without his kind instruction. Generously he gave me an opportunity for this application and took me an apprentice. My sincere and heartfelt gratitude and appreciation to Professor Ito for providing me with a guidance and counsel I need to succeed in the PhD program.

I am also grateful to Professor C Hanashima, Professor T Kato, Professor C-S Lin, Professor Y-C Lin, and Dr. Wendy Hsu (arranged in alphabetical order), who gave me advise and pointing out the weakness of my research. Their suggestions are very useful for revising my thesis and the presentation.

I would also like to thank my colleagues in laboratory: Dr. M-H Tsai who did a preliminary experiment of JDP2-AhR interactions, Dr. C-C Kuo who helped me correction of English in my doctoral thesis, Ms. Betty Kao who cooperated with me to isolate the AhR promoter and its construction; Ms. Laura Ku who helped me to solve the administration problems, Ms. S-W Wang who cooperated to support some experiments and animal care, Ms. Y-H Yang who helped me to do some animal experiments and administration, Mr. J-B Pan who helped to do the con-focal microscope experiments and handle the chores, Ms. Kim Lin and Ms. Judy Lin helped me to cooperation the administration of the experiments.

Lastly, I couldn't have completed it without the support & love of my family throughout. I am thankful to my parents who shared their expertise & encouragement. Thank you for believing in me and encouraging me to work hard. I appreciate all that you have done for me.

I do wish you all for the best.

List of research achievements for application of Doctor of Science, Waseda University

Full Name: Wuputra Kenly seal or signature

Date Submitted(yyyy/mm/dd): 2023/10/18

種類別 (By Type)	題名、 発表・発行掲載誌名、 発表・発行年月、 連名者（申請者含む） (theme, journal name, date & year of publication, name of authors inc. yourself)
○	Dimethyl sulfoxide stimulates the AhR-Jdp2 axis to control ROS accumulation in mouse embryonic fibroblasts. Cell Biology and Toxicology, 38: 203-222 (2022). *Wuputra, K., Tsai, M-H., Kato, K., Yang, Y-H., Pan, J-B., Ku, C-C., Noguchi, N., Kishikawa, S., Nakade, K., Chen, H-L., Liu C-J., Nakamura, Y., Kuo. K-K., Lin, Y-C., Te-Fu, Chan, Wu, D-C., Hou, M-F., Huang, S-K., Lin, C-S., and Yokoyama K.
○	FOXM1-CD44 signaling is critical or the acquisition of regorafenib resistance in human liver cancer cells. International Journal of Molecular Sciences. 23(14): 7782 (2022). *Wuputra, K., Hsiao P-J., Chang, W.T., Wu, P-H., Chen, L-A., Huang, J-W., Su, W-L., Yang, Y-H., Wu, D-C., Yokoyama, K.
○	Jdp2 is a spatiotemporal transcriptional activator of the AhR via the Nrf2 gene battery. Inflammation and Regeneration, 43, 42 (2023). *Wuputra, K., Tsai, M-H., Kato, K., Ku, C-C., Pan, J-B., Yang, Y-H., Saito, S., Wu, C-C., Lin, Y-C., Cheng, K-H., Kuo, K-K., Noguchi, M., Nakamura, Y., Wu, D-C., Lin, C-S., and Yokoyama, K.
	Translational models of 3-D organoids and cancer stem cells in gastric cancer research. Stem Cell Research & Therapy, 12, 492 (2021). *Wuputra K., Ku C-C., Kato K., Wu D-C., Saito S., and Yokoyama K.
	Prevention of tumor risks associated with the reprogramming in human pluripotent stem cells Journal of Experimental & Clinical Cancer Research., 39, 100 (2020). *Wuputra, K., Ku, C-C., Wu, D-C., Lin, Y-C., Saito, S., and Yokoyama K.
	Cancer cell reprogramming to identify the genes component for generating liver cancer stem cells. Inflammation and Regeneration, 37, 15; 10.1186/s41232-017-0041-x (2017). *Wuputra, K., Lin, C-S., Tsai, M-H., Ku, C-C., Lin, W-H., Yang, H-H., Kuo, K-K., and Yokoyama K.
	Roles of HIF family and ROS homeostasis in stem cells and cancer. e-Book, Frontiers in Anti-Cancer Drug Discovery, Bentham Science Publishers, Vol. 6, pp. 91-109 (2015). *Wuputra K., Tsai, M-H., Yokoyama K., and Saito S.

List of research achievements for application of Doctor of Science, Waseda University

Full Name: Wuputra Kenly seal or signature

Date Submitted(yyyy/mm/dd): 2023/10/18

種類別 (By Type)	題名、 発表・発行掲載誌名、 発表・発行年月、 連名者（申請者含む） (theme, journal name, date & year of publication, name of authors inc. yourself)
	Deletion of Jdp2 enhances Slc7a11 expression in Atoh-1 positive cerebellum granule cell progenitor in vivo. Stem Cell Research & Therapy, 12, 369 (2021). *Ku, C-C., Wuputra, K., Kato, K., Pan J-B., Li C-P., Tsai, M-H., Noguchi, M., Nakamura, Y., Liu C-J., Chan, T-F., Hou M-F., Wakana, S., Wu Y-C., Lin C-S, Wu D-C., Yokoyama K. The progress in the study of reprogramming to acquire the feature if stem cells in iPSCs and cancers. Recent Advances in iPSC technology. Springer Nature, Chapter 4 (2021). Saito S., Wuputra, K., Koto, K., Yokoyama K. Jdp2-deficient granule cell progenitors in the cerebellum are resistant to ROS-mediated apoptosis through xCT/Slc7a11 activation. Scientific Reports, 10, 4933 (2020). *Ku, C-C., *Wuputra, K., Kato, K., Lin, W-H., Pan, J-B., Tsi, S-C., Kuo, C-J., Lee, K-H., Lee, Y-L., Lin, Y-C., Saito, S., Noguchi, M., Nakamura, Y., Miyoshi, H., Eckner, R., Nagata, K., Wu, D-C., Lin, C-S., and Yokoyama K. Tissue regulation and healing by ROS-mediated NOX2 and Ca2+ ion uptake. Journal of Stem Cells Research, Reviews & Reports, 5; 1026 (2018). Lin, C-S., Wuputra, K., and Yokoyama, K. Multiple function of histone chaperone Jun dimerization protein 2. Gene, 590, 193-200 (2016). Tsai. M-H., Wuputra, K., Lin Y-C., Lin C-S., and Yokoyama K. Environmental-stress-induced chromatin regulation and its heritability. Journal of Carcinogenesis & Mutagenesis 5, 156 (2014). Fang, L., Wuputra K., Chen D., Li H., Huang, S-K., Jin C., and Yokoyama K. Reactive oxygen (ROS) homeostasis in influenza virus infection. BMC Microbiology, 20, 214 (2020). Chen, K-K., Minakuchi, M., Wuputra, K., Ku, C-C., Pan, J-B., Kuo, K-K., Lin, Y-C., Saito, S., Lin C-S., and Yokoyama K.

List of research achievements for application of Doctor of Science, Waseda University

Full Name: Wuputra Kenly seal or signature

Date Submitted(yyyy/mm/dd): 2023/10/18

種類別 (By Type)	題名、 発表・発行掲載誌名、 発表・発行年月、 連名者（申請者含む） (theme, journal name, date & year of publication, name of authors inc. yourself)
	Application of cancer cell reprogramming technology to human cancer research. Anticancer Research, 37, 3367-3377 (2017). Pan, X-Y., Tsai, M-H., Wuputra K., Ku, C-C., Lin, W-H., Lin, Y-C., Kishikawa, S., Noguchi M., Saito, S., Lin C-S., and Yokoyama K.
	Bovine induced pluripotent stem cells are more resistant to apoptosis than testicular cells in response to mono-(2-ethylhexyl) phthalate. International Journal of Molecular Sciences, 15, 5011-5031 (2014). Lin Y-C., Kuo K-K., Wuputra K., Lin S-H., Ku, C-C., Yang, Y-H., Wang, S-W., Wang, S-W., Wu, D-C., Wu, C-C., Chai, C-Y., Lin, C-L., Lin, C-S., Kajitani, M., Miyoshi, H., Nakamura, Y., Hashimoto, S., Matsushima, K., Jin, C., Huang S-K., Saito S., and Yokoyama K.
	Therapeutic strategies targeting tumor suppressor genes in pancreatic cancer. Cancers, 13, 3920 (2021). Kuo, K-K., Hsiao P-J., Chang, W-T., Chuang, S-C., Yang, Y-H., Wuputra, K., Ku, C-C., Pan, J-B., Li, C-P., Kato, K., Liu, C-J., Wu, D-C., and Yokoyama K.
	Potential application of cell reprogramming technique for cancer. Cellular and Molecular Life Sciences, 76, 45-65 (2019). Saito, S., Lin, Y-C., Nakamura, Y., Eckner, R., Wuputra, K., Kuo, K-K, Lin C-S., and Yokoyama K.
	Reprogramming antagonizes the oncogenicity of HoxA13-Long noncoding RNA HOTTIP axis in gastric cancer cells. Stem Cells, 35, 2115-2128 (2017). Wu, D-C., Wang, S. S-W., Liu, c-J., Wuputra, K., Katoh, K., Lee, Y-l., Lin, Y-C., Tsai, M-H., Ku, C-C., Lin, W-H., Wang, S-W., Kishikawa, S., Noguchi, M., Wu, C-C., Chai, C-Y., Lin, C-L., Kuo, K-K., Yang, Y-H., Miyoshi, H., Nakamura, Y., Saito, S., Nagata, K., Lin, S-C., and Yokoyama, K.
	Positive feedback loop of OCT4 and c-JUN expedites cancer stemness in liver cancer. Stem Cells, 34, 27613-2624 (2016). Kuo, K-K., Lee, K-T., Chen, K-K., Yang, Y-H., Lin, Y-C., Tsai, M-H., Wuputra, K., Lee, Y-L., Ku, C-C. , Miyoshi, H., Nakamura, Y., Saito, S., Wu, C-C., Chai, C-Y., Eckner, R., Lin, S C-L., Wang, S. S-W., Wu, E-C., Lin, C-S., and Yokoyama, K.

List of research achievements for application of Doctor of Science, Waseda University

Full Name: Wuputra Kenly seal or signature

Date Submitted(yyyy/mm/dd): 2023/10/18

種類別 (By Type)	題名、 発表・発行掲載誌名、 発表・発行年月、 連名者（申請者含む） (theme, journal name, date & year of publication, name of authors inc. yourself)
	Control of the cell cycle and mitosis by phosphorylated activating transcription factor 2 and its homologue 7. Journal of Nature and Science, 1, e74 (2015). Ku, C-C., Hasegawa, H., Lin, C-S., Tsai, M-H., Wuputra, K., Eckner, R., Yamaguchi, N., and Yokoyama K. Control of oxidative stress and generation of induced pluripotent stem cell-like cells by Jun dimerization protein 2. Cancers 5, 959-984 (2013). Chiou, S-S., Wang, S-W., Wu, D-C., Lin, Y-C., Kao, L-P., Kuo, K-K., Wu, C-C., Chai, C-Y., Lin, C-C., Lee, C-Y., Liao, Y-M., Wuputra, K., Yang, Y-H., Wang, S-W., Ku, C-C., Nakamura, Y., Saito, S., Hasegawa, H., Yamaguchi, N., Miyoshi, H., Lin, C-S., Eckner, R., and Yokoyama K.